PACIFIC EARTHQUAKE ENGINEERING
RESEARCH CENTER

Moment Resisting Frames Coupled with Rocking Walls Subjected to Earthquakes

Mehrdad Aghagholizadeh

Department of Civil and Environmental Engineering
University of Southern California

Nicos Makris

Department of Civil and Environmental Engineering
Southern Methodist University, Dallas, Texas

PEER Report No. 2022/03

Pacific Earthquake Engineering Research Center
Headquarters at the University of California, Berkeley
June 2022

PEER 2022/03
June 2022

Moment Resisting Frames Coupled with Rocking Walls Subjected to Earthquakes

Mehdad Aghagholizadeh[1]

Nicos Makris[2]

[1]Department of Civil and Environmental Engineering
University of Southern California, Los Angeles, CA

[2]Department of Civil and Environmental Engineering
Southern Methodist University, Dallas, TX

PEER Report 2022/03
Pacific Earthquake Engineering Research Center
Headquarters at the University of California, Berkeley

June 2022

ABSTRACT

The high occupancy levels in urban multistory buildings, in association with current safety considerations inevitably leads to a reconsideration of performance objectives. In view of the appreciable seismic damage and several weak-story failures (some at mid-height) of multistory buildings that have been documented after major earthquakes, there has been a growing effort to develop an alternative hybrid structural system by coupling the response of moment resisting frames with rigid/stiff walls which are allowed to uplift and rock during ground shaking; therefore, enforcing a uniform drift distribution (Meek 1978; Ajrab et al. 2004; Lu 2005; Toranzo et al. 2009; Wada et al. 2011; Hu and Zhang 2012; Qu et al. 2012; Aghagholizadeh and Makris 2018a, 2018b).

Part of the reason for this semi-articulated seismic design alternative is that on several occasions, the further strengthening of the building with fixed-based shear walls leads to the attraction of larger seismic forces and the entire approach reaches an impasse given that the resulting forces that develop cannot be accommodated by cost-effective foundations. Another major issue that is a concern in multistory buildings in which their earthquake performance relies on ductile behavior is that after severe shaking the multi-story building may end up with appreciable permanent displacements and there is a need for re-centering which in most cases leads to demolition (an outcome against the emerging trends of functional recovery) as happened after the 2011 Christchurch, New Zealand earthquake (Elwood 2013).

In this report we first investigate the inelastic response of a yielding single-degree-of-freedom oscillator coupled with a rocking wall. Configurations of both a stepping rocking wall and a pinned rocking wall that have been reported in the literature are examined. The full nonlinear equations of motions are derived, and the report shows that a stepping wall suppresses peak and permanent displacements, with the heavier wall being most effective. In contrast, when the yielding oscillator is coupled with a pinned rocking wall, both peak and permanent displacements increase, with the heavier wall being most unfavorable. This unfavorable response is mainly because the moment from the weight of the pinned wall works against stability, and in most cases, it contributes to larger permanent displacements.

Subsequently, the report investigates the inelastic response of a yielding structure coupled with a vertically restrained rocking wall. The nonlinear equations of motion are extended for of a yielding oscillator coupled with a vertically restrained rocking wall, and the dependability of the one-degree of freedom idealization is validated against the nonlinear time-history response analysis the nine-story SAC steel frame that is coupled with a stepping vertically restrained rocking wall. The planar response analysis is conducted with the open-source software, OpenSees. While the coupling of weak building frames with rocking walls is an efficient strategy that controls inelastic deformations by enforcing a uniform inter-story-drift distribution, therefore, avoiding mid-story failures, our analysis shows that even for medium-rise buildings the effect of vertical tendons on the inelastic structural response is marginal, with the exception of increasing the vertical reactions at the pivoting points of the rocking wall. Accordingly, our planar response analysis concludes that for medium-rise to high-rise buildings, vertical tendons in rocking walls are not beneficial.

Given that the coupling of a moment-resisting building with a stiff rocking wall enforces a first-mode dominating response, our study proceeds by investigating the dynamic response of a yielding single-degree-of-freedom oscillator coupled to a stepping rocking wall with supplemental damping (either hysteretic or linear viscous) along its sides. The full nonlinear equations of motion are derived, and the study presents an earthquake response analysis in terms of inelastic spectra. The study shows that for structures with pre-yielding period $T_1 < 1.0$ s, the effect of supplemental damping along the sides of the rocking wall is marginal even when large values of damping are used. The study uncovers that occasionally, the damped response matches or exceeds the undamped response; however, when this happens, the exceedance is marginal. The report concludes that for yielding structures with strength less than 10% of their weight, the use of supplemental damping along the sides of a rocking wall coupled to a yielding structure is not recommended. Our study concludes that supplemental damping along the sides of the rocking wall may have some limited beneficial effects for structures with longer pre-yielding periods (say $T_1 > 1.0$ s). Nevertheless, no notable further response reduction is observed when larger values of hysteretic or viscous damping are used.

Keywords: seismic response modification, rocking wall, structural dynamics, earthquake engineering, seismic protection

ACKNOWLEDGMENTS AND DISCLAIMER

The opinions, findings, conclusions, and recommendations expressed in this publication are those of the authors and do not necessarily reflect the view of Pacific Earthquake Engineering Research (PEER) Center, and the Regents of the University of California.

CONTENTS

LIST OF TABLES

LIST OF FIGURES

1 INTRODUCTION

1.1 OVERVIEW

In an effort to eliminate the appreciable seismic damage in moment-resisting frames that occasionally resulted to a weak-story failure, the concept of a rigid core system gained appreciable ground (Paulay 1969; Fintel 1975; Emori and Schnobrich 1978; Bertero 1980; Aktan and Bertero 1984). When the core walls in tall buildings are fixed-based, the ductility capacity of the base of the core wall may be limited given the significant axial loads; while the ductility demands are appreciable under long-duration pulse motions (Paulay 1986; Y. Zhang and Wang 2000). Furthermore, the base of the core wall may suffer from cyclic degradation under prolonged shaking which usually results to permanent inelastic deformations. Such inelastic response may result to permanent drifts and lead to large repair costs; therefore, the entire design becomes unsustainable. An example of such failure after an earthquake is shown in Figure 1-1 (left) for a fourteen-story moment-resisting frame with a fixed shear-wall building during 1964 Anchorage, Alaska earthquake.

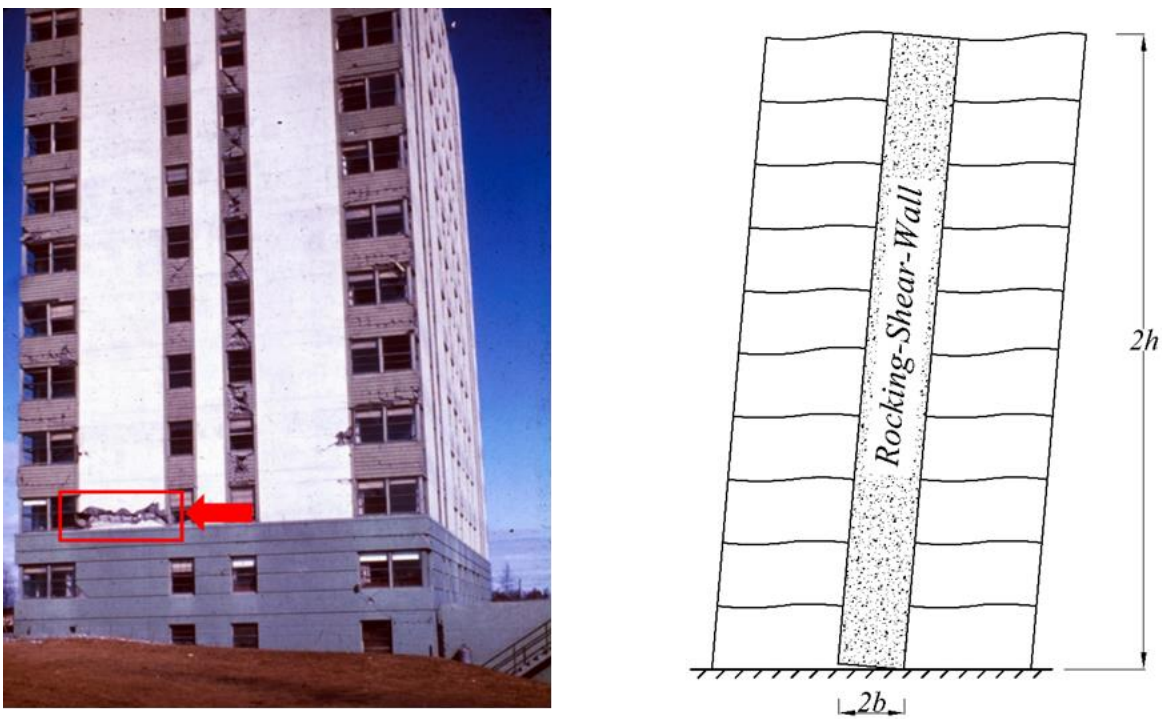

Figure 1-1 Left: A fourteen-story reinforced concrete apartment building in Anchorage, Alaska, was severely damaged during the 1964 Alaska earthquake. One of the main exterior shear walls, shown in this figure, failed at the second floor, exposing the steel reinforced bars within the concrete (Image courtesy of the USGS (2020)). Right: Schematic of the first mode deformation of a tall moment-resisting-frame with a rocking-shear-wall.

The concept of allowing a tall, slender structure to uplift and rock was first advanced and implemented in modern civil engineering in the late 1960s in New Zealand with the design and construction of the stepping piers of the South Rangitikei bridge (Beck and Skinner 1972, 1974; Kelly 1993; Skinner et al. 1993). This unique, at the time, design emerged out of necessity given that the height of the piers of the South Rangitikei Bridge exceeded 75m; therefore, the resulting overturning moments at the foundations of the bridge piers from a traditional capacity design were too large. The design of the South Rangitikei Bridge emerged from the Physics and Engineering Laboratory of the Department of Scientific and Industrial Research (DSIR) in New Zealand (Beck and Skinner 1972, 1974; Kelly 1993; Skinner et al. 1993) in which a material science group led by W. H. Robinson was conducting research on the use of plastically deforming metals (steel and lead) for developing hysteretic energy dissipation devices (Robinson and Greenbank 1976). Their efforts were joined in 1972 by professor J. M. Kelly who visited DSIR during a one-year leave from University of California, Berkeley and resulted to the development of the torsionally yielding steel dampers that was used to enhance the energy dissipation of the base of the stepping piers of the South Rangitikei Rail Bridge (Kelly et al. 1972; Skinner, Kelly, et al. 1974).

Another early study on the concept of shear walls that are able to uplift, and rock was the work by Meek (1978) that studied the possibility of a core shear wall that is able to rock. Inspired by the seminal work on rocking blocks by Housner (1963) this study used a simplified analysis of the core rocking wall and a frame when the wall and footing rock on the soil. In this study it was showed that tipping (rocking) wall greatly reduces the base shear and the moment and the base of the wall when it compared conventional to fixed-base shear walls.

Despite the remarkable originality of these early works and their technical merit, these papers did not receive the attention it deserved, and it was some two decades later that the PRESSS Program (Priestley 1991, 1996) reintroduced the concept of uplifting and rocking of the joint shear wall system (Nakaki et al. 1999; Priestley et al. 1999).

Figure 1-2 Weak-story failure at the higher stories of the buildings after the 1995 Kobe, Japan Earthquake. (Images courtesy of the NOAA (2012)).

Around the same time, after 1994 Northridge, California earthquake followed by 1995 Kobe, Japan earthquake, coherent acceleration pulses (0.8-1.5 sec duration at that time) which result in large monotonic velocity, received revived attention. Makris (1996), Alavi and Krawinkler (2004a) and Makris and Cheng (2000) studied the destructive potential of pulse-like ground motions recorded near the causative fault of earthquakes. In particular, several tall moment-resisting frames that had been designed in accordance with the existing seismic-code provisions exhibited a weak-story failure—in some cases several stories above the ground (see Figure 1-2).

Kurama et al. (1999, 2002) investigated behavior of unbonded post-tensioned precast concrete walls. In these studies, a design procedure based on idealized trilinear base-shear-roof-drift relationship is proposed. In these studies, a trilinear relation is used to define base-shear-roof-drift relation and effect of rotational inertia is not considered. The trilinear relation consists of 4 stages; decompression state (when wall starts the uplift), softening state (linear limit either governed by gap opening of the walls or nonlinear behavior of concrete in compression), yielding state (at this state strain in post-tensioning steel first reaches the linear simit strain) and failure state (in which wall fails) are defined. Kurama et al. (1999) verifies the analytical model using test results of National Institute of Standards and Technology (NIST) (Cheok and Lew 1993). The verification of the analytical model compared with test results shows that the analytical model is reasonably agreed with the test in loading; however, the model is not accurate in unloading phase. This paper concluded that the post-tensioned precast walls are feasible alternative to cast in place walls. These walls can undergo large displacement with minor damages. What is more, precast walls have almost no residual displacement. Additionally, in Kurama et al. (2002) using equal displacement assumption in the analytical model of this study drift results of the model is not predicting the experiment results correctly.

Holden et al. (2003) compared behavior of monolithic reinforced concrete walls with prestressed concrete walls using reversed cyclic quasi-static lateral loading. In this study two geometrically identical (half-scale) concrete wall were tested under quasi-static analysis. One wall was conventional reinforced fixed-end shear wall, and the second specimen was a partially prestressed precast wall which was free to uplift and rock on the pivoting points. The precast wall was also equipped with hysteretic energy dissipating devices. For the rocking wall in this study assumed a bilinear elastic behavior which is inspired by the damage avoidance design (DAD) paradigm (Mander and Cheng 1997) and it ignores effects of wall's mass inertia. In this study it was assumed that after uplifting, system's stiffness is attained from strain-hardening stiffness in energy dissipaters and stiffness of the tendons. Results from this study shows that partially prestressed rocking wall with energy dissipating devices achieved drift level on excess of 3% with no visible damage. This study mostly focused on the advantages of self-centering walls over monolithic shear walls in terms of damage to walls after lateral loadings and residual displacement comparison.

Ajrab et al. (2004) analyzed a rocking wall-reinforced concrete frame system with additional tendon system and dampers. Total damping of the system is assumed to be summation of structural damping, equivalent viscous damping caused by wall and foundation impact, hysteretic damping caused by inelastic action in the frame and additional damping due to supplemental damping devices. In order to calculate lateral capacity demand of the rocking wall-frame system this study adopted a capacity design approach. In the pre-rocking stage, the system behavior governed by structural flexibility, when uplifting of the wall initiated, based on the equilibrium of internal and external works, the base shear capacity of the system is calculated without considering effect of rotational inertia of the rocking wall. Then overall performance of the structure under MCE (Maximum Considered Earthquake) and MAE (Maximum Assumed Earthquake) is compared with the maximum displacement of the structure, calculated using time-history analysis. The results of designed structure under different ground motions showed that the adopted capacity-demand method predicts larger displacements in comparison to what was obtained from time-history analysis. Also, response of an analytical structure with proposed rocking wall-damper system to 1970 Pacoima Dam S18W ground motion is analyzed and compared with the fixed end wall. The results show that the proposed wall-frame system with dampers has smaller roof displacement. Additionally, inter-story drifts are also reduced and became more uniformly distributed through the height of the building.

To strengthen moment-resisting frames to near-fault ground motion effects, Alavi and Krawinkler (2004b) introduced pinned rocking wall system similar to the one shown in Figure 1-3 (right). Because of the nature of near-fault ground motion which cause a highly non-uniform distribution of story ductility demand, in this study effects of coupling MRFs to pinned rocking wall was investigated and it concluded that strengthening with pinned wall is effective and reduces drift demands of structures with a wide range of periods and various performance levels.

In their study, Filiatrault et al. (2004) reviewed self-centering structural systems and discussed advantages of such structures over conventional structural systems in terms of cost, resilience and serviceability after major earthquakes. The paper points the main advantages of these systems as: their large lateral displacement capacity, the lack of structural damage associated with large displacements and their ability to return to the original position upon unloading.

Lu (2005) studied behavior of rocking wall-frame system considering its 3D effect. Purpose of the study was modeling wall's neural axis migration and showing its significance and assessment of 3D effect of the wall in order to control it. This study showed that the uncontrolled wall rocking can cause beam-wall connection failures. In this study planar six story high wall-frame system is also tested under different ground motions. Experiment's main objective was to assess response of the wall-frame system which was designed using Eurocode 8. In this paper test result showed that approximately 80% of the first-story lateral drift was attributed to the wall rigid body rotation about its pivoting points during inelastic response. In this study also, an analytical model of the tested building was investigated. In analytical model walls were modeled as columns and there is no consideration of how wall's inertia was implemented.

Restrepo and Rahman (2007) investigated performance of prestressed self-centering walls with and without additional energy dissipators. Prototype wall tested under quasi-static reversed cyclic loading. In contrast with previous works of Kuramma et al. (1999, 2002) and Holden et al. (2003), instead of trilinear representation of lateral load-displacement relationship, this study utilizes a bi-linear representation. The experiments showed no residual displacement in rocking walls even when the system had no energy dissipators installed and in prestressed wall with dissipators, flag-shaped hysteresis behavior was observed.

Erkmen and Schultz (2009) investigated self-centering behavior of postensioned precast shear walls. Experimental results in this study showed that even though the postensioning force may die-out in cyclic loading but the rocking wall is still capable of recentering.

Tozano et al. (2009) tested a confined-masonry rocking wall-reinforced concrete frame system with supplemental hysteretic damping. In order to design the wall-frame system a performance-based design methodology is used. This study investigates the benefits of masonry rocking wall-reinforced concrete frame, incorporated with low-cost hysteretic damping to reduce maximum roof drifts and dissipate more energy. Prototype structure was a 40% scaled model of a segment of a three-story building. Structure tested under 60 different ground motions which most of them were intended to reproduce the seismic demand of the system in different design levels. The structure showed a good performance under different levels of ground motions and met the design criteria. This study focuses mostly on the performance of the tested prototype structure, the advantage of rocking-wall frame system using ability of self-centering in the rocking wall, and with addition of low-cost hysteretic dampers how these systems can dissipate more energy. Since this study is more focused on the performance of the structure under different design levels, there is no detailed discussion on the dynamic behavior of the rocking wall and effect of walls rotational inertia.

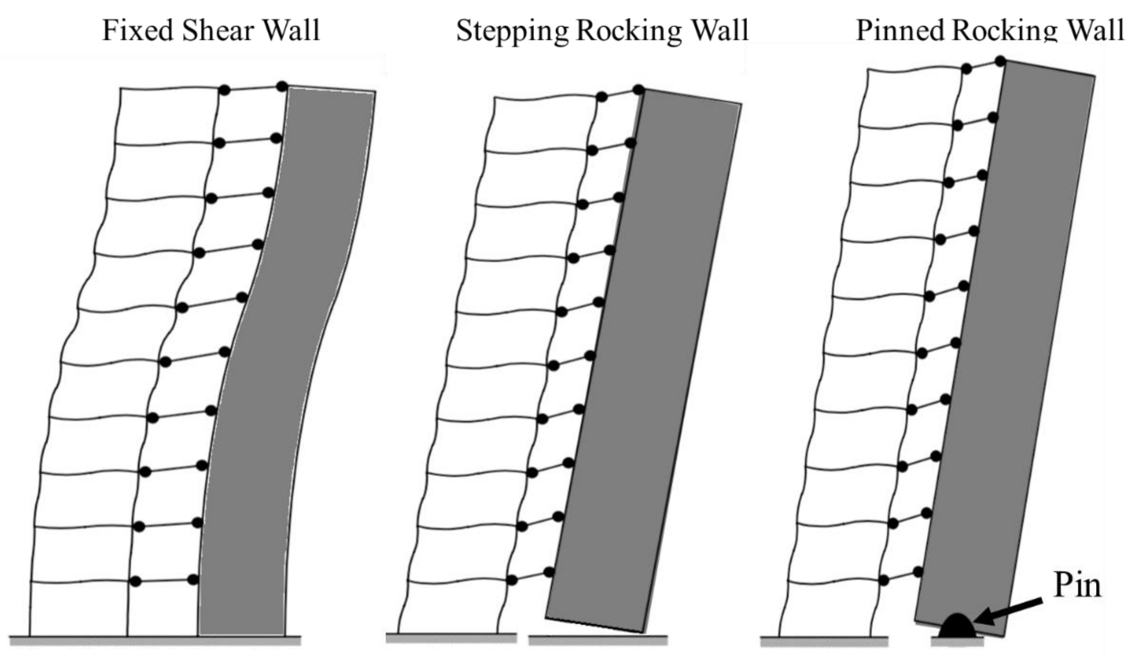

Figure 1-3 Conventional Fixed shear wall (left) compared to stepping rocking wall (center) and Pinned rocking wall (right)

These tests showed that thanks to good performance of rocking masonry wall, this structure performed well under different seismic excitations, and reached a maximum roof drift ratio of 2.5% without visible damage. Finally, the structural system showed no residual deformation because of employing the advantage of self-centering in rocking systems.

Inspired by the idea of coupling a moment-resisting frame with a pinned-rocking wall from the work of Alavi and Krawinkler (2004b), Wada et al. (2011) and Qu et al. (2012) fitted an existing reinforced concrete moment-resisting frame with a pinned-rocking wall and steel damping system. The structure was a 11-story-high reinforced concrete frame building which is in the campus of Tokyo Institute of Technology in Japan. The proposed rocking wall system is a pin-supported concrete wall which is connected to the main frame of the structure. Goal of this retrofitting is enhancing integrity and avoiding weak story failure. Although pin-support connection of the wall prevents the wall foundation impact (when the wall changes its pivot point in rocking), but wall weight cannot help in the self-centering of the system in order to prevent residual displacements. Also, it had showed that strengthening of the frame with hinged walls is effective way of reducing maximum story drift and producing more uniform distribution of story drifts. Performance of the structure assessed through nonlinear dynamic analysis before and after retrofitting. Additionally, energy dissipating devices used between rocking wall and frame. With this approach vertical deformation of the wall can be used in order to dissipate more energy Theoretical analysis of the system in this paper has done in a capacity design manner and while they considered a lateral load at the roof level the failure mechanism is assumed. Because of the nature of this analysis, inertia of the wall is neglected which will not represent the real dynamic behavior of the system. Analytical model of the structure is analyzed under different ground motions for the cases of before and after retrofit using ABAQUS software. The hysteretic behavior of the steel dampers is idealized as elastic-perfectly plastic the nominal yielding strength. The analysis shows the structure undergoes smaller drifts, and deflections are evenly distributed through the structure which shows the damage would be distributed throughout the structure not concentrating at a local part of the structure.

Hu and Zhang (2012) studied retrofitting of concrete frames using hybrid rocking walls (rocking walls with prestressing tendons and dampers). They made a parametric study of the seismic behavior of self-centering walls used for retrofitting of the reinforced concrete frames. This study examined the effect of variety of factors like cross sectional area of prestressing tendons, location of the tendons in the wall and yielding stress of the hysteretic dampers. In the numerical modeling of the system the wall modeled as beam-column element and its mass lumped at the end of nodes (without mentioning any mass inertia consideration). The rocking wall is an infill masonry wall in a reinforce concrete frame with prestressing tendons. Additionally, a prototype structure is selected for numerical analysis. Push over and time history analysis of this numerical model had done using OpenSees (McKenna et al. 2000). The results of this paper compared frame without wall with a frame retrofitted with a rocking wall and showed that after retrofitting the frame dropped the drift from 2-5% to 0.5-0.9% for different ground motions. Additionally, this study investigated the parametric study of the tendons in the rocking wall system and found that the area of the tendons and yield strength of the base dampers play a great role in hysteretic behavior of the hybrid wall system.

Belleri et al. (2014) analyzed a half scaled 3-story high precast concrete building with two unbonded post-tensioned precast walls located at the north and south of the structure, subjected to shake-table testing. In order to provide more energy dissipation ability, energy dissipating devices where used. Through these tests they evaluate the design procedure. The test reported in this paper is the dynamic response of rocking wall to ground motions. Additionally, they investigated higher mode effects on the response of the system and strain distribution at rocking wall's pivoting points. Expected and measured responses of the wall are also presented.

Nicknam and Filiatrault (2014) analyzed and compared experimental results with a numerical model of a structural system which named propped rocking wall (PRW). Proposed structure is a 1:3 scaled structure and goal of the study is to validate direct displacement-based design with experimental outcomes. PRW structure system consists of a concrete frame with a wall which has unbonded post tensioned bars and two diagonally propped hysteretic dampers connected to the wall. In the proposed design method based on a closed-form solution derived for the base shear-roof displacement relationship of the PRW system at its maximum response, even though the wall rotates around its pivoting point but in the calculation no mass inertia of the wall included. An experimental study is performed. A wall with three floors slabs connected to it, and propped hysteretic dampers is designed with this method. This structure then analyzed under different ground motions. The tests showed good seismic behavior of PRW system, but experimentally measured fundamental period of the system was significantly larger than pre-test numerical analysis. Comparison of the experimental and numerical results shows that the results are close but the numerical model's response damps out quicker than the experiment and the maximum roof displacement of the experimental model is higher than the numerical model.

Grigorian and Grigorian (2015; 2016) proposed a new approach based on the principles of design-led analysis for the rocking-wall-moment-frame (RWMF) systems. In this study several generic examples and case studies have been provided to demonstrate application and validation of the proposed procedure. The rocking wall system of this study consists of a pin-supported wall coupled with a frame and the wall-frame system is connected with rigid pin-ended arms. In the analysis, although the wall considered to be rigid, but when the wall tilted no mass rotational inertia was considered.

Nazari et al. (2017) investigated different precast rocking walls with various prestressing and tendon area configurations. In terms of performance under different seismic loadings rocking walls performed satisfactorily and sustained negligible damages. All test walls re-centered with minimum residuals. In this study, prestressed precast wall is also modeled in OpenSees with a single degree idealization of the rocking wall. This analysis was in good agreement with the experimental results.

Most of these aforementioned studies introduce the unique advantages of rocking action by referencing the seminal paper by Housner (1963), who noticed that tall, slender, free-standing columns, while they can easily uplift even when subjected to a moderate ground acceleration (uplifting initiate when $\ddot{u}_g > g\ (\text{base}/\text{height})$); they exhibit remarkable seismic stability due to a size-frequency scale effect. In his 1963 paper Housner shows that there is a safety margin between uplifting and overturning and that as the size of the free-standing column increases or the frequency of the excitation pulse increases, this safety margin increases appreciably to the extent that large free-standing columns enjoy ample seismic stability. Makris (2014a, 2014b) explained that as the size of the free-standing rocking column increases, the enhanced seismic stability primarily originates from the difficulty to mobilize the rotational inertia of the column (wall) which increases with the square of the column (wall) size. Further studies by Makris and Vassiliou (2014; 2015) showed that as the size of the column (wall) increases, the resistance to mobilize the rotational inertia increases to such an extent, that the effect of vertical tendons becomes increasingly marginal.

The motivation for coupling of a moment-resisting frame with a strong rocking wall is to primarily enforce a uniform distribution of interstory drifts; therefore, the first mode of the frame becomes dominant as was first indicated in the seminal paper by Alavi and Krawinler (2004b). Further analytical evidence to the first mode dominated response is offered in the Qu et al. (2012) paper. These results together with additional evidence by other investigators were critically evaluated in a recent paper by Grigorian and Grigorian (2015) who concluded that a moment resisting frame coupled with a rocking wall can be categorized as a single-degree-of-freedom (SDOF) system. Accordingly, in this study we adopted the SDOF idealization shown in Figure 2-1 and Figure 2-2.

Table 1-1 summarizes the studies from the literature and provides the dimensions and modal information of the referenced works.

Table 1-1 Summary of studies in the literature

Paper info.	**Period and Frequency** T_0 , ω_0	**Wall dimensions** $2b \times d \times 2h$	**Slenderness** $\tan(\alpha)$	**Mass Ratio** γ
Lateral load behavior and seismic design of unbonded post-tensioned precast concrete walls (Kurama et al. 1999)	----	$6.1^m \times 0.31^m \times 25.3^m$ $p = 0.752$	0.241	4.85
Seismic Design of Unbonded Post-Tensioned Precast Concrete Walls with Supplemental Viscous Damping. (Kurama 2000)	$T_0 = 0.64$ sec $T_0 = 1.09$ sec $T_0 = 1.65$ sec $\omega_0 = 9.81$ rad/sec $\omega_0 = 5.76$ rad/sec $\omega_0 = 3.81$ rad/sec	$6.1^m \times 0.31^m \times 24.7^m$ $6.1^m \times 0.31^m \times 32.6^m$ $6.1^m \times 0.31^m \times 40.5^m$ $p = 0.761$ $p = 0.666$ $p = 0.599$	0.247 0.187 0.150	---

Paper info.	**Period and Frequency** T_0 , ω_0	**Wall dimensions** $2b \times d \times 2h$	**Slenderness** $\tan(\alpha)$	**Mass Ratio** γ
Rocking Wall–Frame Structures with Supplemental Tendon Systems. (Ajrab et al. 2004)	$T_0 = 1.95$ sec $\omega_0 = 3.22$ rad/sec	$4^m \times 0.4^m \times 21.9^m$ $p = 0.813$	0.183	1.05
Inelastic Behaviour of RC Wall-Frame With A Rocking Wall and Its Analysis Incorporating 3-D Effect. (Lu 2005)	$T_0 = 0.389$ sec $\omega_0 = 16.15$ rad/sec	$3.45^m \times 0.25^m \times 20^m$ $p = 0.852$	0.173	16.90
Shake-Table Tests of Confined-Masonry Rocking Walls with Supplementary Hysteretic Damping. (Toranzo et al. 2009)	$T_0 = 0.14$ sec $\omega_0 = 44.88$ rad/sec	$2.1^m \times 0.61^m \times 11.6^m$ $p = 1.117$	0.181	3.5
Ductility of a Structural Wall with Spread Rebars Tested in Full Scale. (Preti and Giuriani 2011)		$2.8^m \times 0.3^m \times 10^m$ $p = 1.190$	0.280	4.96
Seismic retrofit of existing SRC frames using rocking walls and steel dampers (Wada et al. 2011; Qu et al. 2012)	$T_0 = 0.68$ sec $\omega_0 = 9.24$ rad/sec	$4.4^m \times 0.6^m \times 33^m$ $p = 0.665$	0.133	14.90
Seismic Performance of Reinforced Concrete Frames Retrofitted with Self-Centering Hybrid Wall. (Hu and Zhang 2012)	$T_0 = 0.173$ sec $\omega_0 = 36.32$ rad/sec	$5.3^m \times 0.4^m \times 10.97^m$ $p = 1.094$	0.486	19.08
Dynamic Behavior of Rocking and Hybrid Cantilever Walls in a Precast Concrete Building (Belleri et al. 2014)	$T_0 = 0.187$ sec $\omega_0 = 33.60$ rad/sec	$2.43^m \times 0.2^m \times 7.01^m$ $p = 1.408$	0.347	

Paper info.	**Period and Frequency** T_0 , ω_0	**Wall dimensions** $2b \times d \times 2h$	**Slenderness** $\tan(\alpha)$	**Mass Ratio** γ
Numerical Evaluation of Seismic Response of Buildings Equipped with Propped Rocking Wall Systems (Nicknam and Filiatrault 2014)	$T_0 = 0.18$ sec $\omega_0 = 34.91$ rad/sec	$2.29^m \times 0.6^m \times 11.6^m$ $p = 1.116$	0.197	15.65

2 YIELDING STRUCTURE WITH A STEPPING AND PINNED ROCKING WALL

2.1 INTRODUCTION

The motivation for coupling of a moment-resisting frame with a strong rocking wall is to primarily enforce a uniform distribution of interstory drifts and avoid a soft story collapse; therefore, the first mode of the frame becomes dominant as was first indicated in the seminal paper by Alavi and Krawinler (2004b). Further analytical evidence to the first-mode dominated response is offered in the Qu et al. (2012) and Aghagholizadeh and Makris (2018a) papers. These results together with additional evidence by other investigators were critically evaluated in the paper by Grigorian and Grigorian (2015) who concluded that a moment resisting frame coupled with a rocking wall can be categorized as a single-degree-of-freedom (SDOF) system.

Accordingly, in this study the authors adopted the SDOF idealization shown in Figures 2.1 and 2.2 which is most relevant for stiff rocking walls. Nevertheless, in view of the expected inelastic behavior of the moment resisting frames and the acceptance by the practice of pinned rocking walls that work against the stability of the system (Makris and Aghagholizadeh 2017a, 2017b), the main motivation of this study is to examine to what extent the dynamics of a stepping or a pinned rocking wall influences the dynamic response and permanent displacements of the coupled inelastic oscillator shown in Figures. 2.1 and 2.2.

2.2 DYNAMICS OF A YIELDING OSCILLATOR COUPLED WITH A STEPPING ROCKING WALL

With reference to Figure 2-1, this study first examines the dynamic response of a yielding single-degree-of-freedom (SDOF) structure, with mass, m_s, pre-yielding stiffness, k_1, post yielding stiffness k_2, and strength, Q, that is coupled with a free-standing stepping rocking wall of size $\mathrm{R} = \sqrt{\mathrm{b}^2 + \mathrm{h}^2}$, slenderness, $\tan\alpha = \mathrm{b}/\mathrm{h}$, mass, m_w and moment of inertia about the pivoting (stepping) points O and O', $\mathrm{I} = 4/3\ \mathrm{m_w}\ \mathrm{R}^2$. In the interest of simplicity, the authors assume that the arm with length, L, that couples the motion is articulated at the center of mass of the rocking wall at a height, h, from its foundation as shown in Figure 2-1.

During rocking motion, the center of mass of the rocking wall uplifts by v; therefore, the initially horizontal coupling arm rotates by an angle ψ. Accordingly, the horizontal translation of the center of mass of the rotating wall, x, is related to the horizontal displacement of the SDOF oscillator, u, via the expression, $\cos\psi = 1 - (\mathrm{u} - \mathrm{x})/\mathrm{L}$; whereas $\sin\psi = \mathrm{v}/\mathrm{L}$.

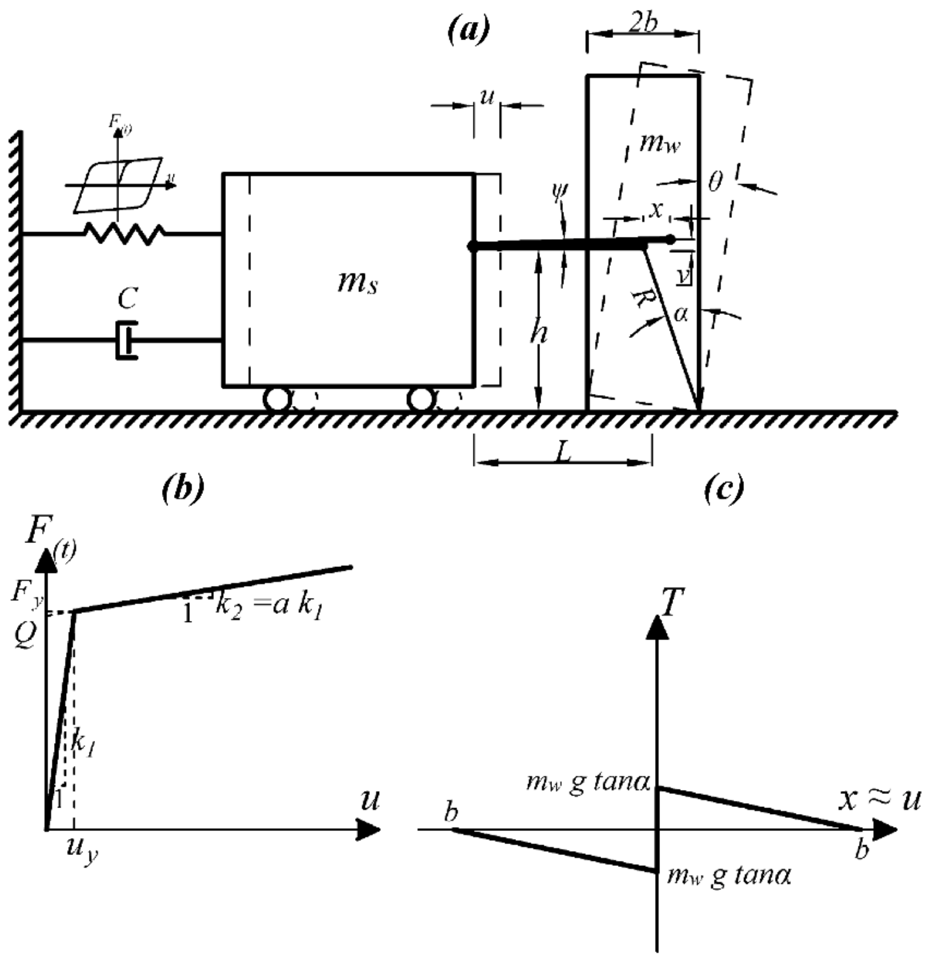

Figure 2-1 Yielding single-degree-of-freedom oscillator coupled with a stepping rocking wall. While schematically the wall is shown to be connected in series with the mass, the dynamics of the wall works in parallel with the nonlinear spring and dashpot because of the rigid connection between the mass and the wall. (b): The bilinear idealization with its control parameters. (c): Force-displacement diagram of the stepping rocking wall.

From the identity, $\cos\psi^2 + \sin\psi^2 = 1$, one concludes that the horizontal displacement, *u* of the SDOF oscillator is related to the horizontal displacement *x* of the center of mass of the rotating wall via the expression:

$$\frac{u}{L} = 1 + \frac{x}{L} - \sqrt{1 - \frac{v^2}{L^2}} \tag{2.1}$$

For the sake of simplicity, in this part of the report, the coupling arm is assumed to be long enough so that v^2/L^2 is much smaller that unity ($v^2/L^2 \ll 1$); and in this case *u*=*x*. Clearly, there are cases where the coupling arm is short and in this case the term v^2/L^2 is not negligible. Nevertheless, a recent study by Makris and Aghagholizadeh (2017a) on the response of an elastic oscillator coupled with a rocking wall showed that the effect due to a shorter coupling arm is negligible. The importance of the length of the coupling arm is also discussed later in this chapter.

The system under consideration shown in Figure 2-1 is a single-degree-of-freedom system where the lateral translation of the mass, u is related to the rotation of the stepping rocking wall θ via the expression:

$$u = \pm R[\sin\alpha - \sin(\alpha \mp \theta)] \tag{2.2}$$

$$\dot{u} = R\dot{\theta}\cos(\alpha \mp \theta) \tag{2.3}$$

$$\ddot{u} = R[\ddot{\theta}\cos(\alpha \mp \theta) \pm \dot{\theta}^2 \sin(\alpha \mp \theta)] \tag{2.4}$$

In equations 2.2 to 2.4 whenever there is a double sign (say$\pm$), the top sign is for $\theta > 0$ and the bottom sign is for $\theta < 0$.

Dynamic equilibrium of the mass m_s gives:

$$m_s(\ddot{u} + \ddot{u}_g) = -F_s - c\dot{u} + T \tag{2.5}$$

where F_s is the force the develops in the nonlinear spring and is described by the Bouc-Wen model (Bouc 1967; Wen 1976).

$$F_s(t) = a\ k_1\ u(t) + (1-a)k_1 u_y\ z(t) \tag{2.6}$$

where $a=k_2/k_1$ is the post–to-pre yielding stiffness ratio and $-1 \leq z(t) \leq 1$ is a dimensionless internal variable described by:

$$\dot{z}(t) = \frac{1}{u_y}[\dot{u}(t) - \beta\dot{u}(t)|z(t)|^n - \gamma|\dot{u}|z(t)|z(t)|^{n-1}] \tag{2.7}$$

In equation 2.7, constants β, γ and n are model parameters to be discussed later in this chapter.

Furthermore, in equation 2.5, T is the axial force (positive = tensile) that develops in the coupling arm.

Case 1: $\theta > 0$

For positive rotations $\theta > 0$, dynamic equilibrium of the rotating wall with mass m_w, gives:

$$I\ddot{\theta} = -TR\cos(\alpha - \theta) - m_w gR\sin(\alpha - \theta) - m_w \ddot{u}_g R\cos(\alpha - \theta) \tag{2.8}$$

The axial force T appearing in equation 2.8 is replaced with the help of equations 2.5 and 2.6 and for a rectangular stepping wall ($I = 4/3\ m_w R^2$), equation 2.8 assumes the form:

$$\begin{aligned}\frac{4}{3}m_w R^2\ddot{\theta} + [m_s(\ddot{u} + \ddot{u}_g) + ak_1 u(t) + (1-a)k_1 u_y z(t) + c\dot{u}]R\cos(\alpha - \theta) \\ = -m_w R[\ddot{u}_g \cos(\alpha - \theta) + g\sin(\alpha - \theta)]\end{aligned} \tag{2.9}$$

Upon dividing with $m_w R$ equation 2.9 gives:

$$\frac{4}{3}R\ddot{\theta}+\left[\sigma(\ddot{u}+\ddot{u}_g)+a\frac{k_1}{m_w}u(t)+(1-a)\frac{k_1}{m_w}u_y z(t)+\frac{c}{m_w}\dot{u}\right]\cos(\alpha-\theta) \\ -\ddot{u}_g\cos(\alpha-\theta)-g\sin(\alpha-\theta) \tag{2.10}$$

in which $\sigma = m_s/m_w$ is the mass ratio parameter.

Substitution of the expressions of the relative displacement, velocity and acceleration given by equations 2.2 to 2.4 for positive rotations and after dividing with *R*, equation 2.10 gives:

$$\Big(\frac{4}{3}+\sigma\cos^2(\alpha-\theta)\Big)\ddot{\theta}+\sigma\cos(\alpha-\theta)\Big\{a\omega_1^2\big(\sin\alpha-sin(\alpha-\theta)\big) \\ +2\xi\omega_1\dot{\theta}\cos(\alpha-\theta)+\dot{\theta}^2\sin(\alpha-\theta)+(1-a)\omega_1^2\frac{u_y}{R}z(t)\Big\} \\ =-\frac{g}{R}\Big[(\sigma+1)\frac{\ddot{u}_g}{g}\cos(\alpha-\theta)+\sin(\alpha-\theta)\Big], \tag{2.11}$$

where $\omega_1 = \sqrt{k_1/m_s}$ = the pre-yielding undamped frequency and $\xi = \frac{c}{2m_s\omega_1^2}$ = the pre-yielding viscous damping ratio of the SDOF oscillator. Equation 2.11 is the equation of motion for positive rotations of the coupled system shown in Figure 2-1.

Case 2: $\theta < 0$

For negative rotations one can follow the same reasoning and the equation of the coupled system shown in Figure 2.1 is:

$$\Big(\frac{4}{3}+\sigma\cos^2(\alpha+\theta)\Big)\ddot{\theta}-\sigma\cos(\alpha+\theta)\Big\{a\omega_1^2\big(\sin\alpha-sin(\alpha+\theta)\big) \\ -2\xi\omega_1\dot{\theta}\cos(\alpha+\theta)+\dot{\theta}^2\sin(\alpha+\theta)-(1-a)\omega_1^2\frac{u_y}{R}z(t)\Big\} \\ =\frac{g}{R}\Big[-(\sigma+1)\frac{\ddot{u}_g}{g}\cos(\alpha+\theta)+\sin(\alpha+\theta)\Big] \tag{2.12}$$

When parameter $a = 1$, the expressions offered by equations 2.11 and 2.12 describe an elastic SDOF oscillator coupled with a stepping rocking wall, and they collapse to the equations of motion presented by Makris and Aghagholizadeh (2017a). In equations 2.11 and 2.12 the terms multiplied with the parameter $\sigma = m_s/m_w$ are associated with the dynamics of the yielding SDOF oscillator, whereas the remaining terms are associated with the dynamics of the rocking wall. When the SDOF oscillator is absent ($\sigma = \omega_1 = \xi = 0$), equations 2.11 and 2.12 reduce to the equations of motion of the free-standing rocking wall (Makris and Roussos 1998, 2000; J. Zhang and Makris 2001; Makris and Black 2002) since the frequency parameter *p* for rectangular walls is $p = \sqrt{3g/4R}$.

During the oscillatory motion of the coupled system shown in Figure 2-1, aside from the energy that is dissipated from the inelastic behavior of the SDOF oscillator and the idealized viscous damping, additional energy is also lost during impact when the angle of rotation reverses. At this instant it is assumed that the rotation of the rocking wall continues smoothly from points *O* to O'; nevertheless, the angular velocity, $\dot{\theta}_2$, after the impact is smaller than the angular velocity, $\dot{\theta}_1$, before the impact. Given that the energy loss during impact is a function of the wall-foundation interface, the coefficient of restitution, $e = \dot{\theta}_2/\dot{\theta}_1$, is introduced as a parameter of the problem. In this study the coefficient of restitution assumes the value of $e=0.9$. The integration of the equations of motion 2.11 and 2.12 together with equation 2.7 is performed via a state-space formulation. The state vector of the system is

$$\{y(t)\} = \begin{Bmatrix} y_1(t) \\ y_2(t) \\ y_3(t) \end{Bmatrix} = \begin{Bmatrix} \theta(t) \\ \dot{\theta}(t) \\ z(t) \end{Bmatrix} \tag{2.13}$$

and the time derivatives of the state vector, $\{\dot{y}(t)\}$ can be expressed solely in terms of the state variables, $y_1(t)$, $y_2(t)$ and $y_3(t)$. For instance, for positive rotations $(\theta > 0)$ the time derivative vector, $\{\dot{y}(t)\}$ is given by:

$$\{\dot{y}\} = \begin{Bmatrix} y_2 \\ \dfrac{\sigma\cos(\alpha - y_1)}{4/3 + \sigma\cos^2(\alpha - y_1)}\Big[a\omega_1^2\big(\sin\alpha - \sin(\alpha - y_1)\big) + 2\xi\omega_1 y_2\cos(\alpha - y_1) + y_2^2\sin(\alpha - y_1) \\ +(1-a)\omega_1^2\dfrac{u_y}{R}y_3\Big] - \dfrac{g}{R\left[4/3 + \sigma\cos^2(\alpha - y_1)\right]}\left[(\sigma+1)\dfrac{\ddot{u}_g}{g}\cos(\alpha - y_1) + \sin(\alpha - y_1)\right] \\ \dfrac{1}{u_y}\left[Ry_2\cos(\alpha - y_1) - \beta Ry_2\cos(\alpha - y_1)|y_3|^n - \gamma|Ry_2\cos(\alpha - y_1)|y_3|y_3|^{n-1}\right] \end{Bmatrix} \tag{2.14}$$

The numerical integration of the time-derivative state vector, $\{\dot{y}(t)\}$, is performed with standard ordinary differential equations (ODE) solvers available in MATLAB[1]. Upon the rotation, θ, and rotational velocity, $\dot{\theta}$, are computed; the relative displacement, *u* and velocity $\dot{u}$ of the mass m_s are offered by equations 2.2 and 2.3. Rocking of the stepping wall initiates when the ground acceleration exceeds the threshold (Makris and Aghagholizadeh 2017a; Aghagholizadeh 2018):

$$\ddot{u}_g^{up} = \frac{1}{\sigma+1} g\tan(\alpha) \tag{2.15}$$

[1] MATLAB. (2021). High performance numerical computation and visualization software. The Math works, Natick, Mass.

2.3 DYNAMICS OF A YIELDING OSCILLATOR COUPLED WITH A PINNED ROCKING WALL

Wada et al. (2011) and Que et al. (2012) proposed a pinned rocking wall for the seismic protection of an 11-story building. The novelty in the Wada at al. (2011), and Qu et al. (2012) studies is that the rocking wall does not alternate pivot points (it is not a stepping wall) given that it is pinned at mid-width as shown in Figure 2-2.

A detail of the specially designed pin bearing is presented in the Wada at al. (2011), and Qu et al. (2012) studies. Given that this configuration has been adopted by other investigators (C. E. Grigorian and Grigorian 2015; M. Grigorian and Grigorian 2016), in this section the dynamics of a yielding SDOF structure with mass, m_s, pre-yielding stiffness, k_1, post-yielding stiffness, k_2, strength, O, yielding displacement, u_y and damping c, that is coupled with pinned wall of size $R = \sqrt{b^2 + h^2}$, slenderness, $\tan\alpha = b/h$, mass, m_w and moment of inertia about the pin O, $I = m_w R^2(1/3 + \cos^2\alpha)$ is examined. As in the previous case (stepping rocking wall) the authors assume that the coupling arm is articulated at the center of mass of the rocking wall at the height of $h = R\cos\alpha$ from the pin bearing as shown in Figure 2.2; whereas the coupling arm is assumed long enough so that $v^2/L^2 \ll 1$; and in this case, $x=u$.

The system shown in Figure 2-2 is a SDOF system where the lateral translation of the mass, u is related to the rotation of the pinned rocking wall,θ via the

$$u = h\sin\theta \tag{2.16}$$

The time derivatives of equation 2.16 are:

$$\dot{u} = h\dot{\theta}\cos\theta \tag{2.17}$$

$$\ddot{u} = h\ddot{\theta}\cos\theta - h\dot{\theta}^2\sin\theta \tag{2.18}$$

Dynamic equilibrium of the mass m_s is given by equation 2.5, where, T, is again the axial force in the coupling arm. In this case, the rocking wall does not alternate pivot points so the same equation of motion for the pinned rocking wall holds for both positive and negative rotations:

$$I\ddot{\theta} = -Th\cos\theta + m_w gh\sin\theta - m_w\ddot{u}_g h\cos\theta \tag{2.19}$$

Note that in equation 2.19 the moment from the weight of the wall $(+m_w gh\sin\theta)$ works against stability, whereas the equivalent term in equation 2.8 for the stepping wall $(-m_w gR\sin(\alpha-\theta))$ works towards stability = recentering.

The axial force T appearing in equation 2.19 is replaced with the help of equation 2.5 and for a rectangular wall pinned at the mid-span of its base $I = m_w R^2(1/3+\cos^2\alpha))$, equation 2.19 assumes the form:

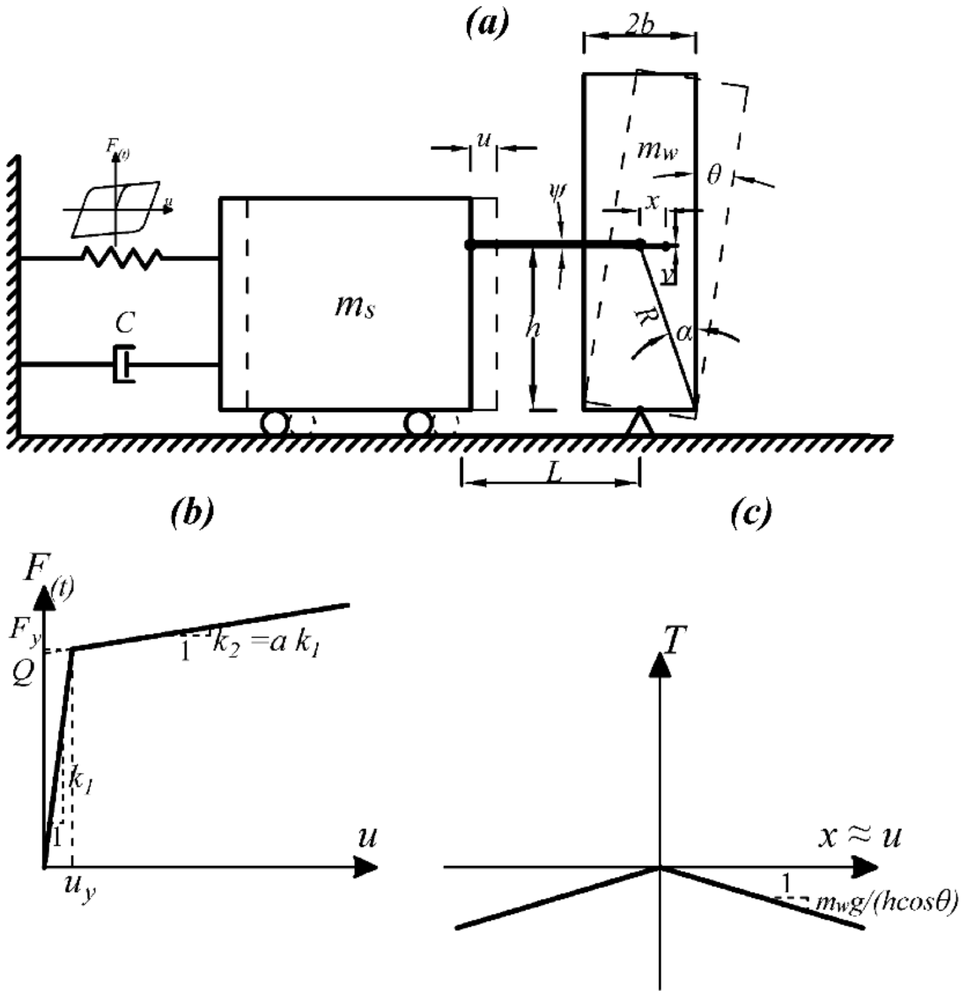

Figure 2-2 (a): Yielding single-degree-of-freedom oscillator coupled with a pinned rocking wall. While schematically the wall is shown to be connected in series with the mass, the dynamics of the wall works in parallel with the nonlinear spring and dashpot because of the rigid connection between the mass and the wall. (b): The bilinear idealization with its control parameters. (c): Force-displacement diagram of the pinned rocking wall.

$$m_w R^2\left(\frac{1}{3}+\cos^2\alpha\right)\ddot{\theta}+\left[m_s(\ddot{u}+\ddot{u}_g)+ak_1u+(1-a)k_1u_yz(t)+c\dot{u}\right]h\cos\theta = -m_w\ddot{u}_g h\cos\theta+m_w gh\sin\theta \tag{2.20}$$

Using that $h = R\cos\alpha$, and upon dividing with $m_w R$, equation 2.20 gives:

$$R\left(\frac{1}{3}+\cos^2\alpha\right)\ddot{\theta}+\left[\sigma(\ddot{u}+\ddot{u}_g)+a\sigma\frac{k_1}{m_s}u+(1-a)\sigma\frac{k_1}{m_s}u_yz(t)+\sigma\frac{c}{m_s}\dot{u}\right]\cos\alpha\cos\theta = -\ddot{u}_g\cos\alpha\cos\theta+g\cos\alpha\sin\theta \tag{2.21}$$

in which $\sigma = m_s / m_w$ as in the case of the stepping wall.

Substitution of the expression of the relative displacement, velocity and acceleration given by equations 2.16 to 2.18 and after dividing with R, equation 2.21 gives:

$$\Big[\frac{1}{3}+(1+\sigma\cos^2\theta)\cos^2\alpha\Big]\ddot{\theta}+\sigma\cos^2\alpha\cos\theta\Big[(a\omega_1^2-\dot{\theta}^2)\sin\theta+(1-a)\omega_1^2\frac{u_y}{R\cos\alpha}z(t)$$
$$+2\xi\omega_1\dot{\theta}\cos\theta\Big]=-\frac{g}{R}\cos\alpha\Big[(\sigma+1)\frac{\ddot{u}_g}{g}\cos\theta-\sin\theta\Big], \tag{2.22}$$

Where $\omega_1=\sqrt{k_1/m_s}$ = the pre-yielding undamped frequency and $\xi=\frac{c}{2m_s\omega_1}$ = the viscous damping ratio of the SDOF oscillator (as in the previous case). Equation 2.22 is the equation of motion for both positive and negative rotations of the coupled system shown in Figure 2-2. Again, the state variables of the system are given by equation 2.13 and the solution is performed with standard ODE solver as described in the case of the stepping wall.

2.4 PARAMETERS OF THE PROBLEM

The Bouc-Wen model described by equations 2.6 and 2.7 is a phenomenological model of hysteresis originally proposed by Bouc (1967) and subsequently generalized by Wen (1975, 1976) and Baber and Wen (1981). It is a versatile model that can capture various details of the nonlinear force-displacement loop. Subsequent studies on the modeling of yielding systems by Constantinou and Adnane (1987) concluded that when certain constraints are imposed on the parameters β and γ (β + γ = 1), the model reduces to a viscoplastic element with well-defined physical characteristics. The Bouc – Wen model essentially builds on the bilinear idealization shown in the bottom-left of Figure 2-1 and Figure 2-2. For the five-parameter system shown with the bilinear idealization. (k_1= pre-yielding stiffness, k_2= post-yielding stiffness, u_y= yield displacement, Q= strength and F_y= yielding force), only three parameters are needed to fully describe the bilinear behavior (see for instance (Makris and Kampas 2013)). In this work, the authors select the pre-yielding stiffness $k_1 = m_s\omega_1^2$, the post-yielding stiffness $k_2 = ak_1$ and the strength of the structure Q. With reference to Figure 2-1 and Figure 2-2 (bottom-left), $F_y = k_1u_y = Q + k_2u_y$ .Accordingly, $u_y = Q/(k_1-k_2)$ and $F_y = k_1Q/(k_1-k_2)$. The parameters β, γ and n appearing in equation 2.7 are established from past studies on the parameter identification of yielding concrete structures and assume the values: β = 0.95, γ = 0.05 and n = 2 ((Kunnath et al. 1997; Goda et al. 2009) among others). With the parameters β = 0.95, γ = 0.05 and n = 2 being established, the peak inelastic displacement, u_{max} of the SDOF system shown in Figure 2-1 and Figure 2-2 is a function of the following parameters:

$$u_{max} = f\Big(\omega_1, \frac{Q}{m_s}, a, \xi, p, \tan\alpha, \sigma, g, \textit{parameters of excitation}\Big) \tag{2.23}$$

In this study, it is assumed that upon yielding, the structure maintains a mild, positive, post-yielding stiffness $= k_2 = 0.05k_1$, therefore $a = 0.05$ (Kunnath et al. 1997; Goda et al. 2009). Furthermore, it is assumed that the pre-yielding damping ratio, $\xi = c/(2m_s\omega_1) = 0.03$ and the authors focus on rocking walls with slenderness, $\tan\alpha = 1/6$. Before proceeding with earthquake response spectra, Figure 2-3 plots force displacement loops, together with displacement, *u(t)* and rotation, θ(t), time histories with a structure having, $T_1 = 0.8s$, $Q/m_s = 0.15g$ which is coupled with a rocking wall with $\omega_1/p = 10$, ($p = 0.778 rad/sec$) and $\sigma = m_s/m_w = 10$ when excited by the Pacoima Dam/164 ground motion recorded during the 1971 San Fernando, California earthquake. The heavy line is when the structure is coupled with the wall, whereas the thin line is when there is no wall ($\sigma = \infty$).

Assuming the bilinear idealization shown at the bottom-left if Figure 2-1 and Figure 2-2, for a given value of pre-yielding period, T_1, normalized strength, $Q/m_s g$ and pre-to-post yielding stiffness ratio, *a=0.05*, the yield displacement is uniquely defined.

$$u_y = \frac{Q}{k_1(1-a)} = \frac{Q}{m_s}\frac{T_1^2}{4\pi^2(1-a)} \tag{2.24}$$

Figure 2-3 (left) indicates that the participation of the stepping rocking wall (even with appreciable size and weight, *p=0.778 rad/sec*, σ=10) has a marginal effect in the suppressing peak inelastic displacement and the only clear benefit is in reducing permanent displacements.

Figure 2-3 (right) plots the corresponding response qualities described in Figure 2-3 (left) for the case where the yielding structure is coupled with a pinned rocking wall. While Figure 2-3 (left) indicates that the stepping rocking wall slightly suppresses the peak response; Figure 2-3 (right) indicates that the pinned rocking wall slightly amplifies the peak response of the structure.

In this case, the pinned rocking wall is also responsible for further increasing the permanent displacements of the inelastic structure, nevertheless, this finding is not uniform along the entire period spectrum of the frame-structures.

Figure 2-4 and Figure 2-5 reveal similar trends than those discussed for the results of Figure 2-3 when the inelastic structural system is subjected to the Takarazuka/000 ground motion recorded during the 1995 Kobe, Japan earthquake (Figure 2-4) and to the Erzincan NS ground motion recorded during the 1992 Erzincan, Turkey earthquake (Figure 2-5).

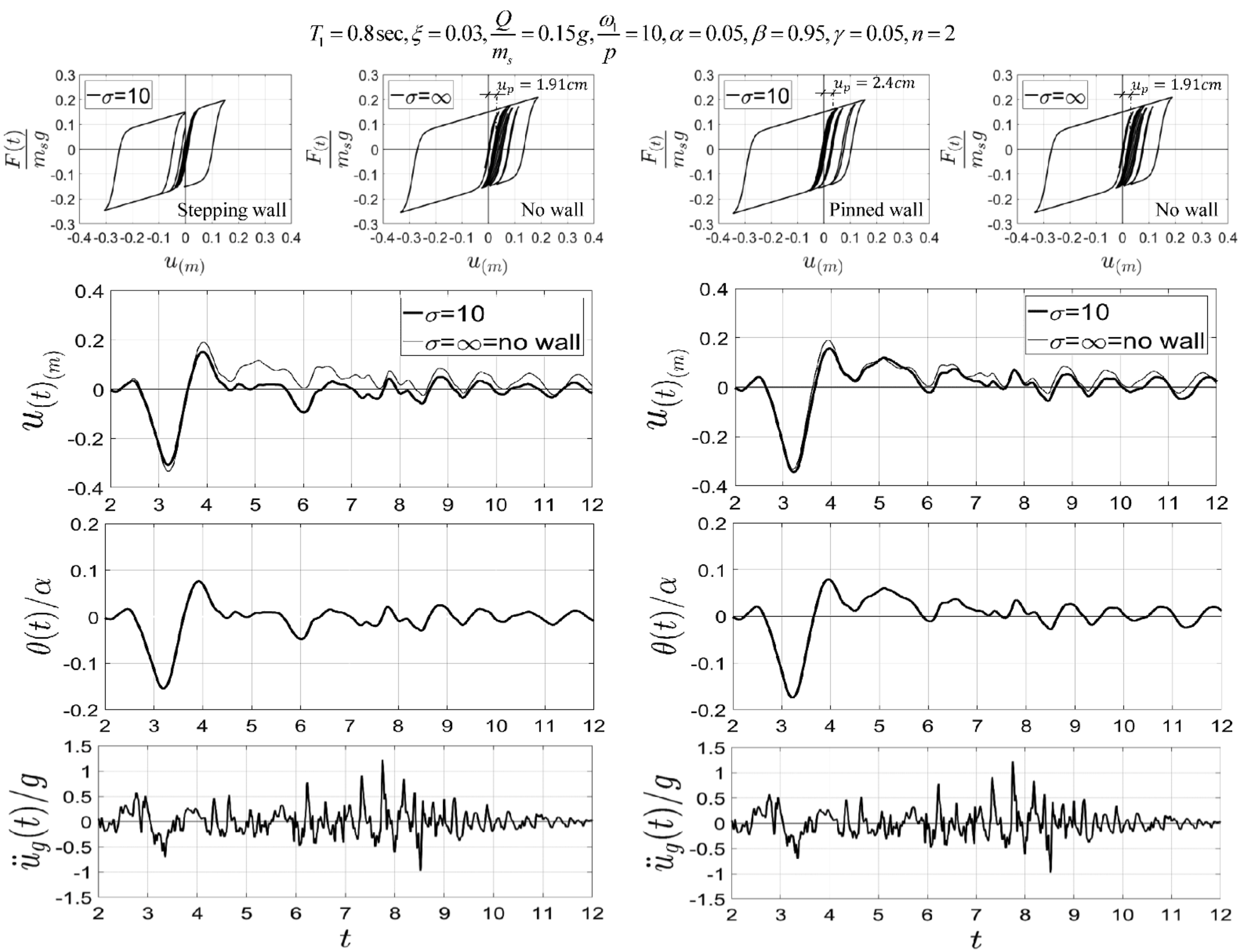

Figure 2-3 Time history analysis of a nonlinear SDOF oscillator coupled with a stepping rocking wall with normalized strength Q/ms = 0:15g, mass ratio, σ= ms/mw = 10, wall size, ω_1/p= 10, and pre-yielding period of T_1 =0.8sec, when subjected to the Pacoima Dam/164 ground motion recorded during the 1971 San Fernando, California earthquake (bottom)

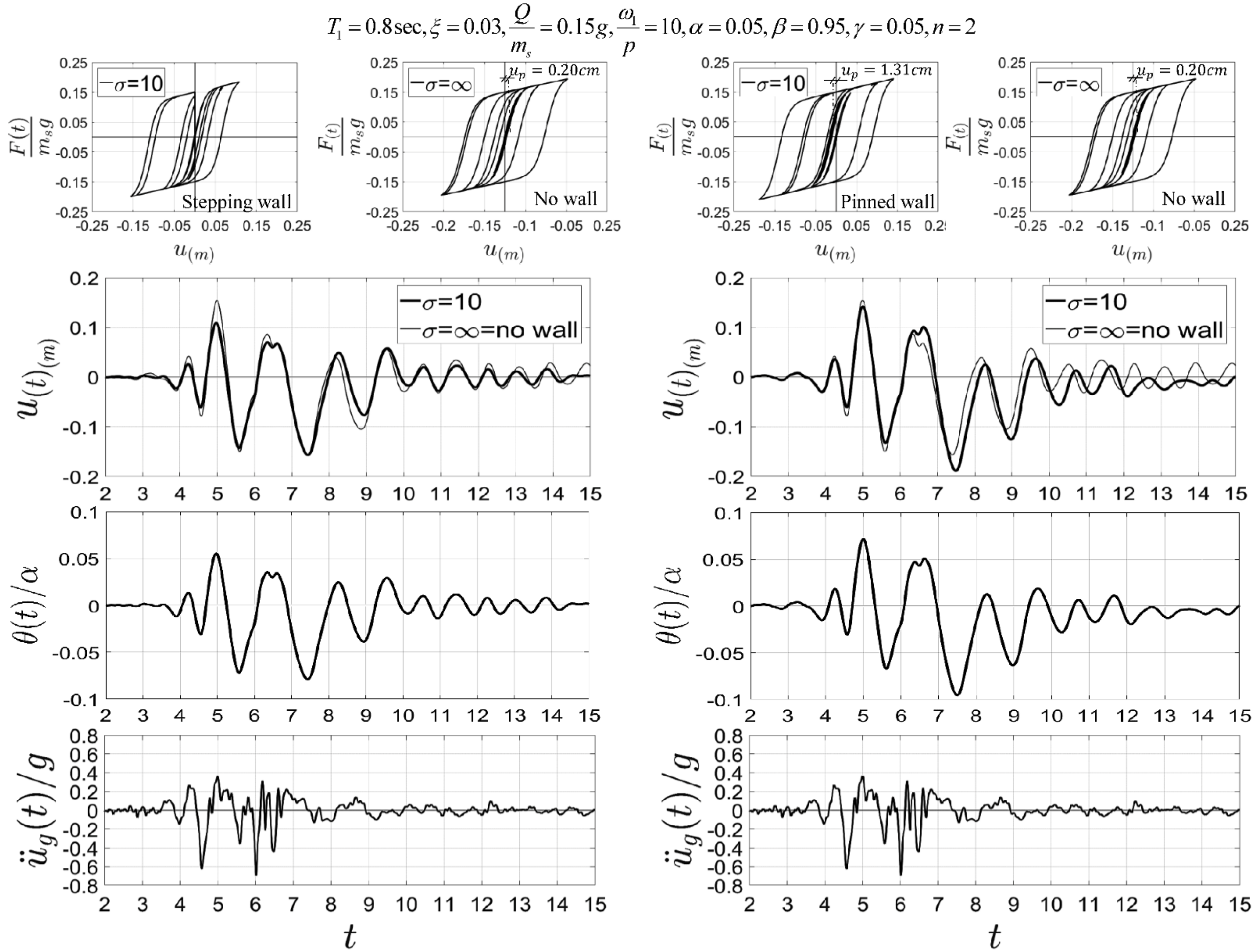

Figure 2-4 Time history analysis of a nonlinear SDOF oscillator coupled with a stepping rocking wall with normalized strength Q/ms = 0:15g, mass ratio, σ= ms/mw = 10, wall size, ω_1/p= 10, and pre-yielding period of T_1 =0.8sec, when subjected to the Takarazuka/000 ground motion recorded during the 1995 Kobe, Japan earthquake (bottom).

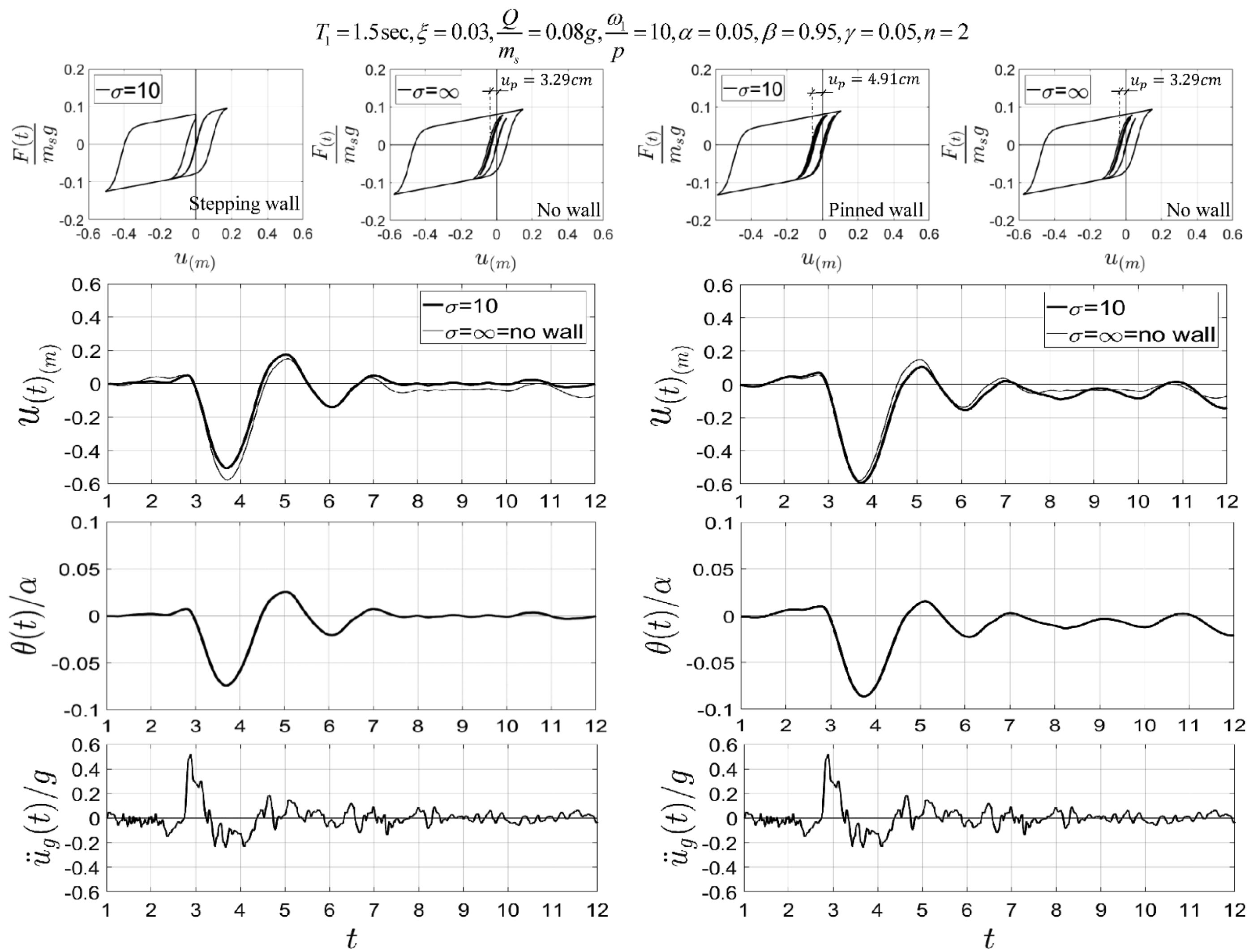

Figure 2-5 Time history analysis of a nonlinear SDOF oscillator coupled with a stepping rocking wall with normalized strength $Q/ms = 0{:}08g$, mass ratio, $\sigma = ms/mw = 10$, wall size, $\omega_1/p = 10$, and pre-yielding period of $T_1 = 1.5sec$, when subjected to the Erzincan NS ground motion recorded during the 1992 Erzincan, Turkey earthquake (bottom)

2.5 VALIDATION OF THE SDOF-IDEALIZATION

In view of small differences between the peak response of a yielding structure coupled with a rocking wall (either stepping or pinned) and the nonlinear response of the solitary yielding structure (other than the reduction of permanent displacements) even for the strong excitations shown in Figures 2.3, 2.4 and 2.5, the dependability of the single-degree-of-freedom idealization shown in Figures 2.1 and 2.2 is examined against the results obtained with the open-source code OpenSees (McKenna et al. 2000) when analyzing the two-bay, four-story frame shown in Figures 2.6 and 2.7 (top-left: (a)). Given that in the SDOF-models shown in Figures 2.1 and 2.2, the coupling arm is connected at the center of mass off the rocking wall, in Figures 2.6 and 2.7 (top-left: (a)), the coupling arms emanating from each story are connected along the center line of the rocking wall.

For the stepping rocking wall shown in Figure 2-6, the mechanical properties of the rocking interface are approximated with a rigid-elastic rotational spring together with a rotational viscous dashpot (Vassiliou et al. 2014) to approximate the energy loss during impact as the rocking wall alternate pivot-points. For a free-standing stepping rocking wall with size R, slenderness,α, and mass m_w, dimensional analysis yields that the expression of the equivalent rotational dashpot is (Vassiliou et al. 2014):

$$c = \lambda \alpha^2 m_w g^{0.5} R^{1.5} \tag{2.25}$$

Where $\lambda = 110$, is a parameter that is calibrated from best fit of the results.

Figure 2-6 (right: (c), (d)) plots response time histories of the second story displacement of a four-story yielding frame with elastic period, $T_1 = 0.5$ s and first modal damping ratio $\xi = 0.03$, when coupled with a stepping rocking wall with $p = 0.952\ \mathrm{rad/sec}$, $(\omega_1/p = 13.2)$ shown in Figure 2.6 (top-left: (a)) when subjected to the 1971 Pacoima Dam/164 ground motion shown at the bottom of Figure 2-3, and the 1995 Takarazuka/000 ground motion shown at the bottom of Figure 2-4.

The response of the nonlinear SDOF idealization shown in Figure 2-1 is in good agreement with the numerical solution from OpenSees for the four-story yielding frame. This favorable comparison validates the SDOF idealization adopted in this study. For any given yielding frame, the parameters of the SDOF model, $k_1 = 4\pi^2 m_s / T_1^2$, Q / m_s and $a = k_1 / k_2$ need to be calibrated to match the push-over curve of the yielding frame as is shown in Figure 2-6 (bottom-left: (b)).

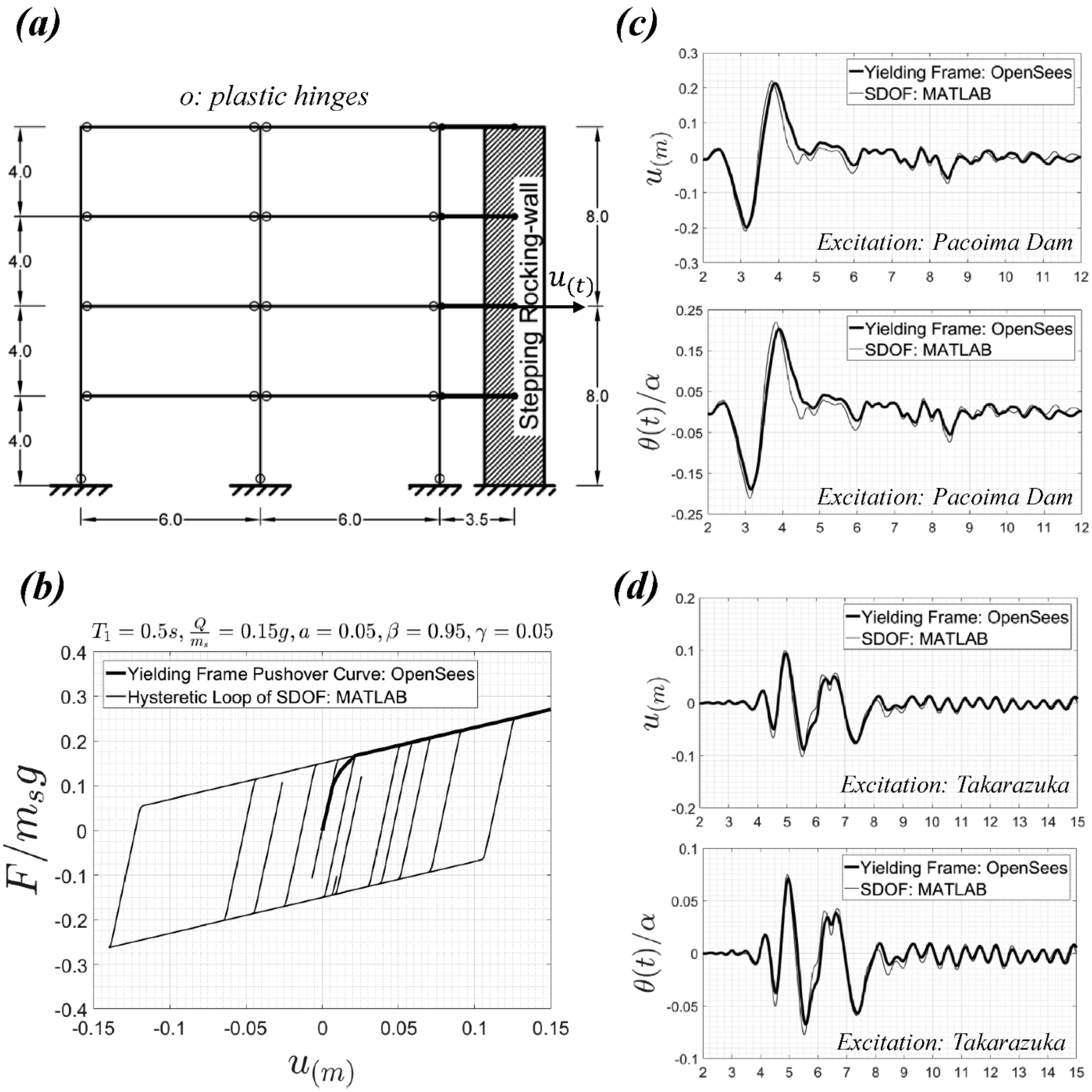

Figure 2-6 (a): Four-story, two-bay yielding frame, with pre-yielding period $\mathbf{T_1 = 0.5}$ **sec coupled with a stepping rocking wall with** $\mathbf{p = 0.952\ rad/sec}$, $\boldsymbol{\omega_1/p = 13.2}$, **and** $\boldsymbol{\sigma = m_s/m_w = 5}$, **(b): pushover curve for frame compared to hysteretic loop of SDOF idealization, response comparison when subjected to the 1971 Pacoima Dam/164 ground motion (c) and the 1995 Takarazuka/000 ground motion (d). Heavy solid lines: OpenSees solution; thin lines: MATLAB solution of the SDOF response.**

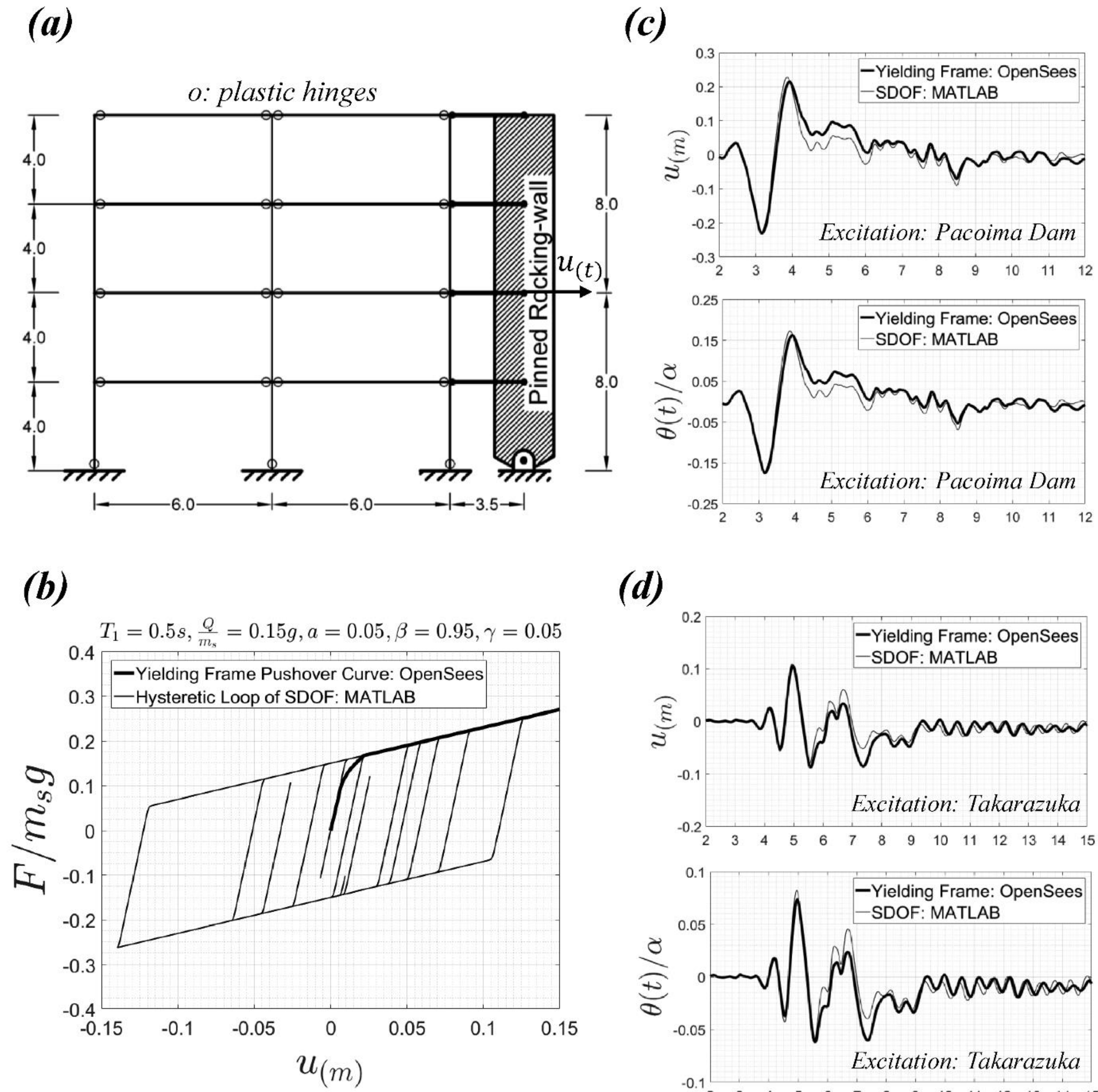

Figure 2-7 (a): Four-story, two-bay yielding frame, with pre-yielding period $T_1 = 0.5$ sec coupled with a pinned rocking wall with $p = 0.952$ rad/sec, $\omega_1/p = 13.2$, and $\sigma = m_s/m_w = 5$, (b): pushover curve for frame compared to hysteretic loop of SDOF idealization, response comparison when subjected to the 1971 Pacoima Dam/164 ground motion (c) and the 1995 Takarazuka/000 ground motion (d). Heavy solid lines: OpenSees solution; thin lines: MATLAB solution of the SDOF response.

Figure 2-7 (right: (c), (d)) plots response time histories of the second story displacement of a four-story yielding frame with elastic period, $T_1 = 0.5$ s and first modal damping ratio $\xi = 0.03$, when coupled with a stepping rocking wall with $p = 0.952$ rad/sec, ($\omega_1/p = 13.2$) shown in Figure

2-7 (top-left: (a)) when subjected to the 1971 Pacoima Dam/164 ground motion shown at the bottom of Figure 2-3 and the 1995 Takarazuka/000 ground motion shown at the bottom of Figure 2-4.

The response of the nonlinear SDOF idealization shown in Figure 2-2 is in good agreement with the numerical solution from OpenSees for the four-story yielding frame. This favorable comparison validates the SDOF idealization adopted in this study. For any given yielding frame, the parameters of the SDOF model, $k_1 = 4\pi^2 m_s / T_1^2$, Q / m_s and $a = k_1 / k_2$ need to be calibrated to match the push-over curve of the yielding frame as is shown in Figure 2-7 (bottom-left: (b)).

2.6 EARTHQUAKE SPECTRA OF A YIELDING OSCILLATOR COUPLED WITH A ROCKING WALL

Following the validation of the single-degree-of-freedom idealization adopted in this study; the equations of motion 2.11 and 2.12 for a structure coupled with a stepping wall, together with equation 2.22 for a structure coupled with a pinned wall are used to generate inelastic earthquake response spectra.

Figure 2-8 plots displacement spectra for the SDOF yielding oscillator coupled with a stepping wall (left) and a pinned wall (right) when excited by the Pacoima Dam/164 ground motion recorded during the 1971 San Fernando, California earthquake. The top plots are for $Q / m_s = 0.15g$; whereas the bottom plots are for a less strong structure with $Q / m_s = 0.08g$. The first observation is that the coupling of a yielding frame with a rocking wall has a limited effect on the peak inelastic deformation. A stepping rocking wall (left, plots in Figure 2-8) reduces the peak inelastic deformations with the heavier wall $(\sigma = 5)$ being more effective; whereas a pinned rocking wall amplifies the inelastic deformations which are accentuated with a heavier wall $(\sigma = 5)$. Stepping rocking walls are effective in reducing or even eliminating permanent displacements (see plots (b) and (f)). When a heavy stepping wall is used permanent displacements are eliminated. In contrast, when a pinned rocking wall is used permanent displacements are in generally larger, with the heavier wall being most detrimental in particular for long-period structures (see plots (d) and (h)).

Figure 2-9 to Figure 2-11 reveal the same trends than those discussed for the spectra appearing in Figure 2-8 when the yielding SDOF oscillator with the same parameters as those shown in Figure 2-8 is subjected to the Takarazuka/000 ground motion recorded during 1995 Kobe, Japan earthquake (Figure 2-9), to the Erzincan NS record from 1992 Erzincan, Turkey (Figure 2-10) and to Newhall/360 ground motion recorded during the 1994 Northridge, California (Figure 2-11) earthquakes.

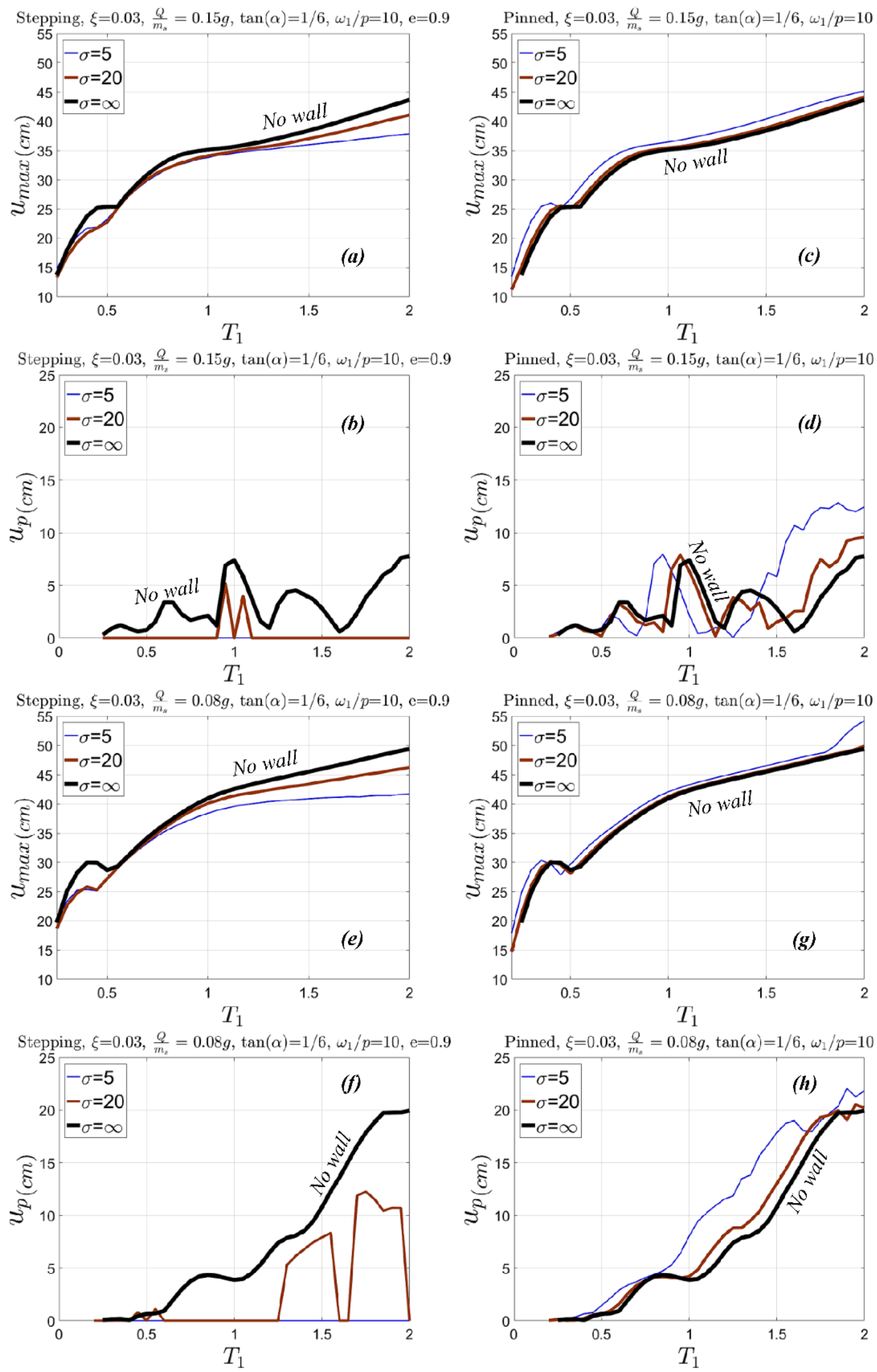

Figure 2-8 Peak displacement (a, c, e, g) and residual displacement (b, d, f, h) spectra of a yielding SDOF oscillator coupled with a stepping wall (a, b, e, f) and pinned wall (c, d, g, h) for two values of the strength, $Q/m_s = 0.15g$ (a, b, c, d) and $Q/m_s = 0.08g$ (e, f, g, h) with, mass ratio, $\sigma = m_s/m_w = 5$ and 20 and wall size, $\omega_1\,/p = 10$, when subjected to the Pacoima Dam/164 ground motion recorded during the 1971 San Fernando, California earthquake.

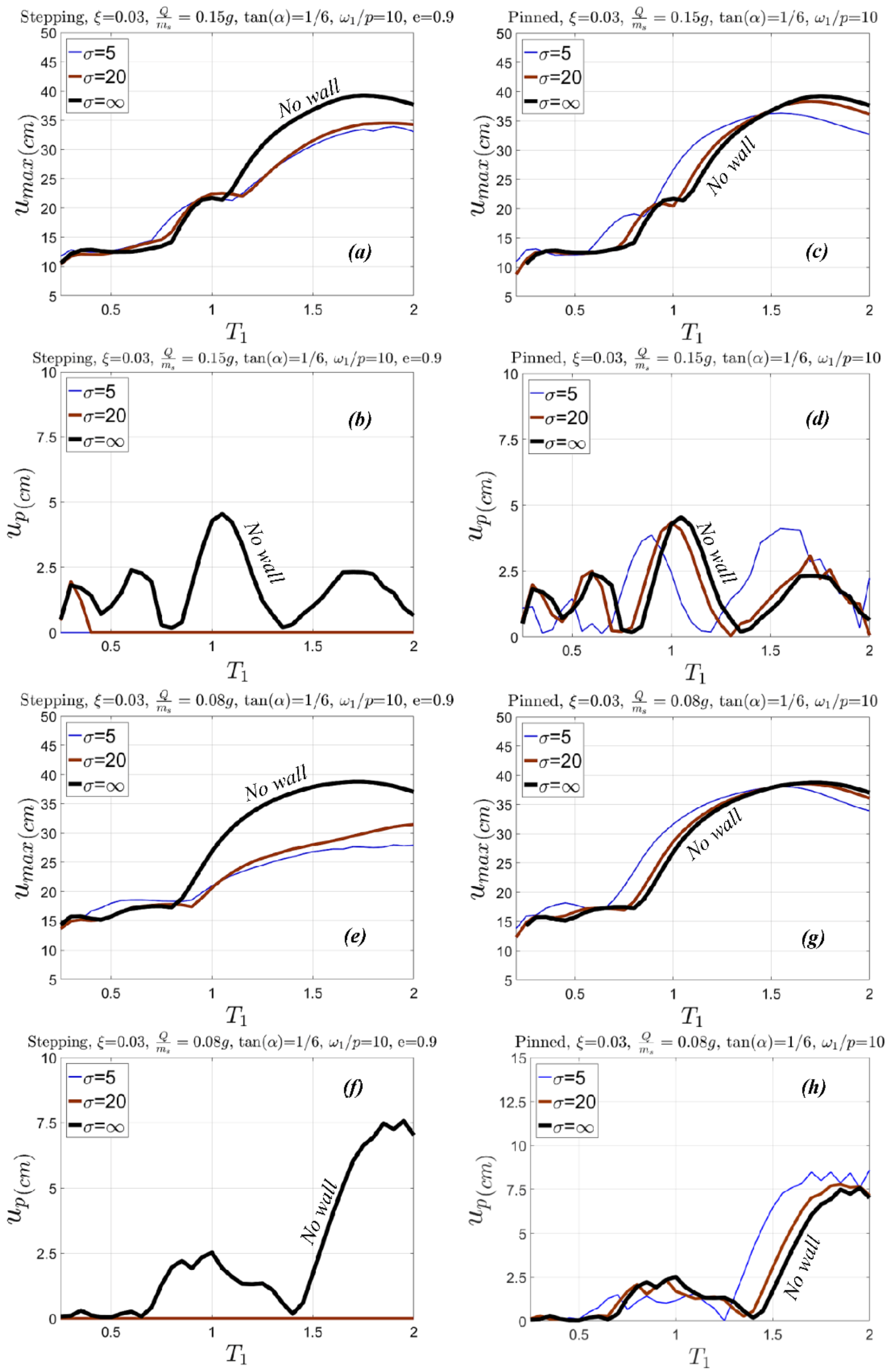

Figure 2-9 Peak displacement (a, c, e, g) and residual displacement (b, d, f, h) spectra of a yielding SDOF oscillator coupled with a stepping wall (a, b, e, f) and pinned wall (c, d, g, h) for two values of the strength, $Q/m_s = 0.15g$ (a, b, c, d) and $Q/m_s = 0.08g$ (e, f, g, h) with, mass ratio, $\sigma = m_s/m_w = 5$ and 20 and wall size, $\omega_1/p = 10$, when subjected to the Takarazuka/000 ground motion recorded during the 1995 Kobe, Japan earthquake.

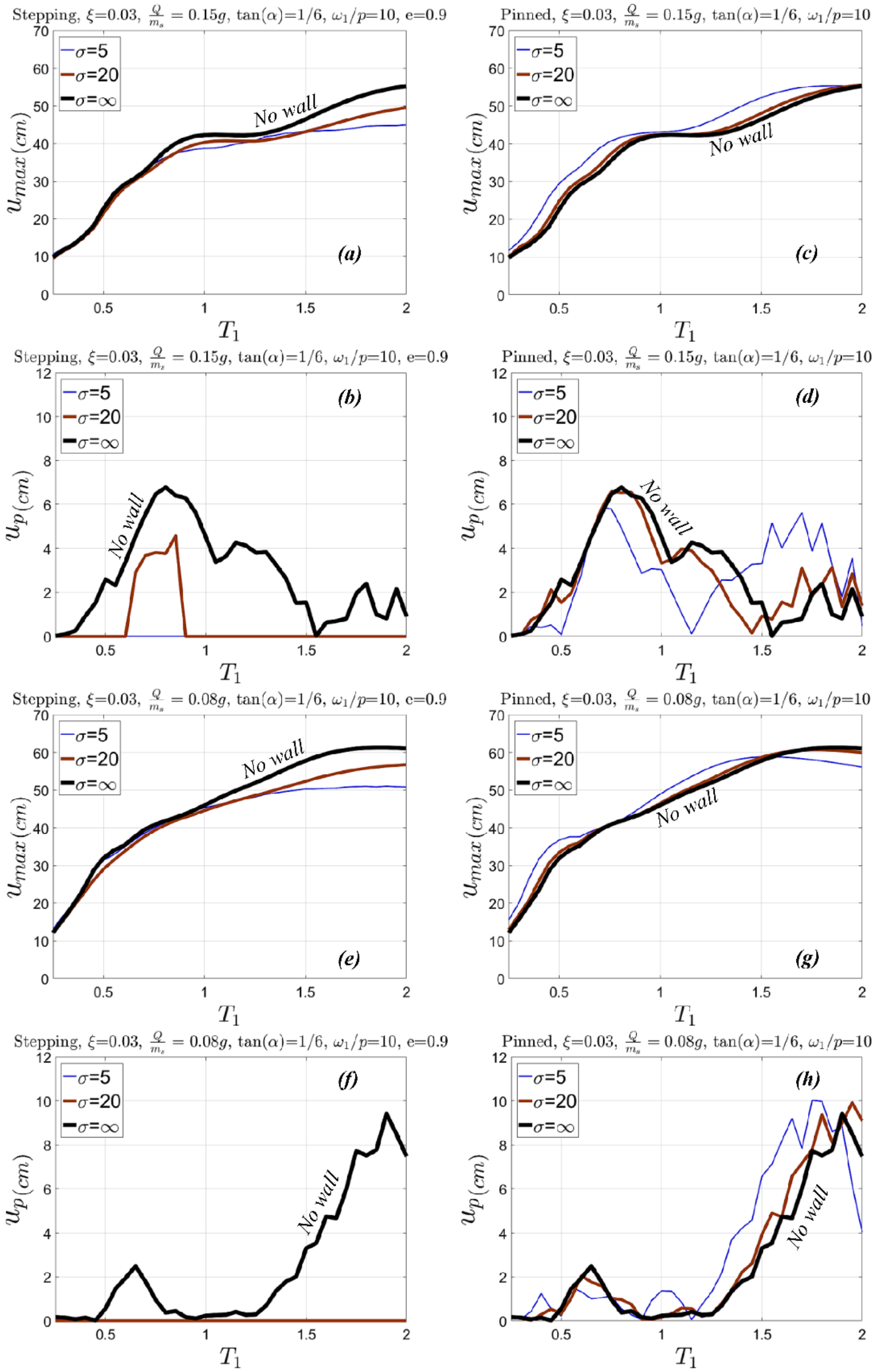

Figure 2-10 Peak displacement (a, c, e, g) and residual displacement (b, d, f, h) spectra of a yielding SDOF oscillator coupled with a stepping wall (a, b, e, f) and pinned wall (c, d, g, h) for two values of the strength, $Q/m_s = 0.15g$ (a, b, c, d) and $Q/m_s = 0.08g$ (e, f, g, h) with, mass ratio, $\sigma = m_s/m_w = 5$ and 20 and wall size, $\omega_1\,/p = 10$, when subjected to the Erzincan NS ground motion recorded during the 1992 Erzincan, Turkey earthquake.

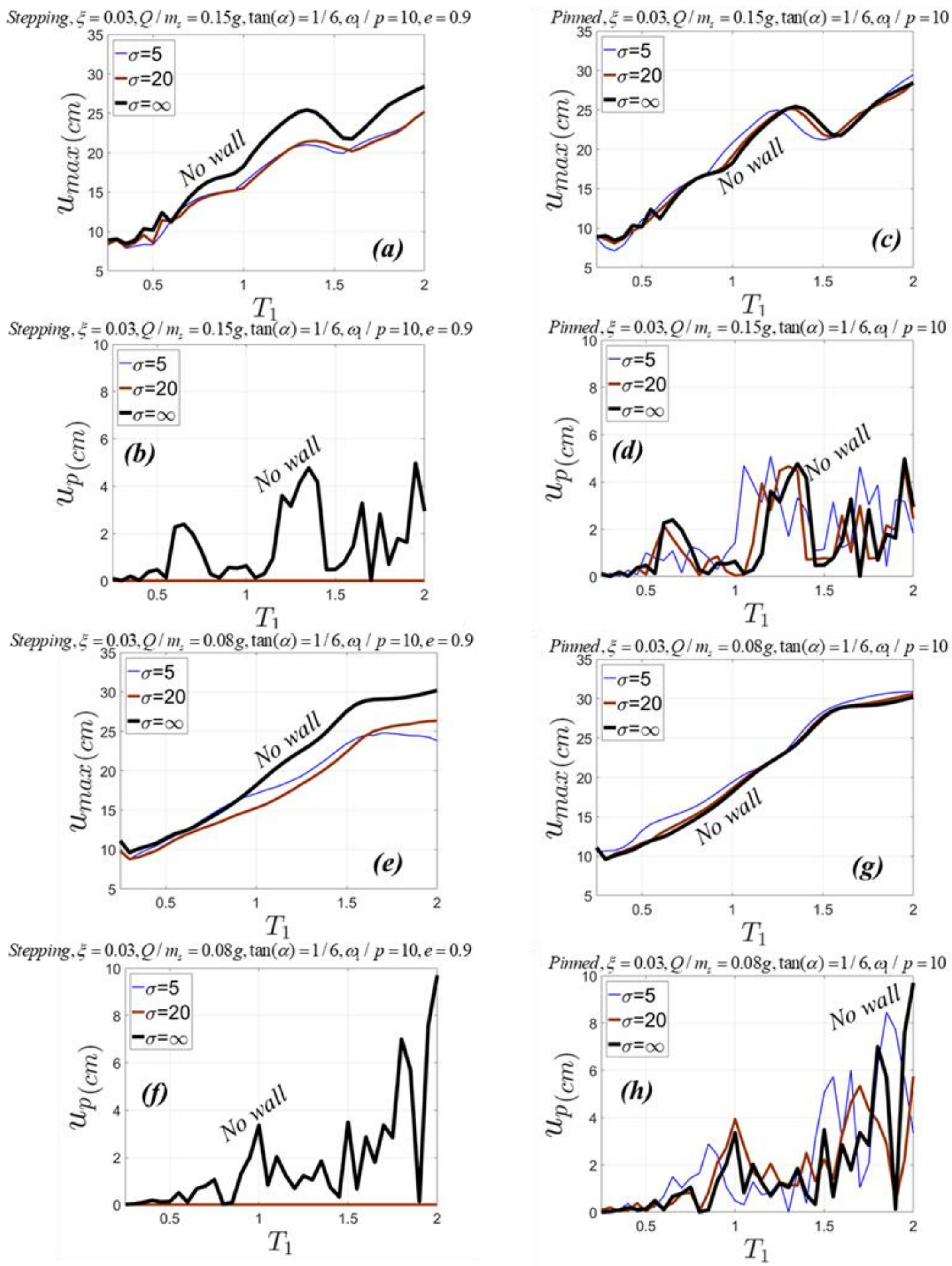

Figure 2-11 Peak displacement (a, c, e, g) and residual displacement (b, d, f, h) spectra of a yielding SDOF oscillator coupled with a stepping wall (a, b, e, f) and pinned wall (c, d, g, h) for two values of the strength, $Q/m_s = 0.15g$ (a, b, c, d) and $Q/m_s = 0.08g$ (e, f, g, h) with, mass ratio, $\sigma = m_s/m_w = 5$ and 20 and wall size, $\omega_1/p = 10$, when subjected to the Newhall/360 ground motion recorded during the 1994 Northridge, California earthquake.

2.7 IMPORTANCE OF THE LENGTH OF THE COUPLING ARMS

In the entire analysis of the study, it was assumed that the length of the coupling arm, L, appearing in Figure 2-1 and Figure 2-2 is sufficiently large so that the quantity v^2/L^2 is much smaller than unity ($v^2/L^2 \ll 1$); and in this case $u = x$. There are cases however where the rocking wall is close enough to the laterally translating structure and in this case the length of the coupling arm, L, becomes an additional parameter of the problem.

Stepping Rocking Wall

For short arm lengths, equation (2) that offers the lateral translation of the elastic oscillator, u as a function of the positive rotation θ of the rocking wall needs to be replaced with:

$$u = L + R\left[\sin\alpha - \sin(\alpha-\theta)\right] - L\sqrt{1 - \frac{R^2}{L^2}[\cos(\alpha-\theta)-\cos\alpha]^2} \tag{2.26}$$

While the last term with the radical in equation (2.26) complicates appreciably the expressions of its time derivatives as follows,

$$\dot{u} = R\dot{\theta}\left(\cos(\alpha-\theta) - \frac{R\sin(\alpha-\theta)[\cos\alpha-\cos(\alpha-\theta)]}{L\sqrt{1-\frac{R^2}{L^2}[\cos(\alpha-\theta)-\cos\alpha]^2}}\right) \tag{2.27}$$

$$\begin{aligned}\ddot{u} = R\dot{\theta}\Bigg\{ & \sin(\alpha-\theta) + \frac{R\cos(\alpha-\theta)[\cos\alpha-\cos(\alpha-\theta)] + R\sin^2(\alpha-\theta)}{L\sqrt{1-\frac{R^2}{L^2}[\cos(\alpha-\theta)-\cos\alpha]^2}} \\ & + \frac{R^3\sin^2(\alpha-\theta)[\cos\alpha-\cos(\alpha-\theta)]^2}{L^3\sqrt{\left(1-\frac{R^2}{L^2}[\cos(\alpha-\theta)-\cos\alpha]^2\right)^3}}\Bigg\} \\ & + R\ddot{\theta}\left\{\cos(\alpha-\theta) - \frac{R\sin(\alpha-\theta)[\cos\alpha-\cos(\alpha-\theta)]}{L\sqrt{1-\frac{R^2}{L^2}[\cos(\alpha-\theta)-\cos\alpha]^2}}\right\}\end{aligned} \tag{2.28}$$

Dynamic equilibrium of the SDOF oscillator shown in Figure 2-1 with a short length link is:

$$m_s(\ddot{u}+\ddot{u}_g) = -F_s - c\dot{u} + T\cos\psi \tag{2.29}$$

while dynamic equilibrium of the stepping rocking wall for $\theta > 0$ gives:

$$\begin{aligned} I\ddot{\theta} = & -(T\cos\psi)R\cos(\alpha-\theta) - (T\sin\psi)R\sin(\alpha-\theta) \\ & -m_w\ddot{u}_g R\cos(\alpha-\theta) - m_w gR\sin(\alpha-\theta) \end{aligned} \tag{2.30}$$

where

$$\sin\psi = \frac{R}{L}\left(\cos(\alpha-\theta) - \cos\alpha\right) \tag{2.31}$$

and $I = \frac{4}{3}m_w R^2$.

Substitution of equations 2.27 and 2.28 into equation 2.29 and after replacing the axial force T in equation 2.30 from 2.29 gives the equation of motion of the coupled SDOF system shown in Figure 2-1 for short coupling arms and $\theta > 0$.

Pinned Rocking Wall

For short arm lengths, equation 2.16 that offers the lateral translation of the elastic oscillator, u as a function of the rotation θ of the rocking wall needs to be replaced with:

$$u = L + h\sin\theta - L\sqrt{1-\frac{h^2}{L^2}(1-\cos\theta)^2} \tag{2.32}$$

Again, the last term with the radical in equation (33) complicates appreciably the expressions of its time derivatives. The time derivatives of the relative displacement offered by equation (2.32) are,

$$\dot{u} = h\dot{\theta}\left(\cos\theta + h\frac{(1-\cos\theta)\sin\theta}{L\sqrt{1-\frac{h^2}{L^2}(1-\cos\theta)^2}}\right) \tag{2.33}$$

$$\ddot{u} = h\ddot{\theta}\left(\cos\theta + h\frac{(1-\cos\theta)\sin\theta}{L\sqrt{1-\frac{h^2}{L^2}(1-\cos\theta)^2}} \right)$$

$$+h\dot{\theta}^2\left\{ -\sin\theta + h\frac{(1-\cos\theta)\sin\theta}{L\sqrt{1-\frac{h^2}{L^2}(1-\cos\theta)^2}} + hh\frac{\sin^2\theta}{L\sqrt{1-\frac{h^2}{L^2}(1-\cos\theta)^2}} \right. \tag{2.34}$$

$$\left. + \frac{h^3(1-\cos\theta)^2\sin^2\theta}{L^3\sqrt{\left(1-\frac{h^2}{L^2}(1-\cos\theta)^2\right)^3}} \right\}$$

Dynamic equilibrium of the SDOF oscillator shown in Figure 2-2 gives:

$$m_s(\ddot{u}+\ddot{u}_g) = -F_s + -c\dot{u} + T\cos\psi \tag{2.35}$$

while dynamic equilibrium of the pinned rocking wall gives:

$$I\ddot{\theta} = -(T\cos\psi)h\cos\theta - (T\sin\psi)h\sin\theta + m_w gh\sin\theta - m_w\ddot{u}_g h\cos\theta \tag{2.36}$$

where

$$\sin\psi = \frac{h}{L}(1-\cos\theta) \tag{2.37}$$

and $I = m_w R^2\left(\frac{1}{3} + \cos^2\alpha\right)$.

Substitution of equations 2.33 and 2.34 into equation (2.35) and after replacing the axial force T in equation 2.36 from 2.35, gives the equation of the motion for short coupling arms of the coupled SDOF system shown in Figure 2-2.

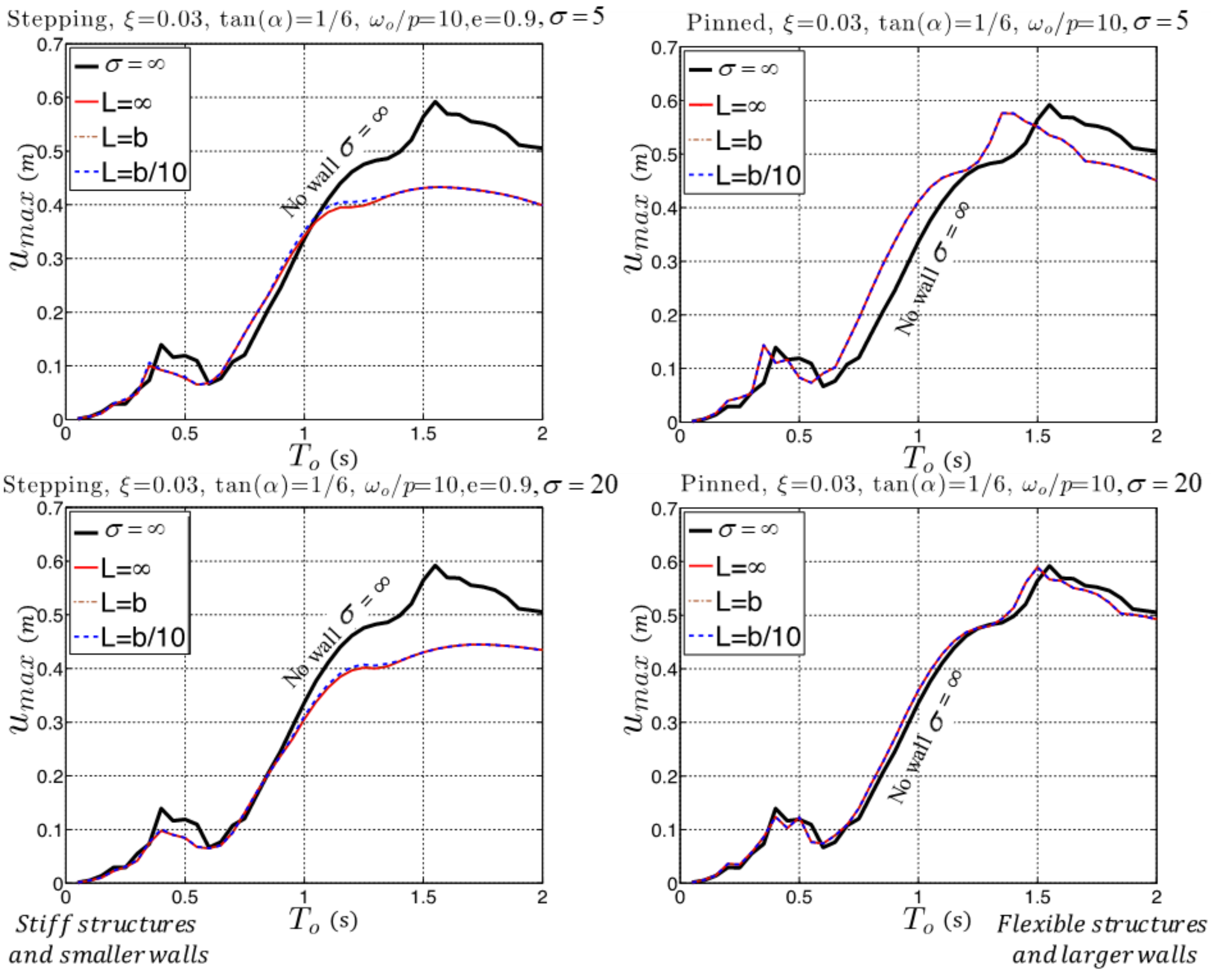

Figure 2-12 Displacement spectra of an elastic SDOF oscillator coupled with a stepping wall (left) and a pinned wall (right) with a short coupling arm for two values of the mass ratio $\boldsymbol{\sigma = m_s/m_w = 5}$ (top) and 20 (bottom) and the wall size, $\boldsymbol{\omega_o/p = 10}$ and three values of the length of the coupling arm, $\boldsymbol{L = \infty, b}$ and $\boldsymbol{b/10}$ when subjected to Pacoima Dam/164 ground motion recorded during the 1971 San Fernando, California earthquake

Figure 2-12 plots displacement spectra of the SDOF oscillator coupled with a stepping wall (left) and a pinned wall (right) with $\frac{\omega_o}{p} = 10$ and three values of the length of the coupling arm, $L = \infty, b$ and $b/10$,when excited by the Pacoima Dam/164 ground motion recorded during the 1971 San Fernando, California earthquake. The top plots are for $\sigma = m_s/m_w = 5$; whereas the bottom plots are for $\sigma = m_s/m_w = 20$ - that is for a lighter wall. The spectra shown on Figure 2-12 indicate that the length of the coupling arm, L, has a marginal effect on the response of the SDOF oscillator when coupled with a stepping wall (either stepping or pinned). Nevertheless, the pinned wall amplifies the response for most of the range of the spectrum. For the sake of simplicity of the analysis, it is assumed that the oscillator is elastic ($a = k_1/k_2 = 1$).

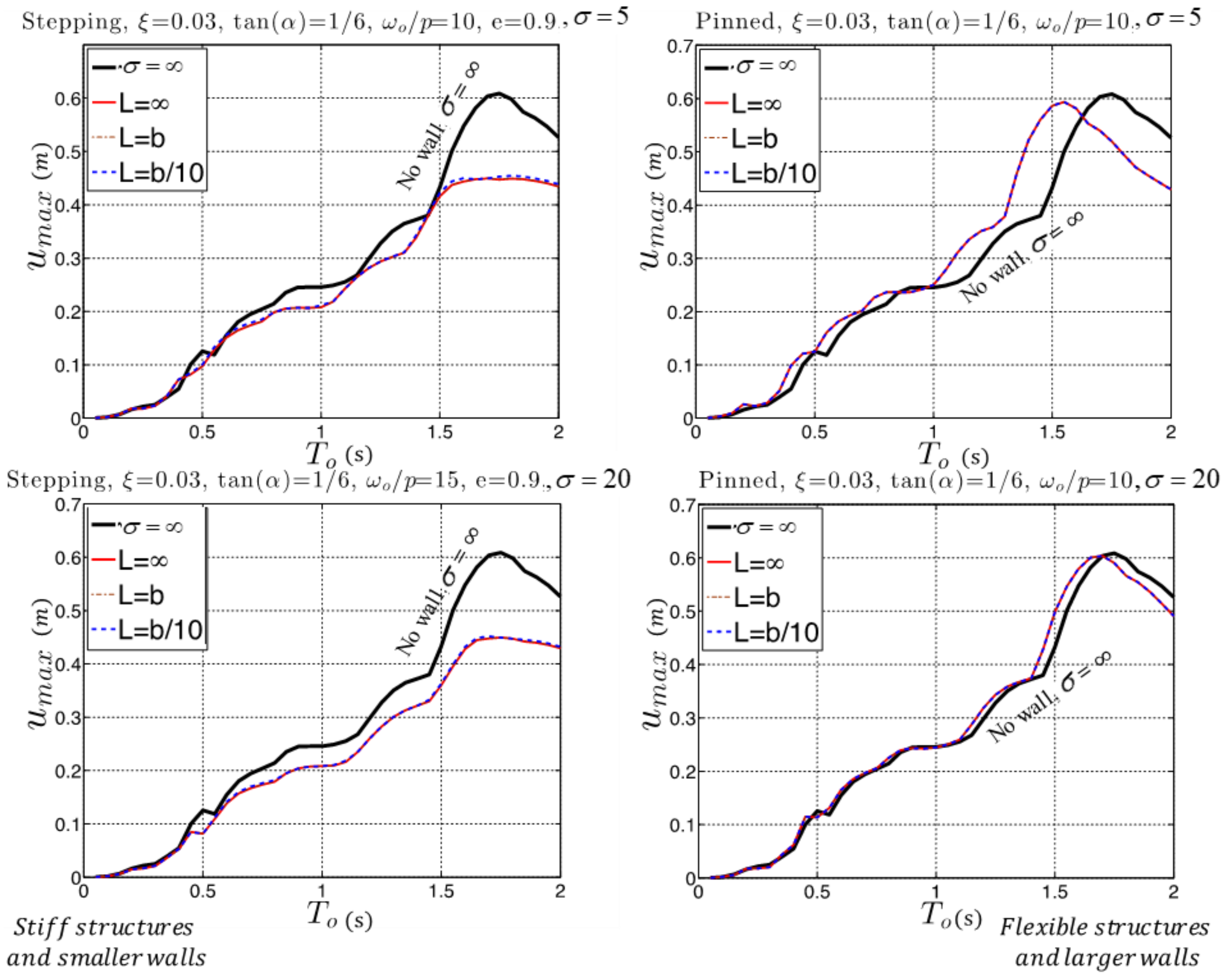

Figure 2-13 Displacement spectra of an elastic SDOF oscillator coupled with a stepping wall (left) and a pinned wall (right) with a short coupling arm for two values of the mass ratio $\sigma = m_s/m_w = 5$ (top) and 20 (bottom) and the wall size, $\omega_o/p = 10$ and three values of the length of the coupling arm, $L = \infty, b$ and $b/10$ when subjected to the Takarazuka/000 ground motion recorded during the 1995 Kobe, Japan earthquake

Same trends are observed in Figure 2-13 that plots displacement spectra of the SDOF oscillator coupled with a stepping wall (left) and a pinned wall (right) with $\frac{\omega_o}{p} = 10$ and three values of the length of the coupling arm, $L = \infty, b$ and $b/10$,when excited by the Takarazuka/000 ground motion recorded during the 1995 Kobe, Japan earthquake. Given that the coupling with a pinned wall invariably amplifies the displacement response, the concept of the pinned wall should be used with caution.

2.8 CONCLUSIONS

The dynamic response of a yielding SDOF oscillator coupled with a rocking wall is investigated in this part. Both configurations of a stepping and a pinned rocking wall that have been reported in the literature are examined. The full nonlinear equations of motions are derived, and the study reaches through a comprehensive parametric analysis the following conclusions.

When the yielding SDOF oscillator is coupled with a stepping rocking wall, the participation of the stepping wall suppresses the peak inelastic displacements in particular for more flexible structures with the heavier wall being most effective. Most importantly, the participation of the stepping rocking wall reduces drastically the permanent displacements which vanish completely as the weight of the wall increases.

When the yielding SDOF oscillator is coupled with a pinned rocking wall, opposite trends are observed:

(a) The participation of the pinned rocking wall increases in general the peak inelastic displacements with the heavier wall being most unfavorable.

(b) the participation of the pinned rocking wall increases the permanent displacements through a wide range of the response spectrum. This unfavorable response is mainly because the moment from the weight of a pinned rocking wall works against the stability of the system. Accordingly, the coupling a yielding frame with a pinned rocking wall may result to unfavorable response and should be used with caution.

The length of the coupling arm has a marginal effect on the response of the SDOF oscillator when coupled with a rocking wall. Nevertheless, the pinned wall amplifies the response for most of the range of the spectrum even when short arm lengths are considered.

3 VERTICALLY RESTRAINED ROCKING WALL

3.1 DYNAMICS OF A YIELDING OSCILLATOR COUPLED WITH A VERTICALLY RESTRAINED STEPPING ROCKING WALL

This chapter of the study examines the dynamic response of a yielding single-degree-of-freedom (SDOF) structure, with mass, m_s, pre-yielding stiffness, k_1 post yielding stiffness, k_2, and strength, Q, that is coupled with a free-standing stepping rocking wall of size, $R = \sqrt{b^2 + h^2}$, slenderness, $\tan\alpha = b/h$, mass, m_w and moment of inertia about the pivoting (stepping) points O and O', $I = 4/3\ m_w R^2$, that is vertically restrained with an elastic tendon with axial stiffness EA which can be prestressed with a prestressing force P_o. In the interest of simplicity, it is assumed that the arm with length, L, that couples the motion is articulated at the center of mass of the rocking wall at a height, h, from its foundation as shown in Figure 3-1.

During rocking motion of the vertically restrained wall, the tendon is elongated by (Vassiliou and Makris 2015)

$$e = \sqrt{2} R \sin\alpha \sqrt{1-\cos\theta} \tag{3.1}$$

In addition to the elongation, e, given by equation 3.1, the analysis accounts for an initial elongation

$$e_o = \frac{P_o}{EA/2h} \tag{3.2}$$

due to a possible initial postensioning force, P_o.

Accordingly, during rocking motion, the restoring moment on the rocking wall from the tendon alone is (Vassiliou and Makris 2015)

$$M_r = -R\sin\alpha\sin\theta\left(\frac{1}{2}EA\tan\alpha + \frac{P_o}{\sqrt{2}\sqrt{1-\cos\theta}}\right) \tag{3.3}$$

With reference to Figure 3-1 (bottom), as the elasticity of the tendon increses it offsets the negative stiffness originating from rocking, The value of the axial stiffness of the tendon that is needed to introduce positive stiffness is

$$\frac{EA}{m_w g} = 2\frac{1}{\tan^2\alpha} \tag{3.4}$$

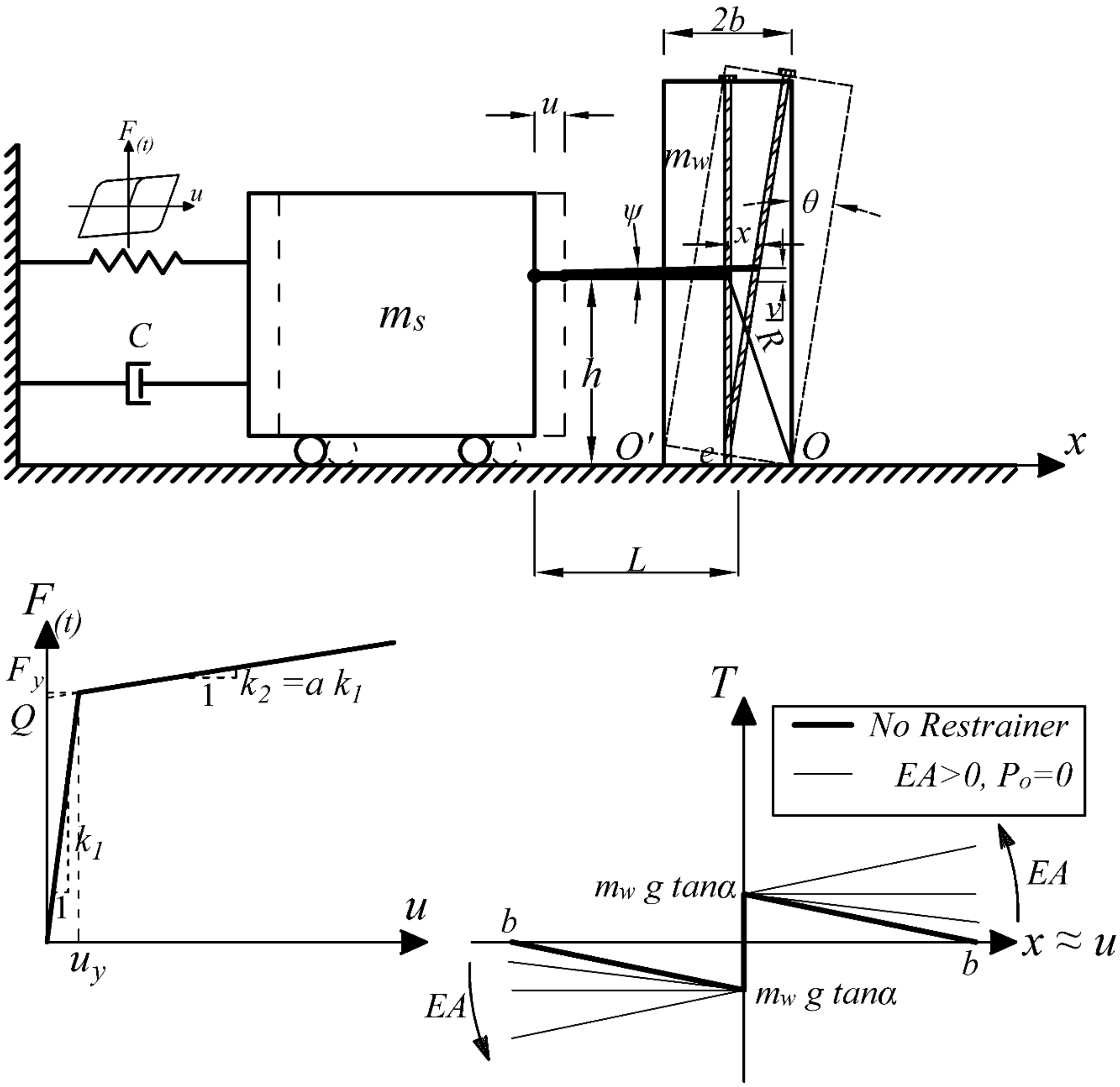

Figure 3-1 Yielding single-degree-of-freedom oscillator coupled with a vertically restrained stepping rocking wall.

For instance, for a slenderness value, $\tan\alpha = 1/6$, a rigid-plastic behavior is reached when $\frac{\mathrm{EA}}{\mathrm{m_w g}} = 72$.

Case 1: $\theta > 0$

For positive rotations ($\theta > 0$), dynamic equilibrium of the vertically restrained stepping rocking wall with mass m_w shown in Figure (1), gives:

$$I\ddot{\theta} = -TR\cos(\alpha-\theta) - m_w gR\sin(\alpha-\theta) - m_w \ddot{u}_g R\cos(\alpha-\theta) \\ - R\sin\alpha\sin\theta\left(\frac{1}{2}EA\tan\alpha + \frac{P_o}{\sqrt{2}\sqrt{1-\cos\theta}}\right) \tag{3.5}$$

where P_o is the initial post-tensioning force and EA is the axial stiffness of the elastic tendon. The axial force T appearing in equation (3.5) is replaced with the help of equations (2.5) and (2.6), whereas for a rectangular stepping wall, $I = 4/3\ m_w\ R^2$. Accordingly, equation (3.5) assumes the form:

$$\frac{4}{3}m_w R^2\ddot{\theta} + [m_s(\ddot{u}+\ddot{u}_g) + ak_1u(t) + (1-a)k_1u_y z(t) + c\dot{u}]R\cos(\alpha-\theta)$$
$$= -m_w R[\ddot{u}_g\cos(\alpha-\theta) + g\sin(\alpha-\theta)] - R\sin\alpha\sin\theta(\frac{1}{2}EA\tan\alpha + \frac{P_o}{\sqrt{2}\sqrt{1-\cos\theta}}) \tag{3.6}$$

Upon dividing with $m_w R$ equation 3.6 gives:

$$\frac{4}{3}R\ddot{\theta} + \left[\sigma(\ddot{u}+\ddot{u}_g) + a\frac{k_1}{m_w}u(t) + (1-a)\frac{k_1}{m_w}u_y z(t) + \frac{c}{m_w}\dot{u}\right]\cos(\alpha-\theta)$$
$$= -\ddot{u}_g\cos(\alpha-\theta) - g\sin(\alpha-\theta) - \sin\alpha\sin\theta(\frac{1}{2}\frac{EA}{m_w}\tan\alpha + \frac{P_o}{m_w\sqrt{2}\sqrt{1-\cos\theta}}) \tag{3.7}$$

in which $\sigma = m_s/m_w$ is the mass ratio parameter.

Substitution of the expressions of the relative displacement, velocity and acceleration given by equations 2.2 to 2.4 for positive rotations, and after dividing with *R* equation 3.7 is expressed only in terms of the variable, $\theta(t)$.

$$\left(\frac{4}{3} + \sigma\cos^2(\alpha-\theta)\right)\ddot{\theta} + \sigma\cos(\alpha-\theta)\left[a\omega_1^2\left(\sin\alpha - \sin(\alpha-\theta)\right) + 2\xi\omega_1\dot{\theta}\cos(\alpha-\theta)\right.$$
$$\left. + \dot{\theta}^2\sin(\alpha-\theta) + (1-a)\omega_1^2\frac{u_y}{R}z(t)\right]$$
$$= -\frac{g}{R}\left[(\sigma+1)\frac{\ddot{u}_g}{g}\cos(\alpha-\theta) + \sin(\alpha-\theta) + \sin\alpha\sin\theta(\frac{1}{2}\frac{EA}{m_w g}\tan\alpha + \frac{P_o}{m_w g}\frac{1}{\sqrt{2}\sqrt{1-\cos\theta}})\right] \tag{3.8}$$

where $\omega_1 = \sqrt{k_1/m_s}$ = the pre-yielding undamped frequency and $\xi = \frac{c}{2m_s\omega_1}$ = the pre-yielding viscous damping ratio of the SDOF oscillator. Equation 3.8 is the equation of motion for positive rotations of the coupled system shown in Figure (1).

Case 2: $\theta < 0$

For negative rotations one can follow the same reasoning and the equation of the coupled system shown in Figure 3-1 is:

$$\left(\frac{4}{3}+\sigma\cos^2(\alpha+\theta)\right)\ddot{\theta}-\sigma\cos(\alpha+\theta)\left[a\omega_1^2\left(\sin\alpha-\sin(\alpha+\theta)\right)-2\xi\omega_1\dot{\theta}\cos(\alpha+\theta)\right.$$
$$\left.+\dot{\theta}^2\sin(\alpha+\theta)-(1-a)\omega_1^2\frac{u_y}{R}z(t)\right]$$
$$=\frac{g}{R}\left[-(\sigma+1)\frac{\ddot{u}_g}{g}\cos(\alpha+\theta)+\sin(\alpha+\theta)-\sin\alpha\sin\theta\left(\frac{1}{2}\frac{EA}{m_w g}\tan\alpha+\frac{P_o}{m_w g}\frac{1}{\sqrt{2}\sqrt{1-\cos\theta}}\right)\right] \tag{3.9}$$

When parameters $EA/m_w g = P_o/m_w g = 0$, equations 3.8 and 3.9 collapse to the equations of motion presented in (Makris and Aghagholizadeh 2017a; Aghagholizadeh 2018) for a yielding SDOF oscillator coupled with a rocking wall with no vertical restrainer. The terms multiplied with the parameter $\sigma = m_s/m_w$ are associated with the dynamics of the yielding SDOF oscillator; whereas, the remaining terms are associated with the dynamics of the rocking wall. When the SDOF oscillator is absent ($\sigma = \omega_1 = \xi = 0$), equations 3.8 and 3.9 reduce to the equations of motion of the solitary restrained rocking wall (Vassiliou et al. 2015) since the frequency parameter *p* for rectangular walls is $p = \sqrt{3g/4R}$ (Makris 2014a, 2014b). Equations 3.8 and 3.9 reveal that the effect of tendon (*EA* and P_o) is different than the effect of a heavier wall (lower σ). These differences are illustrated in the response spectra presented later in the report.

During the oscillatory motion of the coupled system shown in Figure 3-1, aside from the energy that is dissipated from the inelastic behavior of the SDOF oscillator and the idealized viscous damping, additional energy is also lost during impact when the angle of rotation reverses. At this instant it is assumed that the rotation of the rocking wall continues smoothly from points O to O'; nevertheless, the angular velocity, $\dot{\theta}_2$, after the impact is smaller than the angular velocity, $\dot{\theta}_1$, before the impact. Given that the energy loss during impact is a function of the wall-foundation interface, the coefficient of restitution, $e = \dot{\theta}_2/\dot{\theta}_1 < 1$, is introduced as a parameter of the problem. In this study the coefficient of restitution assumes the value of $e = 0.9$.

3.2 MINIMUM ACCELERATION NEEDED TO INITIATE UPLIFT OF THE COUPLED, VERTICALLY RESTRAINED ROCKING WALL

With reference to Figure 3-1, during an infinitesimal admissible horizontal displacement δu, application of the principle of virtual work (when damping forces are neglected) gives

$$m_s\ddot{u}_g\delta u+m_w\ddot{u}_g\delta u=m_w g\delta v+\frac{1}{2}k\delta u^2+\frac{1}{2}\frac{EA}{L}\delta v^2+P_o\delta v \tag{3.10}$$

where δv is the corresponding infinitesimal vertical displacement of the center of mass of the rocking wall that is associated with δu. Assuming a positive rotation, for a horizontal displacement, u, given by equation 2.2, the associated vertical displacement v is

$$v=R[\cos(\alpha-\theta)-\cos\alpha] \tag{3.11}$$

From the calculus of variations (Lanczos 1979)

$$\delta u = \frac{du}{d\theta}\delta\theta \quad and \quad \delta v = \frac{dv}{d\theta}\delta\theta \tag{3.12}$$

Equation 3.12, in association with equations 2.2 and 3.11 give

$$\delta u = R\cos(\alpha - \theta)\,\delta\theta \tag{3.13}$$

and

$$\delta v = R\sin(\alpha - \theta)\,\delta\theta \tag{3.14}$$

Substitution of equations 3.13 and 3.14 into the equation of virtual work 3.10, after dropping the terms $\frac{1}{2}k\delta u^2$ and $\frac{EA}{L}\delta v^2$ which involve second order variations, gives

$$m_w(\sigma+1)\ddot{u}_g R\cos(\alpha-\theta)\delta\theta = (m_w g + P_o)R\sin(\alpha-\theta)\delta\theta \tag{3.15}$$

At the initiation of uplift, $\theta = 0$; therefore, equation 3.15 indicates that the uplift acceleration of the system is:

$$\ddot{u}_g = \frac{1}{\sigma+1} g\, tan\alpha\left(1+\frac{P_o}{m_w\, g}\right) \tag{3.16}$$

3.3 Parameters of The Problem

The Bouc-Wen model described by equations 2.6 and 2.7 is a phenomenological model of hysteresis originally proposed by Bouc (1967) and subsequently generalized by Wen (1975; 1976) and Baber and Wen (1981). It is a versatile model that can capture various details of the nonlinear force-displacement loop. Subsequent studies on the modeling of yielding systems by Constantinou and Adnane (1987) concluded that when certain constraints are imposed on the parameters β and γ $(\beta+\gamma=1)$, the model reduces to a viscoplastic element with well-defined physical characteristics. The Bouc-Wen model essentially builds on the bilinear idealization shown in the bottom-left of Figure 1.

For the five-parameter system shown with the bilinear idealization. (k_1= pre-yielding stiffness, k_2= post-yielding stiffness, u_y= yield displacement, Q= strength and F_y= yielding force), only three parameters are needed to fully describe the bilinear behavior (see for instance (Makris and Kampas 2013)). In this work, the authors select the pre-yielding stiffness $k_1 = m_s\,\omega_1^2$, the post-yielding stiffness $k_2 = a\,k_1$ and the strength of the structure Q. With reference to Figure 3.1 (bottom-left), $F_y = k_1\,u_y = Q + k_2\,u_y$. Accordingly, $u_y = Q/(k_1 - k_2)$ and $F_y = k_1\,Q/(k_1 - k_2)$. The parameters β, γ and n appearing in equation 2.7 are established from past studies on the parameter identification of yielding concrete structures and assume the values: $\beta = 0.95, \gamma = 0.05$ and $n = 2$ (Goda et al. 2009; Kunnath et al. 1997). With the parameters $\beta = 0.95$, $\gamma = 0.05$ and $n = 2$ being established, the peak inelastic displacement, u_{max} of the SDOF system shown in Figure 3-1 is a function of the following parameters:

$$u_{max} = f\left(\omega_1, \frac{Q}{m_s}, a, \xi, p, \tan\alpha, \sigma, g, EA, P_o, \textit{parameters of excitation}\right) \tag{3.17}$$

In this study, it is assumed that upon yielding, the structure maintains a mild, positive, post-yielding stiffness = $k_2 = 0.05k_1$, therefore $a = 0.05$ (Goda et al. 2009; Kunnath et al. 1997). Furthermore, it is assumed that the pre-yielding damping ratio, $\xi = c/(2m_s\,\omega_1) = 0.03$ and the authors focus on rocking walls with slenderness, $\tan\alpha = 1/6$.

3.4 Normal Force at The Pivoting Corners

By increasing the axial stiffness, EA, of the vertical tendon one increases the lateral stiffness of the entire structural system; nevertheless, at present it is not clear to what extent a stiffer vertical tendon improves the seismic performance of the overall structure, or it merely contributes to accentuate the vertical reaction force at the pivoting points. With reference to Figure 3-2, a rotation of the wall = θ creates an elongation to the tendon = e, given by equation (8). In addition to gravity and inertia forces, the vertical reaction at the pivot corner, *N*, balances the vertical forces from the tendon

$$F_v = \frac{EA}{2h} e\cos\phi + P_o\cos\phi \tag{3.18}$$

Using that $e\cos\phi = b\sin\theta$ and $\cos\phi = (1/\sqrt{2}\,)\sqrt{1+\cos\theta}$, equation 3.18 assumes the form

$$F_v = \frac{1}{2} EA\tan\alpha\sin\theta + \frac{P_o}{\sqrt{2}}\sqrt{1+\cos\theta} \tag{3.19}$$

During rocking motion, the vertical reaction at the pivoting corners, N, balances the weight of the wall, the inertia forces and the vertical force, F_v, from the tendon gives by equation 3.19

$$N(t) = m_w\ddot{v} + m_w g + EA\left(\frac{1}{2}\tan\alpha\sin\theta + \frac{P_o}{EA}\frac{\sqrt{1+\cos\theta}}{\sqrt{2}}\right) \tag{3.20}$$

where $\ddot{v}$ is the vertical acceleration of the center of mass of the wall. For instance, for a positive rotation ($\theta > 0$), the vertical uplift of the center of mass of the wall is given by 3.11 and successive differentiation gives,

$$\dot{v} = R\dot{\theta}\sin(\alpha-\theta) \tag{3.21}$$

$$\ddot{v} = R\left[\ddot{\theta}\sin(\alpha-\theta) - \dot{\theta}^2\cos(\alpha-\theta)\right] \tag{3.22}$$

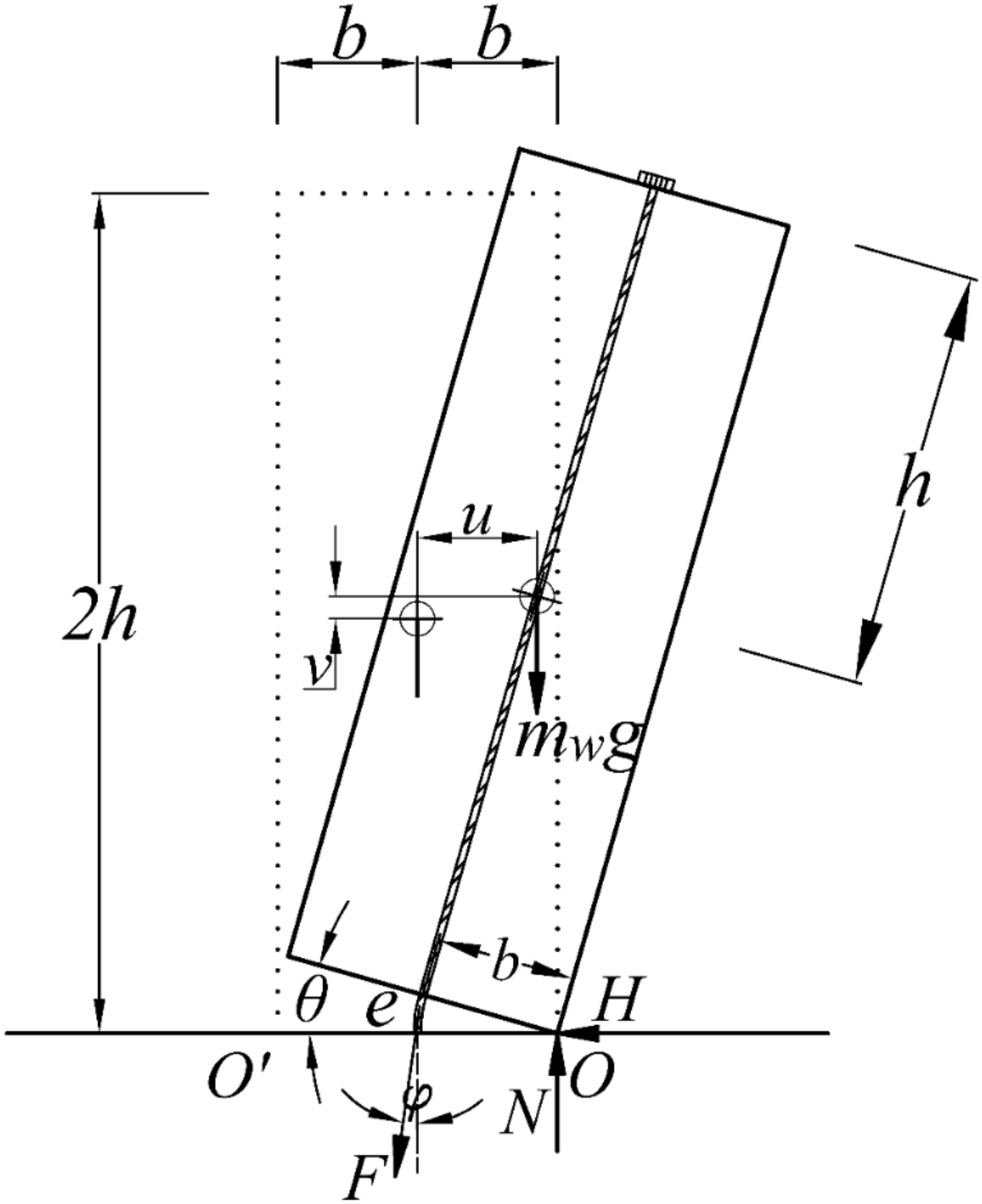

Figure 3-2 Free-body diagram of a rocking wall with an elastic tendon passing through its center-line.

By virtue of equation 3.22, the normalized to the weight of the wall vertical reaction of the pivoting point is given by

$$\frac{N(t)}{m_w g} = 1 + \frac{R}{g}\left[\ddot{\theta}\sin(\alpha-\theta) - \dot{\theta}^2\cos(\alpha-\theta)\right] + \frac{1}{2}\frac{EA}{m_w g}\tan\alpha\sin\theta + \frac{1}{\sqrt{2}}\frac{P_o}{m_w g}\sqrt{1+\cos\theta} \tag{3.23}$$

Figure 3-3 (left) plots displacement, $u(t)$, rotation, $\theta(t)$ and vertical-reaction, $N(t)$ (at the pivot points) time histories for a structure having, $T_1 = 0.8$ sec, $Q/m_s = 0.08g$ which is coupled with a rocking wall with $\omega_1/p = 10$ ($p = 0.778$ rad/sec), $\tan\alpha = 1/6$ and $\sigma = m_s/m_w = 10$ when excited by the Pacoima Dam/164 ground motion recorded during the 1971 San Fernando, California earthquake. The dashed line is when there is no wall, the heavy dark line is where there is a rocking wall without tendon; whereas the thinner solid lines show the response when a tendon is present without being pretensioned ($P_o = 0$). Figure 3-3 (left) shows that whereas a stiff tendon ($\frac{EA}{m_w g} = 200$) increases the vertical reaction at the pivot points by more than 50% its effect in reducing peak inelastic deformations is marginal. Figure 3-3 (right) reveals similar trends as those discussed for the results of Figure 3-3 (left) when the inelastic structure is subjected to Erzincan NS ground motion recorded during 1992 Erzincan, Turkey earthquake.

Figure 3-4 plots displacement, $u(t)$, rotation $\theta(t)$ and vertical reaction at the pivot points, $N(t)$ time histories for a structure having $T_1 = 1.5$ sec, $Q/m_s = 0.12g$ which is coupled with a rocking wall with $\omega_1/p = 10$ ($p = 0.778$ rad/sec), $\tan\alpha = 1/6$ and $\sigma = m_s/m_w = 10$ when excited by the same ground motions used in Figure 3.3. Figure 3.5 plots displacement, $u(t)$, rotation, θ(t), and vertical reaction at the pivot points, $N(t)$, time histories for a structure having the same parameters as those of the structural system of Figure 3-4; yet, now the vertical tendon is prestressed with $P_o = 0.5 m_w g$ and subjected to the Newhall/360 ground motion recorded during 1994 Northridge, California earthquake (left) and the Takarazuka/000 ground motion recorded during the 1995, Kobe, Japan earthquake (right). Similar to the results presented in Figure 3-3, Figure 3-4 and Figure 3-5 show that the effect of the vertical tendon is marginal other than increasing by more than 50% the vertical reaction of the pivot points.

While equations 3.8 and 3.9 only describe the dynamics of the SDOF idealization shown in Figure 3.1, they are of engineering value since they show the relative contribution of the various parameters of the problem. For instance, consider a moment frame-rocking wall system with mass ration, $\sigma = m_s/m_w = 10$, when the rocking wall with slenderness, $\tan\alpha = 1/6$, restrained with a stiff vertical tendon (say $EA/m_w g = 200$) and subjected to a ground motion with an acceleration amplitude of $\ddot{u}_g = 0.5g$. The right-hand side of equations 3.8 and 3.9 show that the term associated with the input ground acceleration, $(\sigma + 1)\frac{\ddot{u}_g}{g}\cos(\alpha - \theta)$, is of the order of 5; whereas, the term associated with the contribution of the tendon is $\frac{1}{2}\sin\alpha\tan\alpha\frac{EA}{m_w g}\sin\theta \approx 2.74\theta$. Given that for most cases of interest θ_{max} is less than $\alpha/10 \approx (\tan\alpha)/10$ (see Figure 3-4 and Figure 3-5), the contribution of the tendons at peak wall rotation = θ_{max}, is of the order of $2.74\,(\tan\alpha)/10 \approx 0.05$—that is two order of magnitude smaller than the term associated with the input ground acceleration. This explains the marginal contribution of the vertical tendons even if they are stiff.

$$T_1 = 0.8s, \frac{Q}{m_s g} = 0.08, \frac{\omega_1}{p} = 10, tan\, \alpha = \frac{1}{6}, \sigma = 10, \xi = 0.03, \frac{P_o}{m_w g} = 0$$

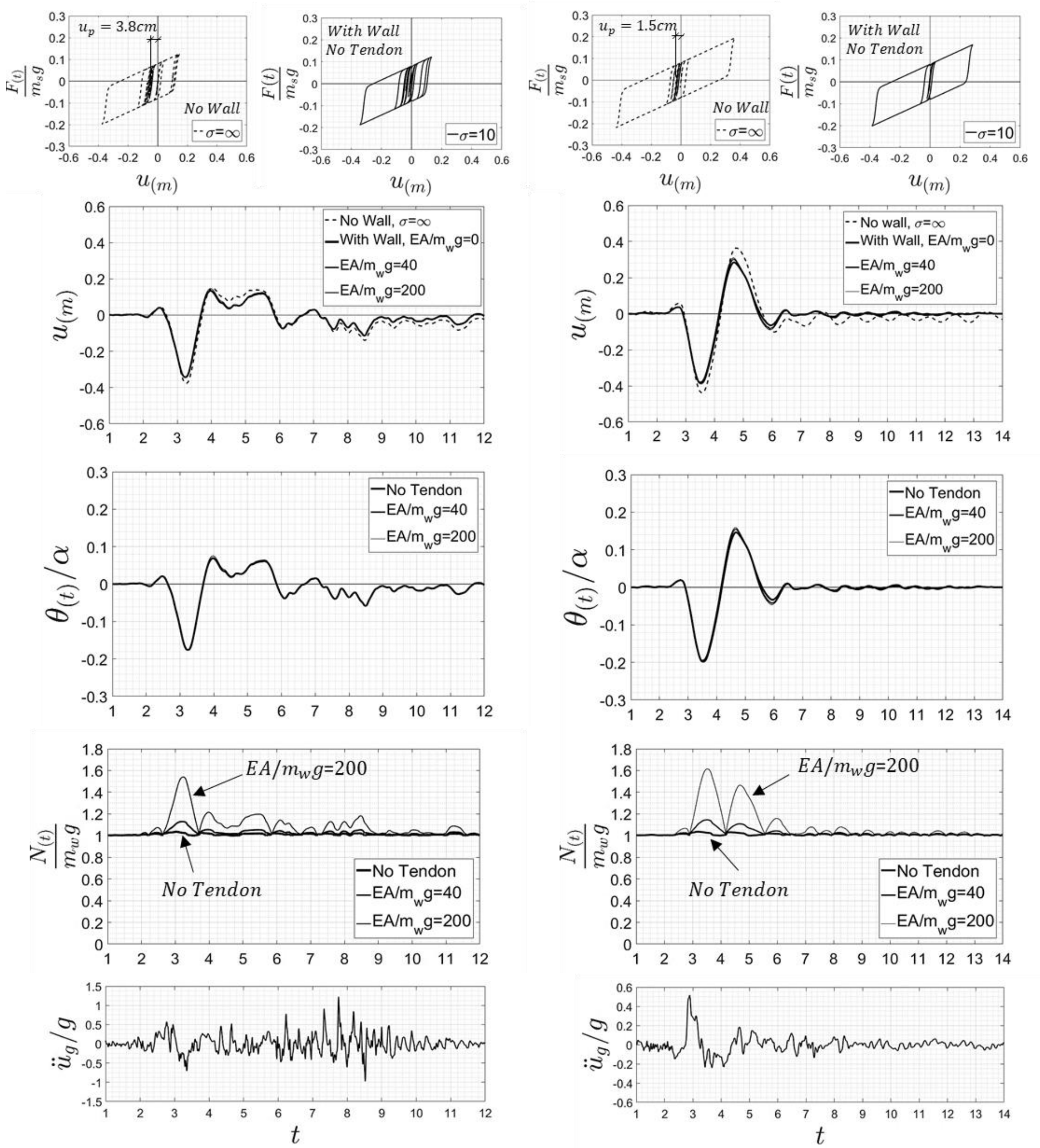

Figure 3-3 Time-history analysis of a nonlinear SDOF oscillator coupled with a vertically restrained stepping rocking wall with preyielding period, $T_1 = 0.8$ sec, normalized strength $Q/m_s = 0.08g$, wall size ratio, $\omega_1/p = 10$ and structure-to-wall mass ration, $\sigma = 10$ when subjected to the 1971 Pacoima Dam/164 ground motion (left) and the 1992 Erzincan NS, Turkey ground motion (right). Even stiff tendons ($EA/m_w g = 200$) have a marginal effect on the response, except of drastically increasing the vertical reaction (more than 50%) at the pivot points. Tendons are not prestressed, $P_o/m_w g = 0$.

$$T_1 = 1.5s, \frac{Q}{m_s g} = 0.12, \frac{\omega_1}{p} = 10, tan\,\alpha = \frac{1}{6}, \sigma = 10, \xi = 0.03, \frac{P_o}{m_w g} = 0$$

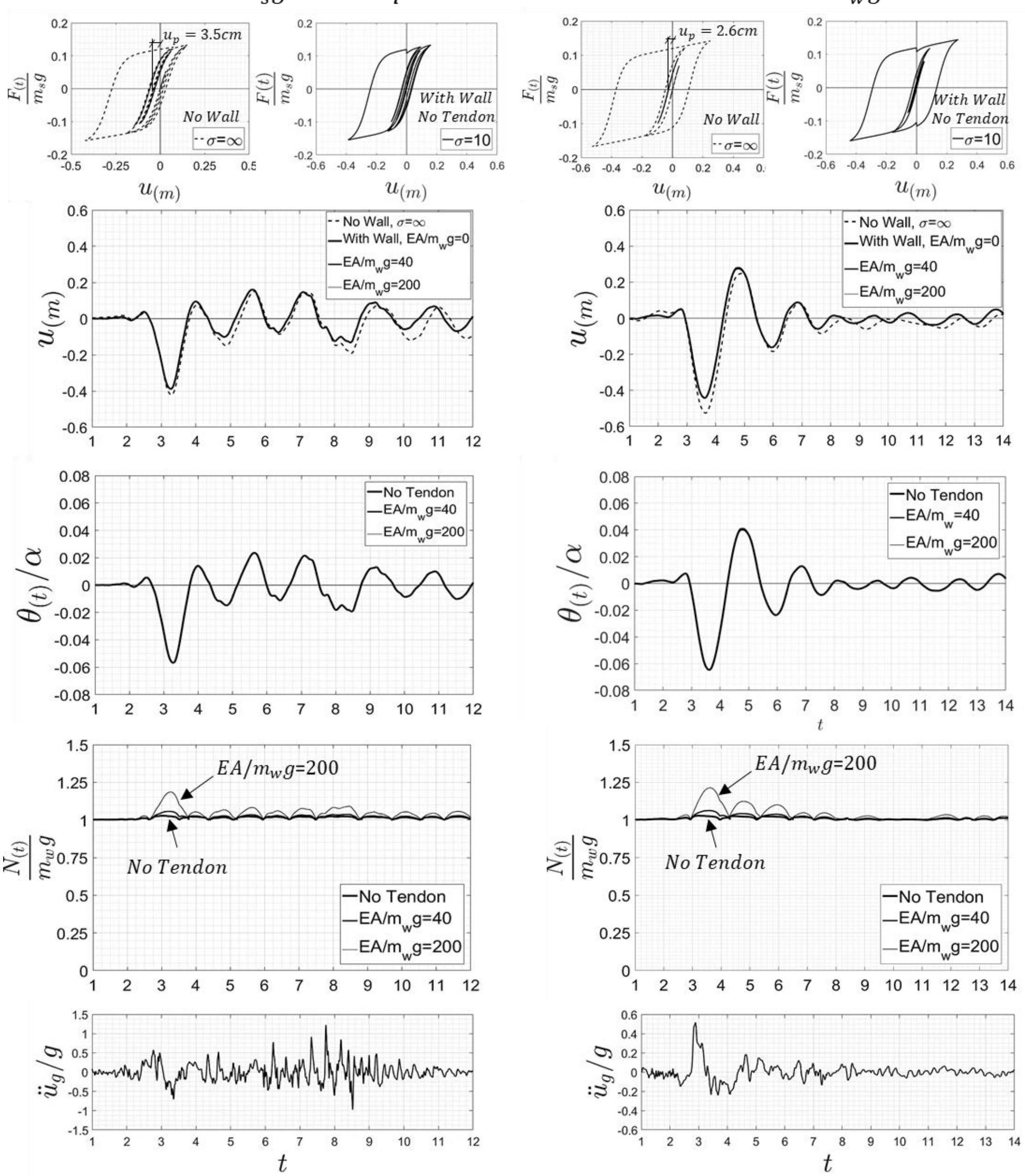

Figure 3-4 Time-history analysis of a nonlinear SDOF oscillator coupled with a vertically restrained stepping rocking wall with preyielding period, $T_1 = 1.5$ sec, normalized strength $Q/m_s = 0.12g$, wall size ratio, $\omega_1/p = 10$ and structure-to-wall mass ration, $\sigma = 10$ when subjected to the 1971 Pacoima Dam/164 ground motion (left) and the 1992 Erzincan NS, Turkey ground motion (right). Even stiff tendons ($EA/m_w g = 200$) have a marginal effect on the response, except of drastically increasing the vertical reaction at the pivot points. Tendons are not prestressed, $P_o/m_w g = 0$.

$$T_1 = 1.5s, \frac{Q}{m_s g} = 0.12, \frac{\omega_1}{p} = 10, tan\,\alpha = \frac{1}{6}, \sigma = 10, \xi = 0.03, \frac{P_o}{m_w g} = 0.5$$

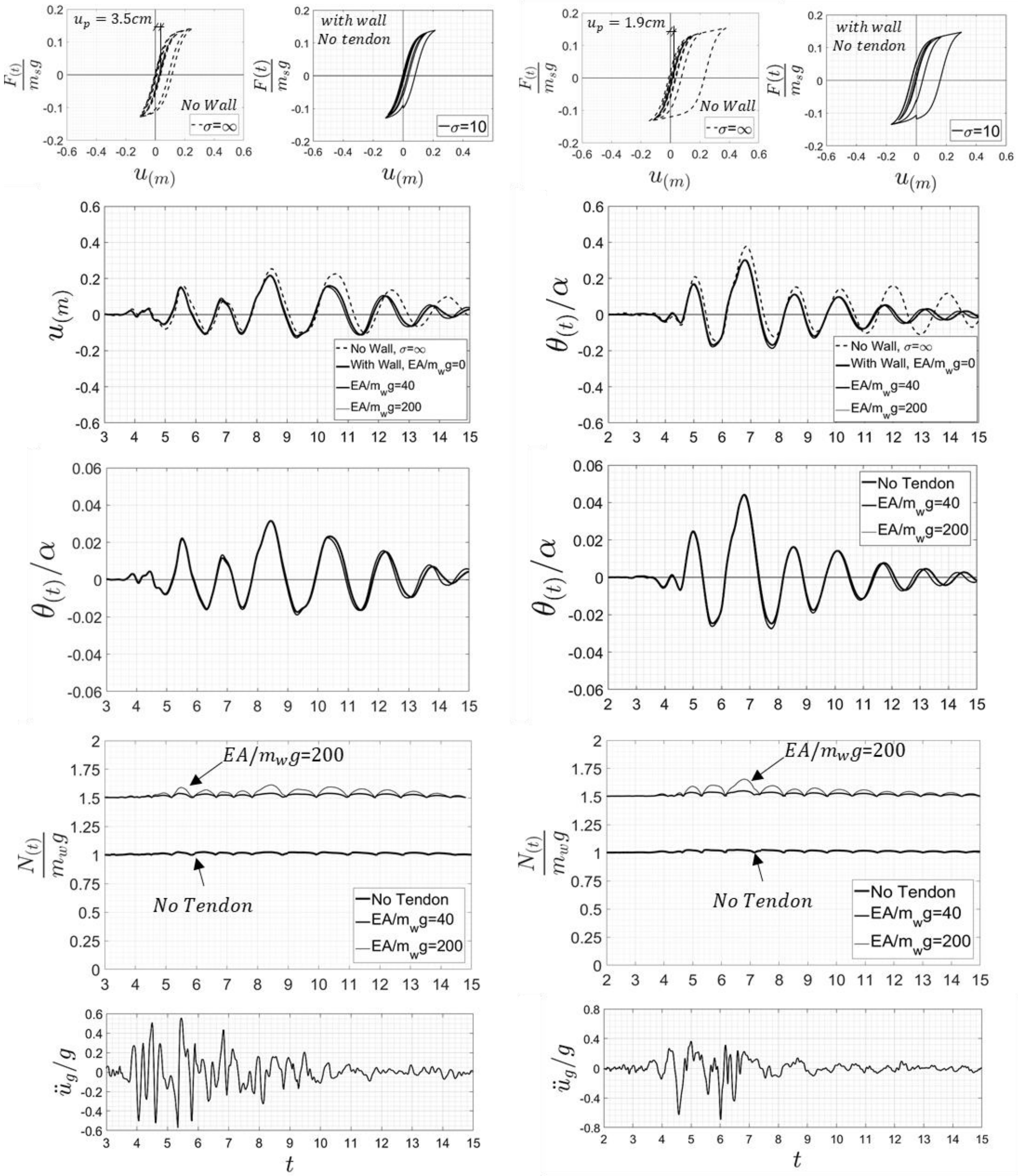

Figure 3-5 Time-history analysis of a nonlinear SDOF oscillator coupled with a vertically restrained stepping rocking wall with preyielding period, $T_1 = 1.5$ sec, normalized strength $Q/m_s = 0.12g$, wall size ratio, $\omega_1/p = 10$ and structure-to-wall mass ration, $\sigma = 10$ when subjected to the 1994 Newhall/360 ground motion (left) and the 1995 Takarazuke/000, Japan ground motion (right). Even stiff tendons ($EA/m_w g = 200$) have a marginal effect on the response, except of drastically increasing the vertical reaction (more than 50%) at the pivot points. Tendons are prestressed with, $P_o/m_w g = 0.5$.

3.5 VALIDATION OF THE SDOF – IDEALIZATION

In view of the small differences between the peak response of a yielding structure coupled with a stepping rocking wall (either free-standing or vertically restrained) and the nonlinear response of the solitary yielding structure (other than the reduction of permeant displacements – see Figures 3-3, 3-4 and 3-5), the dependability of the single-degree-of-freedom idealization shown in Figure 3.1 is examined against the results obtained with the open-source code OpenSees[1] (McKenna et al. 2000) when analyzing the nine-story moment resisting steel structure designed for the SAC Phase II Project (2000). This structure that is well-known to the literature (Gupta and Krawinkler 1999, 2000; Chopra and Goel 2002) was designed to meet the seismic code (pre-Northridge Earthquake) and represents typical medium-rise buildings designed for the greater area of Los Angeles, California.

This moment-resisting, steel building is 40.82 m tall with 9-stories above ground level and a basement. The bays are 9.15 m wide, with five bays in north-south (N-S) and east-west (E-W) directions. Floor-to-floor height of each story is 3.96 m, except for the basement and first floor which are 3.65 m and 5.49 m respectively as shown in Figure 3-6. Columns splices are on the 1st, 3rd, 5th and 7th floors and located 1.83 m above the beam-column joint. The column bases are modeled as pinned connection and it is assumed that the surrounding soil and concrete foundation walls are restraining the structure in horizontal direction at the ground level. The columns are 345 MPa wide-flange steel sections and the floor beams are composed of 248 MPa wide-flanges steel sections. All beam column connections of the frames are rigid except for the corner columns which are pinned in order to avoid bi-axial bending of the members. In this study, the exterior frame in N-S direction is chosen for the 2-D validation of our planar analysis.

Figure 3-7 (top) plots the computed push-over curve (base shear vs roof displacement) of the 9-story moment resisting steel building without rocking wall, which is compared with the push-over curve presented in past investigations (Gupta and Krawinkler 1999, 2000; Chopra and Goel 2002). The resulting pre-yielding period of the building is $\mathrm{T_1} = 2.27\ \mathrm{sec}$, while its normalized strength is $\mathrm{Q/m_s} = 0.17\mathrm{g}$. The remaining four subplots in Figure 3-7 plot the base-shear versus the mid-height displacement of the 9-story building without rocking wall together with the corresponding force-displacement loops computed with Matlab of the SDOF inelastic model shown in Figure 3-1 when excited with the 1994 Newhall/360, Northridge (b), 1992 Erzincan NS, Turkey (c), the 1995 Takarazuka/000, Kobe (d) and the 1971 Pacoima Dam/164, Imperial Valley (e) ground motions. All four subplots show that the inelastic force-displacement loops of the SDOF model shown in Figure 3-1 follow with fidelity the inelastic back-bone curve of the 9-story SAC building that is computed with OpenSees.

When analyzing with OpenSees the 9-story SAC building coupled with the stepping rocking wall as shown in Figure 3-6, the properties of the rocking interface are approximated with a rigid-elastic

[1] https://opensees.berkeley.edu/

rotational spring together with a rotational viscous dashpot to approximate the energy loss during impact as the rocking wall alternate pivot-points.

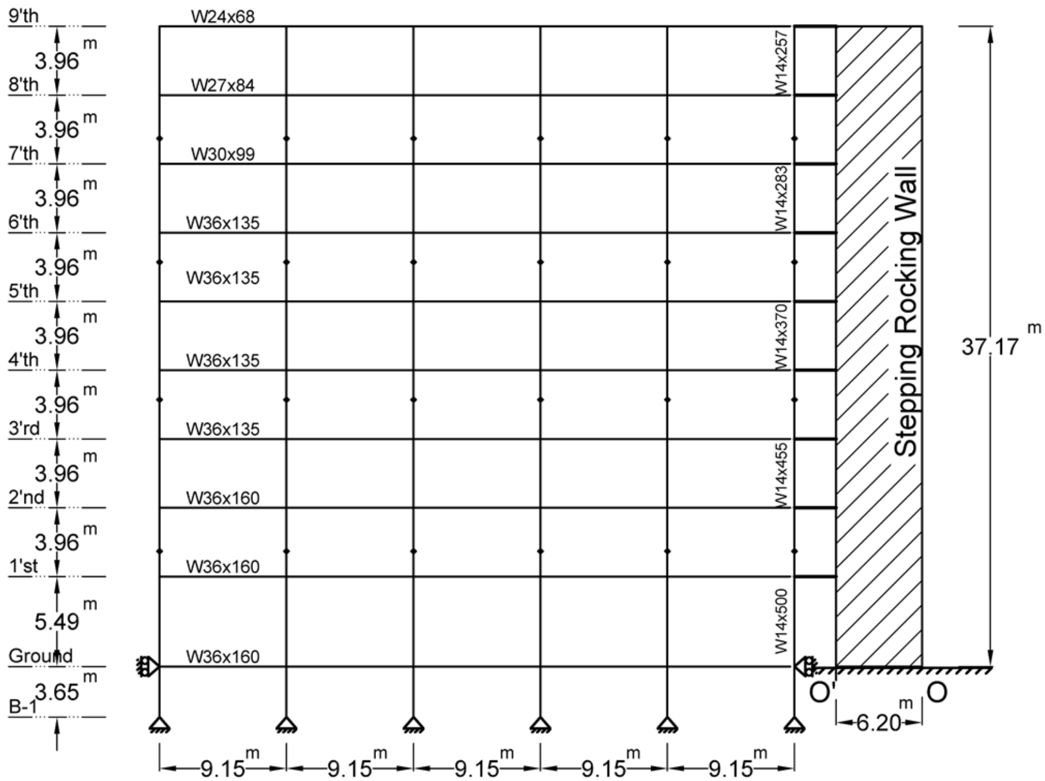

Geometric and Physical Characteristics			
Beams [248 MPa]		Columns [345 MPa]	
• Ground-2nd level	W36x160	• B1-1st level	W14x500
• 3rd-6th level	W36x135	• 1st-3rd level	W14x455
• 7th level	W30x99	• 3rd-5th level	W14x370
• 8th level	W27x84	• 5th-7th level	W14x283
• 9th level	W24x68	• 7th-9th level	W14x257
Columns • Column sizes change at splices and they are marked on the figure. Indicates column splices			
Seismic mass: • Ground level $9.5 \times 10^5\ kg$ • 1st level $1.0 \times 10^6\ kg$ • 2nd-8th level $9.89 \times 10^5\ kg$ • 9th level $1.07 \times 10^6\ kg$		Restraints: Column splices are at 1.83 m w.r.t. beam-to-column joint; Columns pinned at base; Structure laterally restrained at 1st level.	

Figure 3-6 Top: Nine-story moment-resisting steel frame designed for the SAC Phase II Project coupled with a stepping rocking wall. Bottom: Geometric and physical characteristics pertinent to the 9-story SAC building.

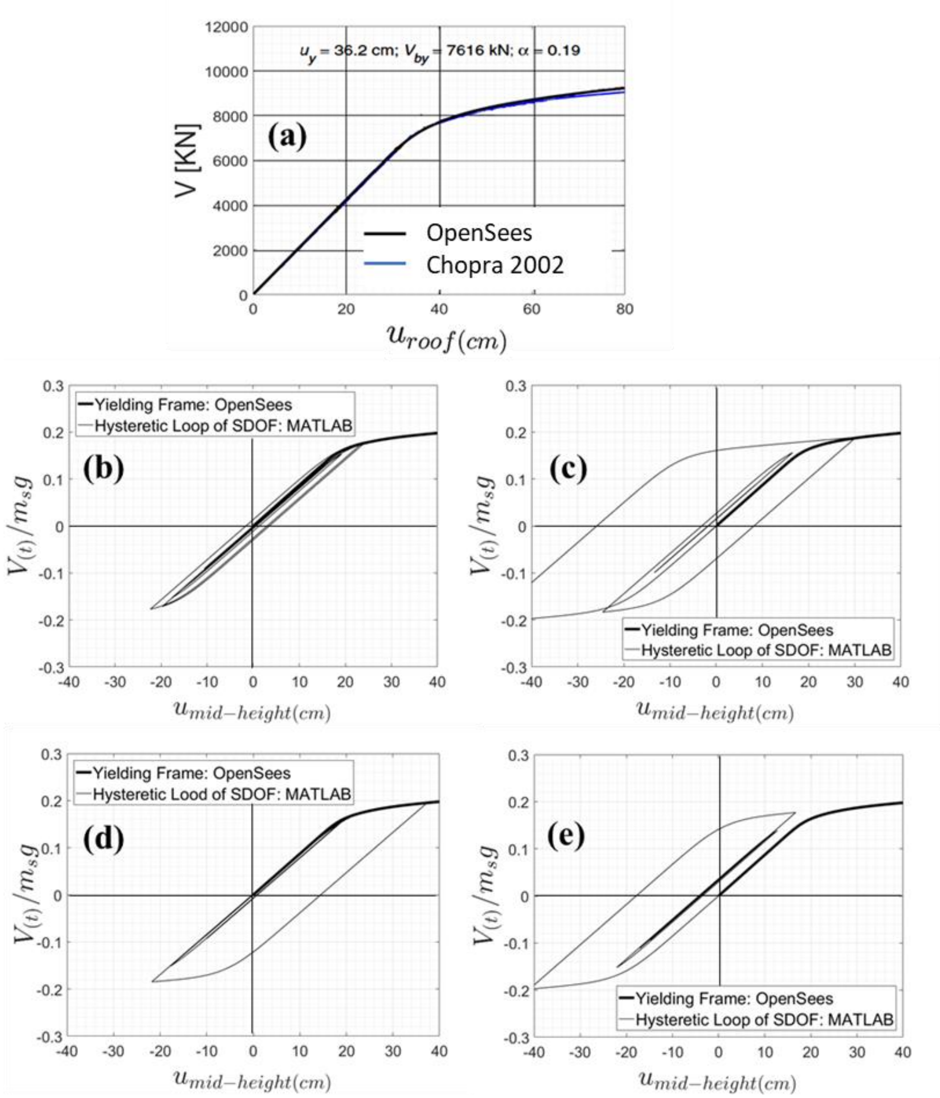

Figure 3-7 (a): Comparison of the computed push-over curve (base-shear vs roof displacement) of the 9-story moment-resisting steel building with the results reported by (Chopra and Goel 2002). Base-shear versus displacement at mid-height computed with OpenSees of the 9-story steel building without rocking wall together with the corresponding force-displacement loops computed with MATLAB of the SDOF inelastic model shown in Figure 1 when excited with the 1994 Newhall/360, Northridge (b), the 1992 Erzincan NS, Turkey (c), the 1995 Takarazuka/000, Kobe (d) and the 1971 Pacoima Dam/164, Imperial Valley (e) ground motions.

For a free-standing stepping rocking wall with size R, slenderness, α, and mass m_w, dimensional analysis yields that the expression of the equivalent rotational dashpot is (Vassiliou et al. 2014; Aghagholizadeh 2020)

$$c = \lambda \alpha^2 m_w g^{0.5} R^{1.5} \tag{3.24}$$

where, $\lambda = 250$, parameter that is calibrated for best fit of the result.

Figure 3-8 compares response histories computed with OpenSees at mid-height of the 9-story SAC steel building with the solutions obtained with MATLAB for the SDOF idealization shown in Figure 3-1. The top plots are when the rocking wall is not restrained (No tendon), the center plots are when the rocking wall is restrained with a stiff tendon with $\mathrm{EA/m_w g} = 200$ without being prestressed ($\mathrm{P_o} = 0$); while the bottom plots are when the tendon with $\mathrm{EA/m_w g} = 200$ is prestressed with $\mathrm{P_o} = \mathrm{m_w g}$. The left plots are when the structure is subjected to the Pacoima Dam/164 ground motion recorded during the 1971 San Fernando, California earthquake whereas the right plots are when the structure is subjected to the Erzincan NS ground motion recorded during the 1992 Erzincan, Turkey earthquake. The comparison of the OpenSees and Matlab solutions are in good agreement—in particular for the peak-response values and supports the use of the SDOF idealization introduced in Figure 3-1.

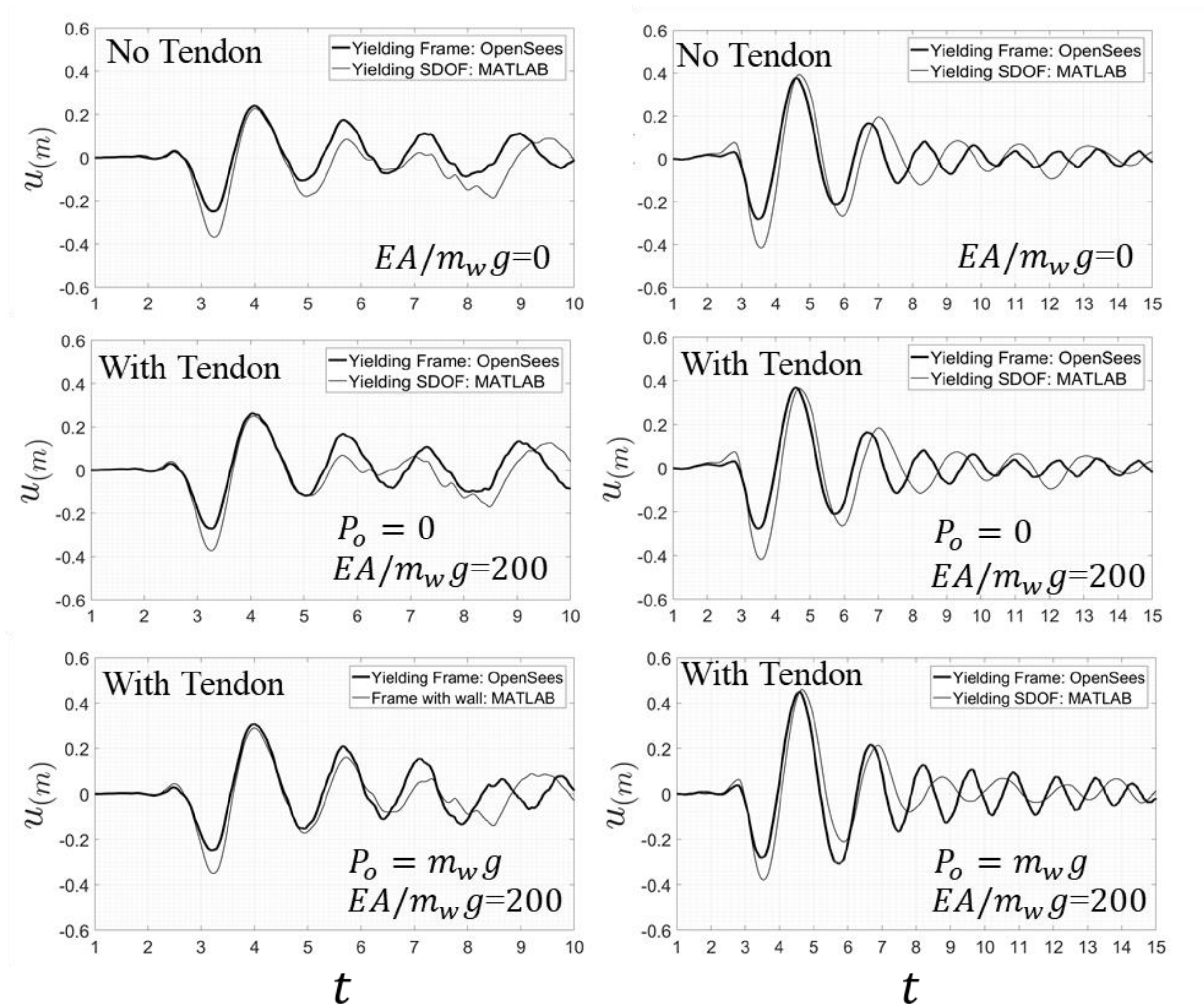

Figure 3-8 Comparison of the displacement time histories at mid-height of the 9-story steel building shown in Figure 6, computed with OpenSees with the displacement time-histories of the SDOF idealization shown in Figure 1, when excited with the 1971 Pacoima Dam/164, San Fernando, California (left) and the 1992 Erzincan NS, Turkey (right) ground motions.

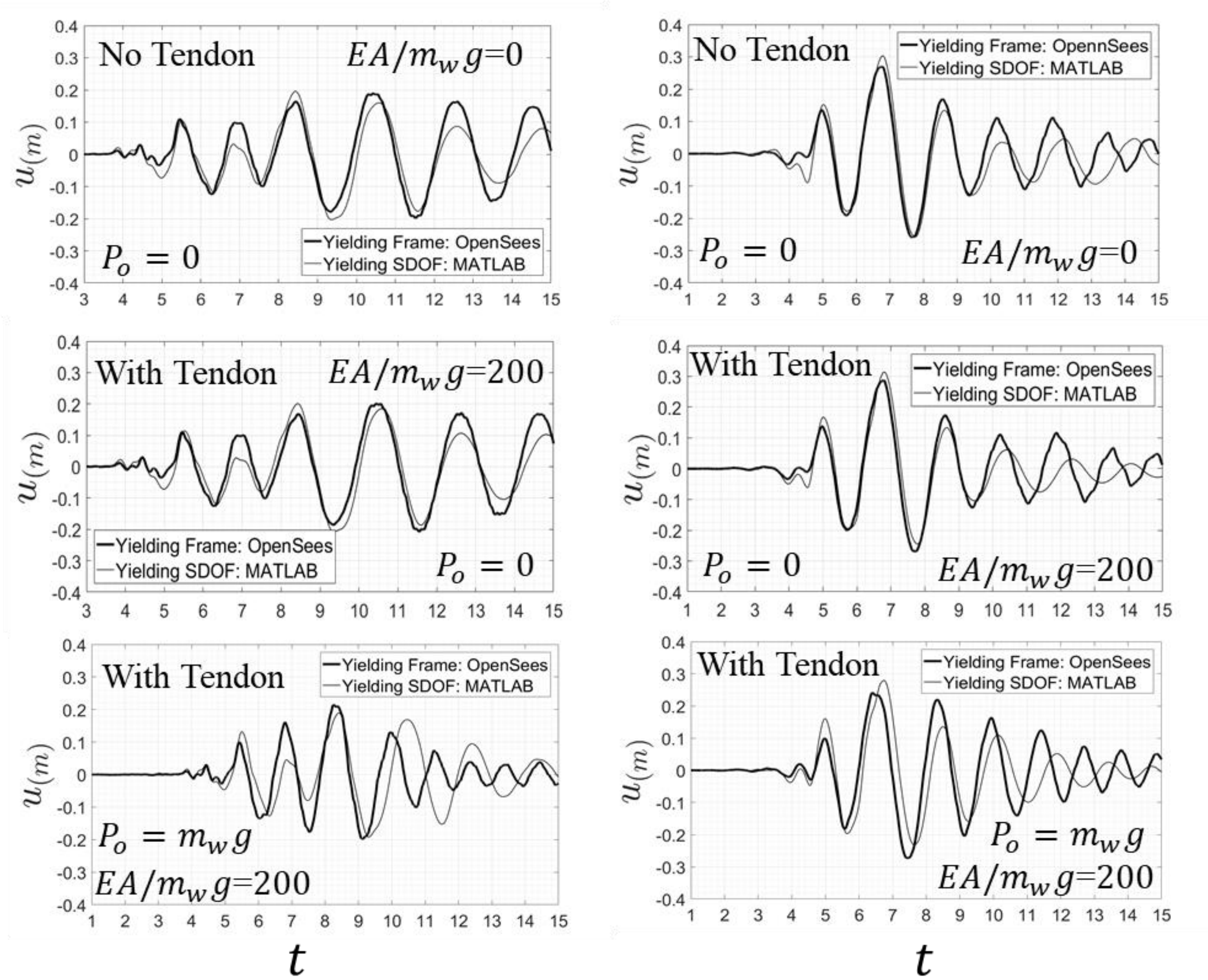

Figure 3-9 Comparison of the displacement time histories at mid-height of the 9-story steel building shown in Figure 6, computed with OpenSees with the displacement time-histories of the SDOF idealization shown in Figure 1, when excited with the 1994 Newhall/360, Northridge, California (left) and the 1995 Takarazuka/000, Kobe, Japan (right) ground motions.

Equally good comparisons are plotted in Figure 3-9 when the inelastic structure coupled with the rocking wall is subjected to the Newhall/360 ground motion recorded during the 1994 Northridge, California earthquake (left plots) and the Takarazuka/000 ground motion recorded during the 1995 Kobe, Japan earthquake.

3.6 EARTHQUAKE SPECTRA OF A YIELDING OSCILLATOR COUPLED WITH A ROCKING WALL

Following the verification of the single-degree of freedom idealization by comparing its response with that of the 9-story steel SAC building computed with OpenSees, the equations of motion 3.8 and 3.9 are used to generate inelastic response spectra.

Figure 3-10 plots displacement spectra of a yielding SDOF oscillator coupled with a vertically prestressed, stepping rocking wall when excited by the Newhall/360 ground motion recorded during the 1994 Northridge, California earthquake. The left plots are for a structure with a yielding strength $Q/m_s = 0.15g$; whereas, the right plots are for a weaker structure, $Q/m_s = 0.08g$. The first and most important observation is that the effect of vertical tendons even when they are stiff ($EA/(m_w\ g) = 200$) and highly prestressed ($p_o = m_w\ g$) is marginal. In contrast, the weight of the rocking wall has more noticeable effects with the heavier wall (σ=5) being more effective in some regions of the spectra. The same conclusions are drawn from the inelastic spectra presented in Figure 3-11 and Figure 3-12 where the inelastic structure-rocking wall system is excited by the Pacoima Dam/164 ground motion recorded during the 1971 San Fernando, California earthquake and the Erzincan NS ground motion recorded during the 1992 Erzincan, Turkey earthquake.

3.7 CONCLUSION

This chapter investigates the dynamic response of a yielding SDOF oscillator coupled with a vertically restrained, stepping rocking wall. The full nonlinear equations of motion were derived, and the dependability of the one-degree-of-freedom idealization is validated against the nonlinear time-history response analysis of the 9-story SAC steel building. The equations of motion of the SDOF idealization show explicitly that the contribution of vertical tendons, even when they are stiff, is two orders of magnitude less than the inertia forces on the moment frame-rocking wall system. This study offers a comprehensive parametric analysis which reaches the following conclusions.

The participation of the stepping rocking wall suppresses peak inelastic displacements with the heavier wall being in most cases more effective. In contrast, the effect of the vertical tendons even when they are stiff ($\frac{\mathrm{EA}}{\mathrm{m_w g}} = 200$) and highly prestressed ($\mathrm{P_o} = \mathrm{m_w g}$) is marginal. Given than the vertical tendons increase the vertical reactions at the pivoting corners by more than 50%, this chapter concludes that for medium- to high-rise buildings, vertical tendons in rocking walls are not recommended.

The SDOF idealization presented in this report compares satisfactory with finite-element analysis of a 9-story steel SAC building coupled with a stepping rocking wall; therefore, the SDOF idealization can be used with confidence for preliminary analysis and design.

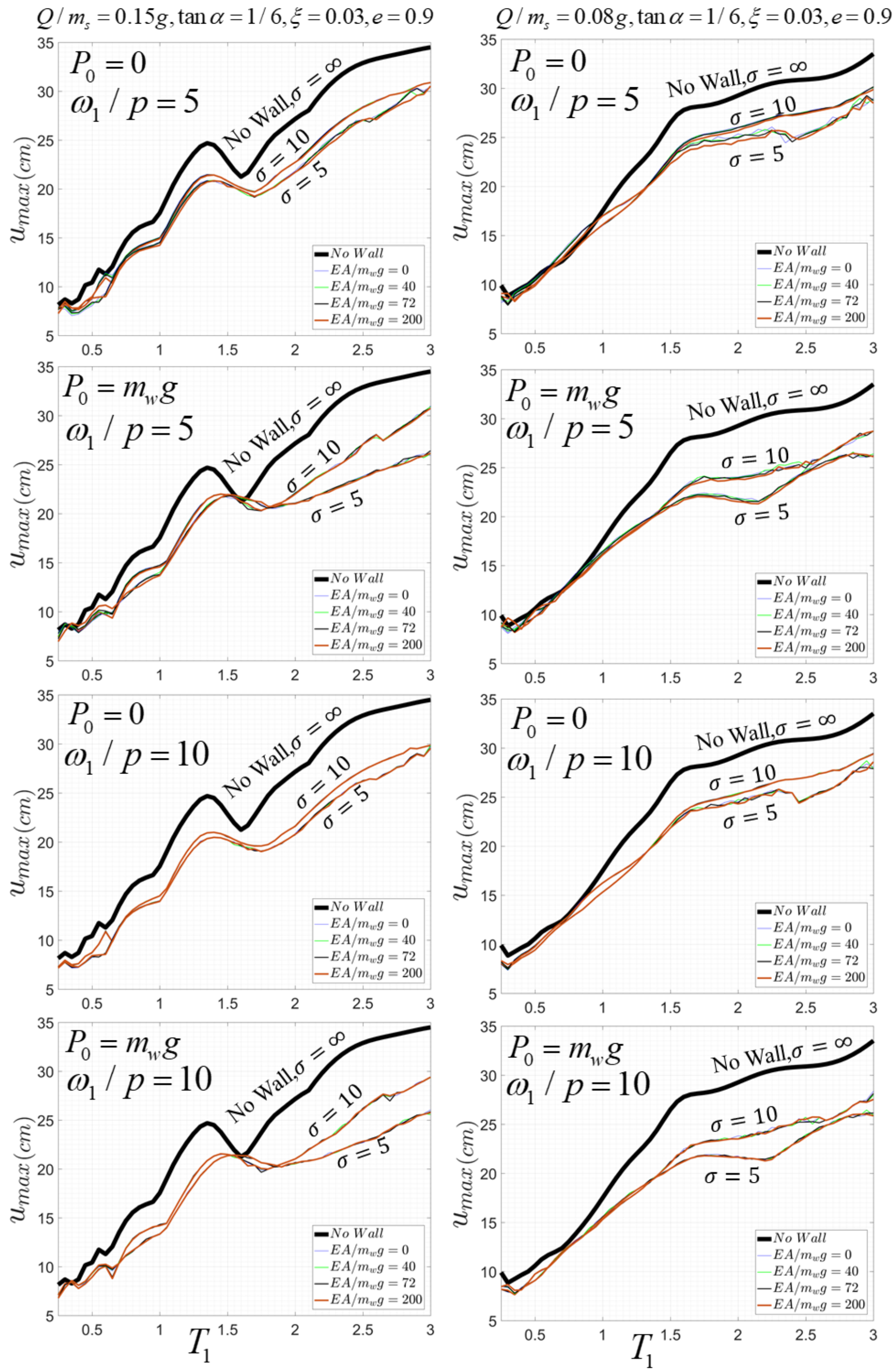

Figure 3-10 Displacement spectra of a yielding SDOF oscillator coupled with a vertically restrained stepping rocking wall with slenderness $\tan\alpha = 1/6$, for two valued of strength, $Q/m_s = 0.15g$ (left column) and $Q/m_s = 0.08g$ (right column) with mass ratios, $\sigma = 5, 10$ and ∞ (no wall); several values of tendon stiffness ($EA/m_w g$=0, 40, 72 and 200) with ($P_o = m_w g$) and without ($P_o = 0$) pre-tensioning when subjected to the Newhall/360 ground motion recorded during the 1994, Northridge California earthquake.

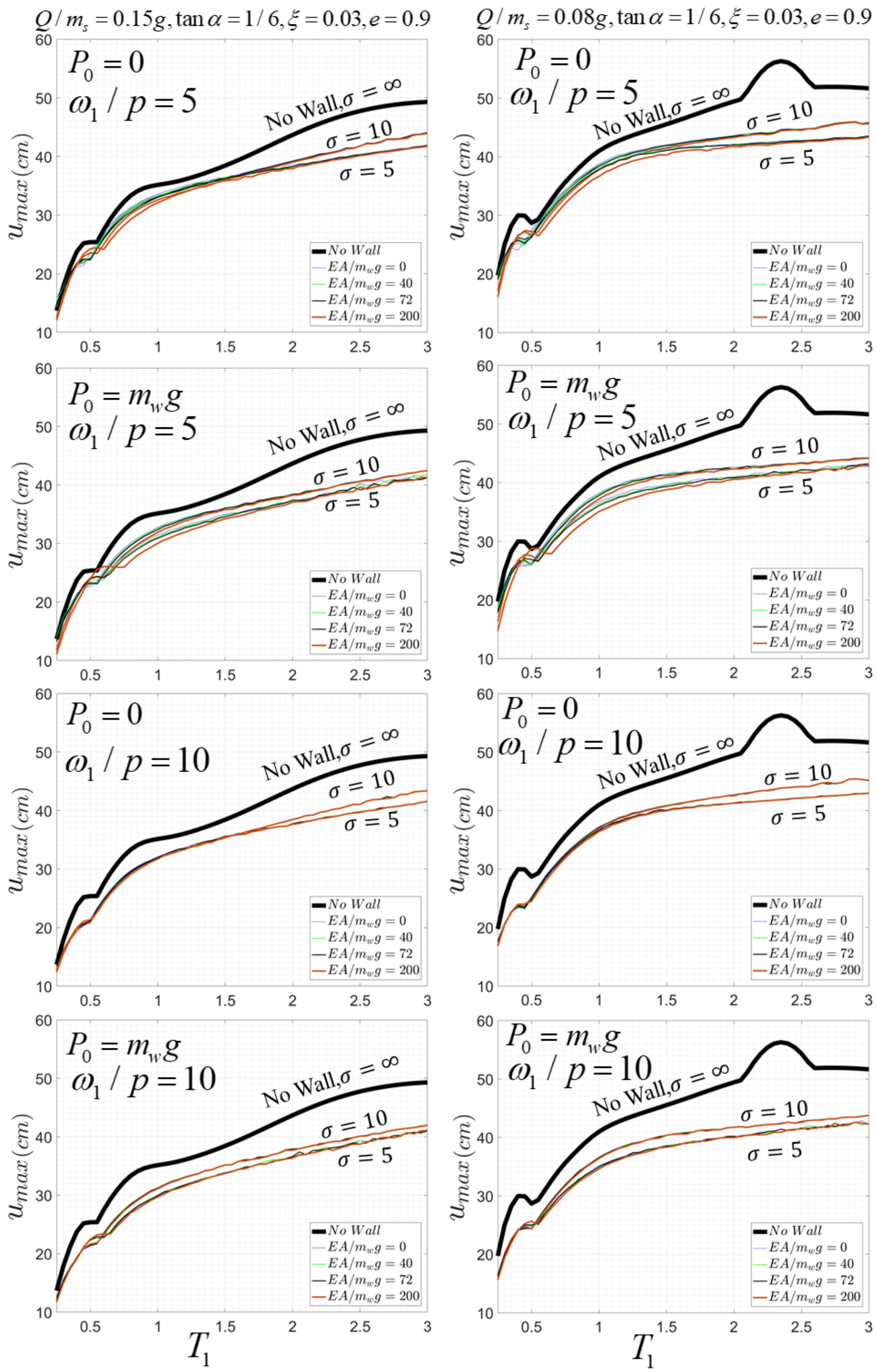

Figure 3-11 Displacement spectra of a yielding SDOF oscillator coupled with a vertically restrained stepping rocking wall with slenderness $\tan\alpha = 1/6$, for two valued of strength, $Q/m_s = 0.15g$ (left column) and $Q/m_s = 0.08g$ (right column) with mass ratios, $\sigma = 5, 10$ and ∞ (no wall); several values of tendon stiffness ($EA/m_w g$=0, 40, 72 and 200) with ($P_o = m_w g$) and without ($P_o = 0$) pre-tensioning when subjected to the Pacoima Dam/164 ground motion recorded during the 1971 San Fernando, California earthquake.

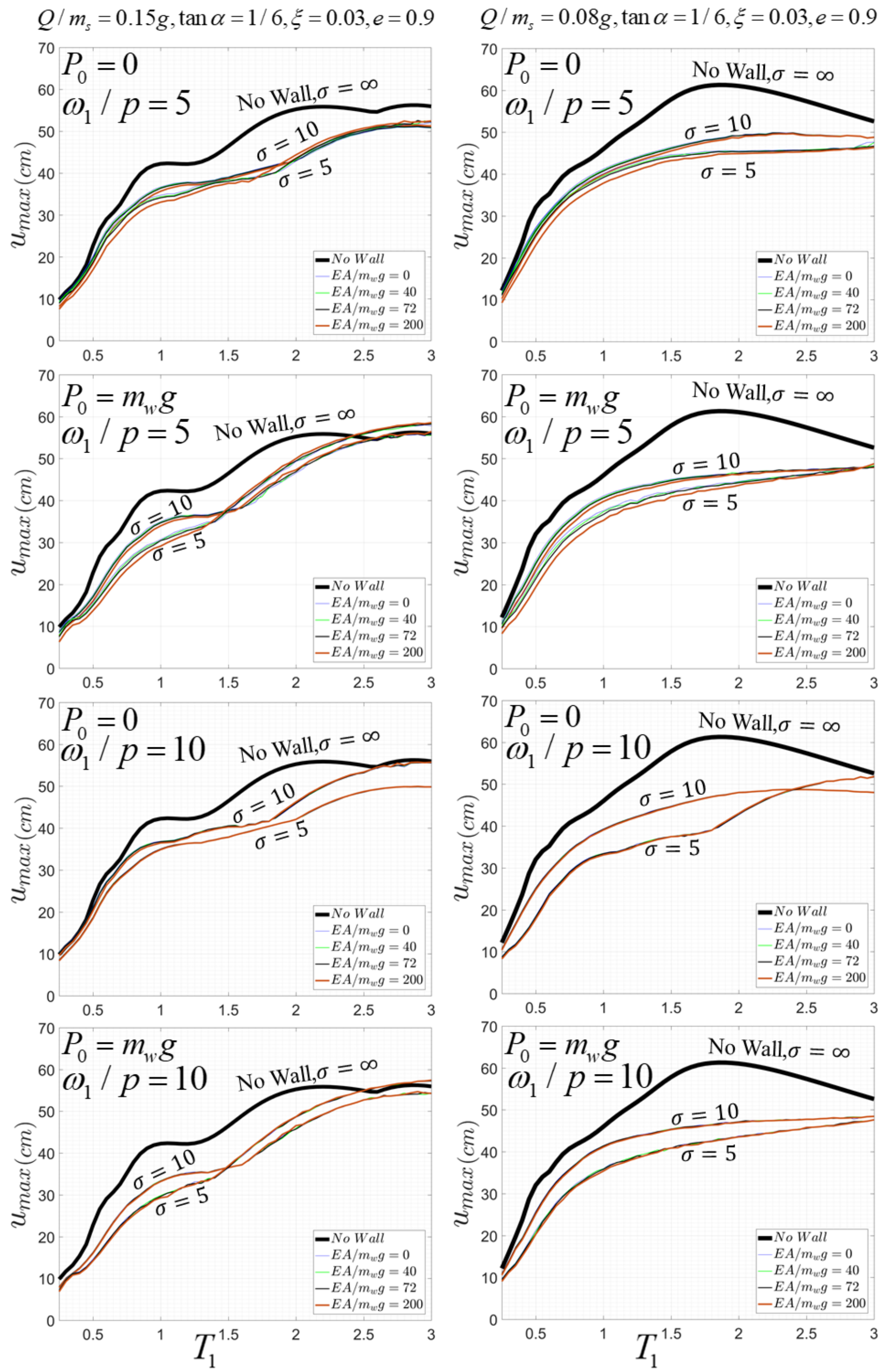

Figure 3-12 Displacement spectra of a yielding SDOF oscillator coupled with a vertically restrained stepping rocking wall with slenderness $\tan\alpha = 1/6$, for two valued of strength, $Q/m_s = 0.15g$ (left column) and $Q/m_s = 0.08g$ (right column) with mass ratios, $\sigma = 5, 10$ and ∞ (no wall); several values of tendon stiffness ($EA/m_w g$=0, 40, 72 and 200) with ($P_o = m_w g$) and without ($P_o = 0$) pre-tensioning when subjected to the Erzincan NS ground motion recorded during the 1992 Erzincan, Turkey earthquake.

4 VERTICAL DAMPERS/BRBS

The concept of coupling the lateral response of a moment resisting frame with a rigid core system goes back to the early works of Paulay (1969) and Fintel (1975) With this design, interstory drift demands are reduced at the expense of transferring appreciable shear-forces and bending moments at the foundation of the rigid core wall. In the early 1970s a new concept for seismic protection, by modifying the earthquake response of structures with specially designed supplemental devices, was brought forward in the seminal papers by Kelly et al. (1972) and Skinner et al. (1974) and implemented in important structures that were under design at that time such as the South Rangitikei Rail Bridge, (Beck and Skinner 1974; Skinner, Beck, et al. 1974; Kelly 1993) the Union Building (Boardman et al. 1983) and the Wellington Central Police Station in Auckland, New Zealand (Charleson et al. 1987).

Clearly, the paper by Kelly et al. (1972) marks the beginning of the use of response modification devices for the seismic protection of structures and among several original contributions it suggests the use of rocking shear-walls in association with energy dissipation devices for the seismic protection of moment-resisting frames (Fig. 2 of the paper by Kelly et al. (1972) that is reproduced in this chapter as Figure 4-1)). In this way, the stepping core wall does not suffer from large ductility demands and possible cyclic degradation while recentering happens due to gravity. Despite its remarkable originality and technical merit, the paper by Kelly et al. (1972) did not receive the attention it deserved, and it was some two decades later that the PRESSS Program (Priestley 1991, 1996) reintroduced the concept of uplifting and rocking of the joint shear wall system (Nakaki et al. 1999; Priestley et al. 1999).

Following the PRESSS program a number of publications presented experimental and analytical studies on the cyclic loading of structural systems coupled with vertically restrained rocking walls (Kurama et al. 1999, 2002). Given that damping during impact as the wall alternate pivot points is low, (Beck and Skinner 1972, 1974; Makris 2014b) the idea of introducing supplemental energy dissipation devices in structural systems coupled with rocking walls received revived attention (Holden et al. 2003; Ajrab et al. 2004; Filiatrault et al. 2004; Lu 2005) some 30 years after the original idea presented by Kelly et al. (1972). These subsequent studies were partly motivated from the need to eliminate the generation of a weak-story failure in multi-story buildings together with the need to ensure recentering of the yielding frame (Alavi and Krawinkler 2004b; Toranzo et al. 2009; Nicknam and Filiatrault 2014). At the same time alternative proposals with the use of pinned rocking walls, (C. E. Grigorian et al. 2015; Qu et al. 2012; Wada et al. 2011) where the weight of the wall works against the stability of the structure motivated a series of recent studies that revisited the dynamics of a moment-resisting frame coupled with a rocking wall either stepping or pinned (Aghagholizadeh and Makris 2018a, 2018b) by accounting explicitly of the role of the of the rotational inertia of the rocking wall. These studies led to valuable conclusions associated with the challenges that emerge when pinned rocking walls are used, and that vertical tendons in tall, stiff, stepping rocking walls have marginal contribution even when they offer a high axial stiffness (Aghagholizadeh and Makris 2018b).

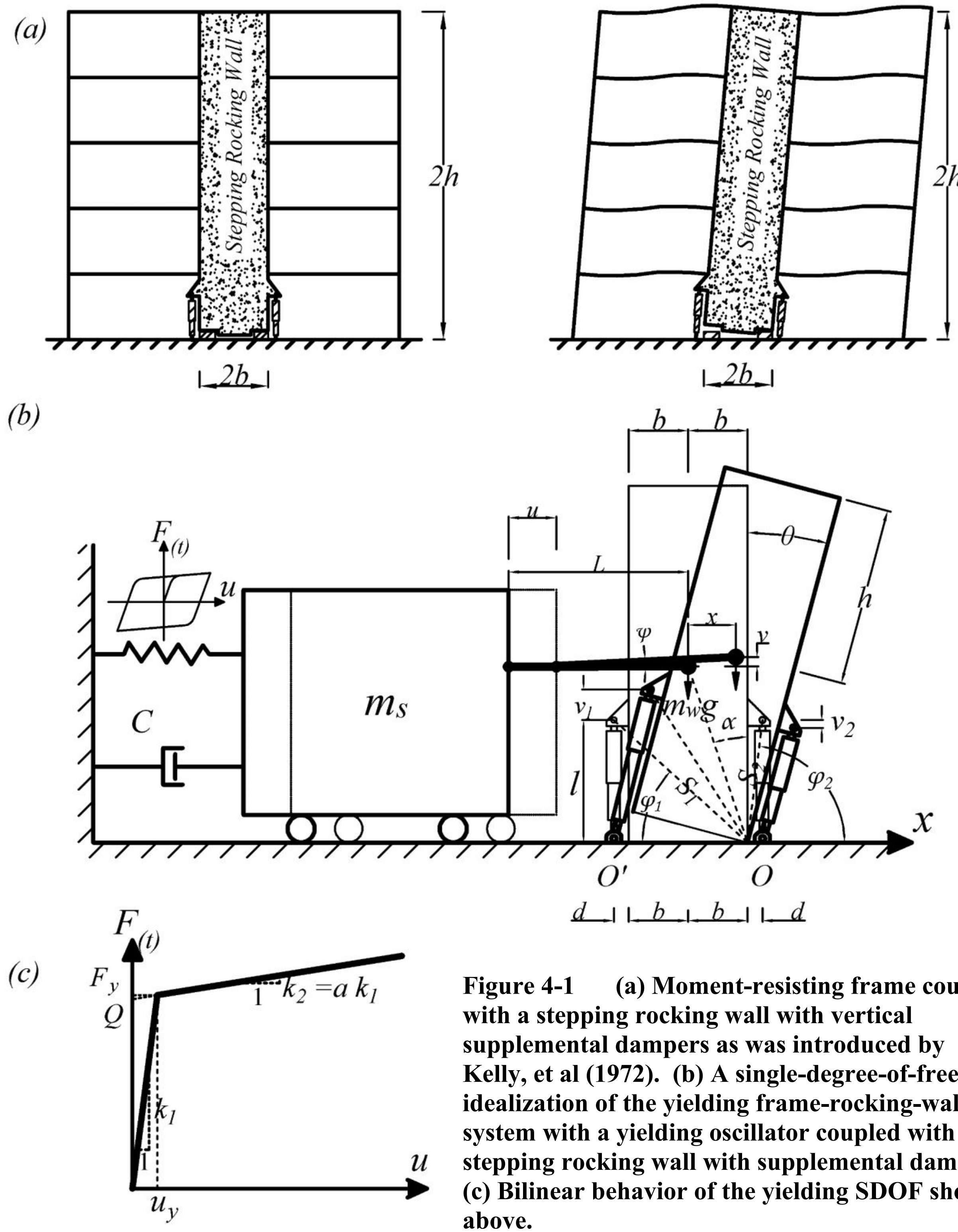

Figure 4-1 (a) Moment-resisting frame coupled with a stepping rocking wall with vertical supplemental dampers as was introduced by Kelly, et al (1972). (b) A single-degree-of-freedom idealization of the yielding frame-rocking-wall system with a yielding oscillator coupled with a stepping rocking wall with supplemental dampers. (c) Bilinear behavior of the yielding SDOF shown above.

In view of these recent findings, this chapter examines the contribution of viscous and hysteretic dampers to the response of a yielding frame coupled with a rocking wall shown in Figure 4-1.

4.1 DYNAMICS OF A YIELDING OSCILLATOR COUPLED TO A ROCKING WALL WITH SUPPLEMENTAL DAMPING

With reference to Figure 4-1 (b), this study examines the dynamic response of a yielding single-degree-of-freedom (SDOF) structure, with mass, m_s, pre-yielding stiffness, k_1, post-yielding stiffness, k_2 and strength, Q, that is coupled with a free-standing stepping rocking wall of size, $R=\sqrt{b^2+h^2}$, slenderness, $\tan\alpha = b/h$, mass m_w and moment of inertia about the pivoting (stepping) points O and O', $I=4/3m_wR^2$. Vertical energy dissipation devices are mounted to the rocking wall at a distance, d, from the pivoting points of the wall as shown in Figure 4-1 (b) and Figure 4-2. In the interest of simplicity, it is assumed that the arm with length L, that couples the motion is articulated at the center mass of the rocking wall at a height, h from its foundation as shown in Figure 4-1 (b).

4.1.1 Kinematics of the SDOF Yielding Oscillator-Rocking Wall System

During rocking motion of the wall, the upward displacement; v_1 of the damper appended at the side of the wall across the pivoting point is

$$v_1 = S_1[\sin(\phi_1 \pm \theta) - \sin\phi_1] \tag{4-1}$$

whereas the downward displacement; v_2 of the damper appended at the side of the wall that is stepping on the pivoting point is

$$v_2 = S_2[\sin\phi_2 - \sin(\phi_2 \mp \theta)] \tag{4-2}$$

where $S_1=\sqrt{(2b+d)^2+l^2}$, $S_2=\sqrt{d^2+l^2}$, $sin\phi_1 = l/S_1$ and $\sin\phi_2 = l/S_2$.

The elongation of damper, e_1 appended at the side of the column across the pivoting point is: $e_1=\delta_1 - l$, where δ_1 is offered by the cosine rule:

$$\delta_1 = S_1\sqrt{1+\cos^2\varphi_1 - 2\cos\varphi_1\cos(\varphi_1 \pm \theta)} \tag{4-3}$$

and by using that $e_1=\delta_1 - l$, the elongation of the damper is

$$e_1(t) = S_1\left[\sqrt{1+\cos^2\varphi_1 - 2\cos\varphi_1\cos(\varphi_1 \pm \theta)} - \sin\varphi_1\right] \tag{4-4}$$

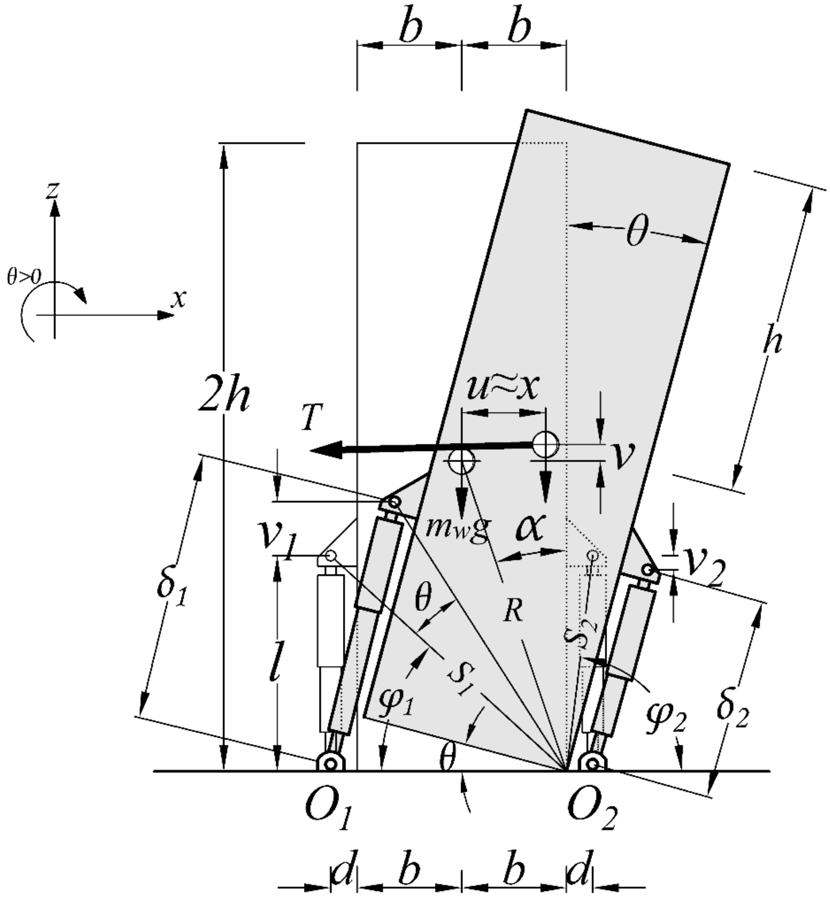

Figure 4-2 Geometric quantities pertinent to the dynamic analysis of a rocking wall with additional energy dissipators.

The time derivative of the elongation $e_1(t)$ is expressed in terms of the independent variable θ and its time derivative, $\dot{\theta}$:

$$\dot{e}_1(t) = \frac{S_1 \cos\varphi_1 \dot{\theta} \sin(\varphi_1 \pm \theta)}{\sqrt{1+\cos^2\varphi_1 - 2\cos\varphi_1 \cos(\varphi_1 \pm \theta)}} \tag{4-5}$$

Similarly, the contraction of the dampers appended at the side of the column that is stepping on the pivoting point is $e_2 = l - \delta_2$, where δ_2 is

$$\delta_2 = S_2 \sqrt{1+\cos^2\varphi_2 - 2\cos\varphi_2 \cos(\varphi_2 \mp \theta)} \tag{4-6}$$

and by using that $e_2 = l - \delta_2$, the contraction of the damper is

$$e_2(t) = S_2\left[\sin\varphi_2 - \sqrt{1+\cos^2\varphi_2 - 2\cos\varphi_2\cos(\varphi_2 \mp \theta)}\right] \tag{4-7}$$

The time derivative of the contraction $e_2(t)$ is expressed in terms of the independent variable θ and its time derivative, $\dot{\theta}$ (Makris and Aghagholizadeh 2019; Aghagholizadeh and Makris 2021)

$$\dot{e}_2(t) = \frac{S_2\cos\varphi_2\dot{\theta}\sin(\varphi_2 \mp \theta)}{\sqrt{1+\cos^2\varphi_2 - 2\cos\varphi_2\cos(\varphi_2 \mp \theta)}} \tag{4-8}$$

4.1.2 Constitutive Laws of Non-Linear Viscous and Hysteretic Dissipation Devices

The energy dissipation devices appended to the rocking wall as shown in Figure 4-2 can be either linear or nonlinear fluid dampers (Wada et al. 1989; Black et al. 2002, 2004) or hysteretic (yielding) dampers such as torsionally yielding steel-dampers, (Kelly et al. 1972; Skinner, Kelly, et al. 1974) or buckling restrained braces (Bouc 1967; Wen 1976; Baber and Wen 1981; Makris and Chang 2000).

When nonlinear fluid dampers are employed, their force-displacement relation follows a power-law:

$$F_d = C_q|\dot{e}(t)|^q \operatorname{sgn}\left[\dot{e}(t)\right] \tag{4-9}$$

where $0 < q < 1$ is the exponent of the damper, C_q is the damping constant with units: $[m]\ [L]^{1-q}\ [T]^{q-2}$, and $sgn[\ ]$ is the signum function *e(t)* is the stroke of the damper that is given by equation (4-1) when the damper is in elongation ($e(t) = e_1$(t)) and by equation (4-7) when the damper is in contraction ($e(t) = e_2(t)$). When $q=1$, equation (4-9) reduces to a linear viscous law: $F_d = c_1\dot{e}(t)$.

When torsionally yielding steel-beam dampers, buckling restrained braces (BRBs) or other yielding devices are used, their constitutive law can be expressed by the Bouc-Wen model (Constantinou and Adnane 1987; Makris and Aghagholizadeh 2019)

$$F_d = a_d k_d\, e(t) + (1-a_d)k_d\, u_{yd}\, z_d(t) \tag{4-10}$$

in which, k_d is the pre-yielding stiffness of the device, u_{yd} is the yield displacement, a_d is the post-to-pre- yielding stiffness ratio and $z_d(t)$ is the dimensionless internal variable described by

$$\dot{z}_d(t) = \frac{1}{u_{yd}}\left[\dot{e}(t) - \beta\dot{e}(t)\left|z_d(t)\right|^n - \gamma\left|\dot{e}(t)\right|z_d(t)\left|z_d(t)\right|^{n-1}\right] \tag{4-11}$$

Again, *e(t)* is the stroke of the hysteretic device that is given by equation (4-1) when the damper is in elongation ($e(t) = e_1(t)$) and by equation (4-7) when the damper is in contraction ($e(t) = e_2$(t)). In equation (4-11), constants β, γ and n are model parameters to be discussed later in the chapter. When $\beta + \gamma = 1$, the dimensionless parameter, $z_d(t)$ is bounded $-1 \leq z_d(t) \leq 1$ (Kunnath et al. 1997).

4.1.3 Equation of Motion of the Entire System

For positive rotation ($\theta > 0$):

For positive rotations ($\theta > 0$), dynamic equilibrium of the rotating wall with mass, m_w, equipped with vertical dampers installed on each of its side as shown in Figure 4-1 (b) and Figure 4-2 gives

$$I\ddot{\theta} = -TR\cos(\alpha-\theta) - m_w gR\sin(\alpha-\theta) - m_w\ddot{u}_g R\cos(\alpha-\theta) - F_{d_1}r_1 - F_{d_2}r_2 \tag{4-12}$$

in which F_{d_1} and F_{d_2} are the damping forces from the damper across the pivoting point and from the damper at the pivoting point side respectively and r_1 and r_2 are moment arms of the damper forces about the pivoting point

$$r_1 = S_1\cos\varphi_1 \frac{\sin(\varphi_1 \pm \theta)}{\sqrt{1+\cos^2\varphi_1 - 2\cos\varphi_1\cos(\varphi_1 \pm \theta)}} \tag{4-13}$$

$$r_2 = S_2\cos\varphi_2 \frac{\sin(\varphi_2 \mp \theta)}{\sqrt{1+\cos^2\varphi_2 - 2\cos\varphi_2\cos(\varphi_2 \mp \theta)}} \tag{4-14}$$

The axial force *T* appearing in equation (4-12) is replaced with the help of equations (2.5) and (2.6); whereas, for a rectangular stepping wall, $I = 4/3m_w R^2$. Accordingly, equation (4-12) assumes the form:

$$\begin{aligned}&\frac{4}{3}m_w R^2\ddot{\theta} + \left[m_s(\ddot{u}+\ddot{u}_g) + ak_1u(t) + (1-a)k_1u_y z(t) + c\dot{u}\right]R\cos(\alpha-\theta)\\ &= -m_w R\left[\ddot{u}_g\cos(\alpha-\theta) + g\sin(\alpha-\theta)\right] - F_{d_1}r_1 - F_{d_2}r_2\end{aligned} \tag{4-15}$$

upon dividing with m_w R equation (4-15) gives:

$$\frac{4}{3}R\ddot{\theta}+\left[\sigma(\ddot{u}+\ddot{u}_g)+a_s\frac{k_{1s}}{m_w}u(t)+(1-a_s)\frac{k_{1s}}{m_w}u_{ys}z_s(t)+\frac{c_s}{m_w}\dot{u}\right]\cos(\alpha-\theta)$$
$$=-\left[\ddot{u}_g\cos(\alpha-\theta)+g\sin(\alpha-\theta)\right]-\frac{F_{d_1}}{m_w}\frac{r_1}{R}-\frac{F_{d_2}}{m_w}\frac{r_2}{R} \tag{4-16}$$

in which $\sigma = m_s/m_w$ is the mass ratio parameter.

Substitution of the expressions of the relative displacement, velocity and acceleration given by equations (2.2) to (2.4) for positive rotations, and after dividing with R, equation (4-16) is expressed only in terms of the variable, $\theta(t)$.

$$\left(\frac{4}{3}+\sigma\cos^2(\alpha-\theta)\right)\ddot{\theta}+\sigma\cos(\alpha-\theta)\Big[a\omega_1^2(\sin\alpha-\sin(\alpha-\theta))+2\xi\omega_1\dot{\theta}\cos(\alpha-\theta)$$
$$+\dot{\theta}^2\sin(\alpha-\theta)+(1-a)\omega_1^2\frac{u_y}{R}z(t)\Big]$$
$$=-\frac{g}{R}\left[(\sigma+1)\frac{\ddot{u}_g}{g}\cos(\alpha-\theta)+\sin(\alpha-\theta)+\frac{F_{d_1}}{m_w g}\frac{r_1}{R}+\frac{F_{d_2}}{m_w g}\frac{r_2}{R}\right] \tag{4-17}$$

<u>*For negative rotation ($\theta < 0$):*</u>

For negative rotations one can follow the same reasoning and the equation of the coupled system is:

$$\left(\frac{4}{3}+\sigma\cos^2(\alpha+\theta)\right)\ddot{\theta}-\sigma\cos(\alpha+\theta)\Big[a\omega_1^2(\sin\alpha-\sin(\alpha+\theta))-2\xi\omega_1\dot{\theta}\cos(\alpha+\theta)$$
$$+\dot{\theta}^2\sin(\alpha+\theta)-(1-a)\omega_1^2\frac{u_y}{R}z(t)\Big]$$
$$=-\frac{g}{R}\left[(\sigma+1)\frac{\ddot{u}_g}{g}\cos(\alpha+\theta)-\sin(\alpha+\theta)+\frac{F_{d_1}}{m_w g}\frac{r_1}{R}+\frac{F_{d_2}}{m_w g}\frac{r_2}{R}\right] \tag{4-18}$$

In equations (4-17) and (4-18), the terms multiplied with the parameter $\sigma = m_s/m_w$ are associated with the dynamics of the nonlinear oscillator whereas the remaining terms are associated with the dynamics of the rocking wall with vertical dampers. When the yielding oscillator is absent ($\sigma = \omega_1 = \xi = 0$), equations (4-17) and (4-18) reduce to the equations of motion of the free-standing rocking wall equipped with dampers (Makris and Aghagholizadeh 2019).

4.2 PARAMETERS OF THE PROBLEM

The Bouc-Wen model described by equations (2.6) and (2.7) is a phenomenological model of hysteresis that essentially builds on the bilinear idealization shown in the bottom of Figure 4-1. Only three of the five constitutive parameters (k_1= pre-yielding stiffness, k_2= post-yielding stiffness, u_y= yield displacement, Q= strength and F_y= yielding force) of the bilinear Bouc-Wen model are independent and needed to be defined.

In this work, the authors select the pre-yielding stiffness $k_1 = m\,\omega_1^2$, the post-yielding stiffness $k_2 = a\,k_1$ and the strength of the structure Q. With reference to Figure 4-1 (bottom), $F_y = k_1\,u_y = Q + k_2\,u_y$. Accordingly, $u_y = Q/(k_1 - k_2)$ and $F_y = k_1\,Q/(k_1 - k_2)$. The parameters β, γ and n appearing in equation (2.7) are established from past studies on the parameter identification of yielding concrete structures and assume the values: $\beta = 0.95, \gamma = 0.05$ and $n = 2$ (Goda et al. 2009; Kunnath et al. 1997). With the parameters $\beta = 0.95, \gamma = 0.05$ and $n = 2$ being established, the peak inelastic displacement, u_{max} of the SDOF system shown in the Figure 4-1 (bottom) is a function of the following parameters:

$$u_{max} = f\left(T_1, \frac{Q}{m_s}, a, \xi, p, \tan\alpha, \sigma, g, \frac{F_d}{m_w}, d, \textit{parameters of excitation}\right) \tag{4-19}$$

where $T_1 = \frac{2\pi}{\omega_1} = 2\pi\sqrt{\frac{m_s}{k_1}}$ is the pre-yielding natural periods of the SDOF oscillator when decoupled from the rocking wall.

Here, it is assumed that upon yielding, the structure maintains a mild, positive, post-yielding stiffness = $k_2 = 0.05k_1$, therefore $a = 0.05$ (Goda et al. 2009; Kunnath et al. 1997). Furthermore, it is assumed that the pre-yielding damping ratio, $\xi = c_s/(2m_s\omega_1) = 0.03$ and that the rocking wall assumes a slenderness, $\tan\alpha = 1/6$. F_d/m_s are the supplemental normalized damping forces from the vertical dampers appended to the rocking wall expressed either by equation (4-9) when nonlinear fluid dampers are used, or equation (4-10) when hysteretic yielding steel dampers are used.

When the dampers are attached at the pivoting points of the rocking wall ($l = \phi_1 = \phi_2 = d = S_2 = 0 \textit{ and } S_1 = 2b$), they become essentially zero-length elements (as is the configuration of the torsionally yielding steel beam dampers installed in the piers of the South Rangitikei Rail Bridge (Makris et al. 2019; Skinner et al. 1974)), equations (4-4) and (4-5) simplifies to:

$$e_1(t) = 2\sqrt{2}b\sqrt{1-\cos\theta} \qquad \textit{and} \qquad \dot{e}_1(t) = \sqrt{2}b\dot{\theta}\sqrt{1+\cos\theta} \tag{4-20}$$

while

$$r_1(t) = \sqrt{2}\,\frac{b\sin\theta}{\sqrt{1-\cos\theta}} \tag{4-21}$$

with $e_2(t) = \dot{e}_2(t) = r_2(t) = 0$.

For small rotations $\cos\theta = 1-\theta^2/2$ and $\sin\theta = \tan\theta = \theta$, therefore, the expressions given by equations (4-20) and (4-21) further simplify to

$$e_1(t) = 2b\theta(t)\ , \qquad \dot{e}_1(t) = 2b\dot{\theta}(t) \quad and \quad r_1(t) = 2b\frac{\sin\theta}{\theta} \approx 2b \tag{4-22}$$

When torsionally yielding steel beam dampers, buckling restrained braces (BRBs) or other yielding devices are used, the strength of the hysteretic devices, $(1-a_d)K_d u_{yd}$ is taken as a fraction of the strength of the nonlinear spring of the structure Q. Accordingly

$$(1-a_d)k_d u_{yd} = \epsilon Q \tag{4-23}$$

In terms of the weight of the rocking wall, $m_w\ g$ the strength of the supplemental yielding dampers at the sides of the wall is

$$\frac{(1-a_d)k_d u_{yd}}{m_w g} = \epsilon\frac{m_s}{m_w}\frac{Q}{m_s g} = \epsilon\sigma\frac{Q}{m_s g} \tag{4-24}$$

So assuming a typical structural strength $Q = 0.1m_s\ g$ and that each of the supplemental yielding dampers have 20% of that strength ($\epsilon = 0.2$), for a wall when $\sigma = m_s/m_w = 10$, the normalized strength of the supplemental yielding damper to the weight of the rocking wall is $\frac{(1-a_d)k_d u_{yd}}{m_w g} = 0.1\times 10\times 0.2 = 0.2$. In this study the parametric analysis includes values of ϵ up to $\epsilon = 0.5$ so that the benefits of a rocking wall are not suppressed from the presence of over strength yielding devices.

By comparing the right-hand side of the equations (4-9) and (4-10) in association with equation (4-22), the peak damping force from a nonlinear viscous damper, $C_q\left|2b\dot{\theta}_{max}\right|^q$, will match the yielding capacity of a hysteretic, yielding damper when

$$C_q = \frac{(1-a_d)k_d u_{yd}}{(2b\dot{\theta}_{max})^q} = \frac{\epsilon Q}{(2b\dot{\theta}_{max})^q} \tag{4-25}$$

Before proceeding with earthquake response spectra, Figure 4-3 plots force-displacement loops, together with displacement, $u(t)$ and rotation $\theta(t)$ time histories for a structure having $T_1 = 1.2s$ and $Q/m_s = 0.08g$, that is coupled with a rocking wall with $\omega_1/p = 5$ ($p = 1.05\ rad/sec$) and $\sigma = m_s/m_w = 5$ when excited by the CO2/065 ground motion recorded during the 1966 Parkfield, California earthquake. The heavy line plots the inelastic response of the structure without wall, whereas the heavy dashed line plots the inelastic response of the structure coupled to the rocking wall without dampers on its sides. Figure 4-3 (a) indicates that the participation of the stepping rocking wall (which in this case has appreciable weight, $\sigma = m_s/m_w = 5$) suppresses the peak inelastic displacement; yet most importantly it eliminates permanent displacements. The thin solid lines plot the inelastic response of the structure coupled to the rocking wall with hysteretic damper (say Buckling Restrained Braces) where each damper delivers a yield strength, $(1-a_d)k_d u_{yd}$, equal to 1/2 of the strength of the structure, Q, $(\epsilon = (1-a_d)k_d u_{yd} / Q = 0.5)$ and uncovers that the presence of supplemental dampers along the sides of the wall have a marginal effect. Similar trends are observed in Figure 4-3 (e) which shows the response of the same yielding frame-rocking wall system in which $C_1 = \frac{\epsilon Q}{2b\dot{\theta}_{max}} = 1217$ kNs/m=1217 Mg/s. Again, the effect of the viscous dampers that deliver a peak viscous force of the viscous force of the order of 20% of the weight of the wall $m_w g$ is marginal.

Figure 4-4 plots force-displacement loops, together with displacement $u(t)$, velocity $\dot{\theta}$, time histories for the same structural system examined in Figure 4-3, yet with larger yielding strength, $Q/m_s = 0.15g$ when excited by the Newhall/360 ground motion recorded during 1994 Northridge, California earthquake. Similar trends to theses reported from the findings shown on Figure 4-3 are observed with the supplemental dampers having a marginal effect on the response, despite producing peak-output forces of the order of 30% of the weight of the rocking wall.

In terms of the strength of the inelastic structure, Q, the ratio F_d/Q is computed from the identity

$$\frac{F_d}{Q} = \frac{F_d}{m_w g}\frac{m_w g}{Q} = \frac{F_d}{m_w g}\frac{m_w}{m_s}\frac{m_s g}{Q} = \frac{F_d}{m_w g}\frac{1}{\sigma}\frac{m_s g}{Q} \tag{4-26}$$

So with reference to Figure 4-3 (d) for $\sigma = 5$, $Q = 0.08 m_s g$ and an approximate peak value of $F_{d,max}/m_w g = 0.35$ equation (4-26) gives a value of $F_{d,max}/Q = 0.875$. Accordingly, the peak forces originating from the vertical dampers placed along the sides of the rocking wall are of the same order of magnitude as the strength of the yielding structure. Clearly higher values of supplemental damping forces can be used; yet it needs to be recognized, that as the strength of the yielding dampers further increase, the entire response modification strategy tends to an “added strength” strategy rather to an “added damping” strategy.

The dependability of the SDOF idealization shown in Figure 4-1 (b) has been examined and confirmed with the results obtained with the open-source code OpenSees when analyzing the nine-story moment resisting steel structure designed for the SAC Phase II Project by the authors in the previous works (Aghagholizadeh and Makris 2018a, 2018b). This nine-story structure that is well-known to the literature (Gupta and Krawinkler 1999; Chopra and Goel 2002) was designed to meet the seismic code (pre-Northridge Earthquake) and represents typical medium-rise buildings designed for the greater area of Los Angeles, California. Accordingly, this study proceeds with the generation of earthquake spectra of a yielding oscillator coupled to a rocking wall with supplemental damping shown in in Figure 4-1 (b).

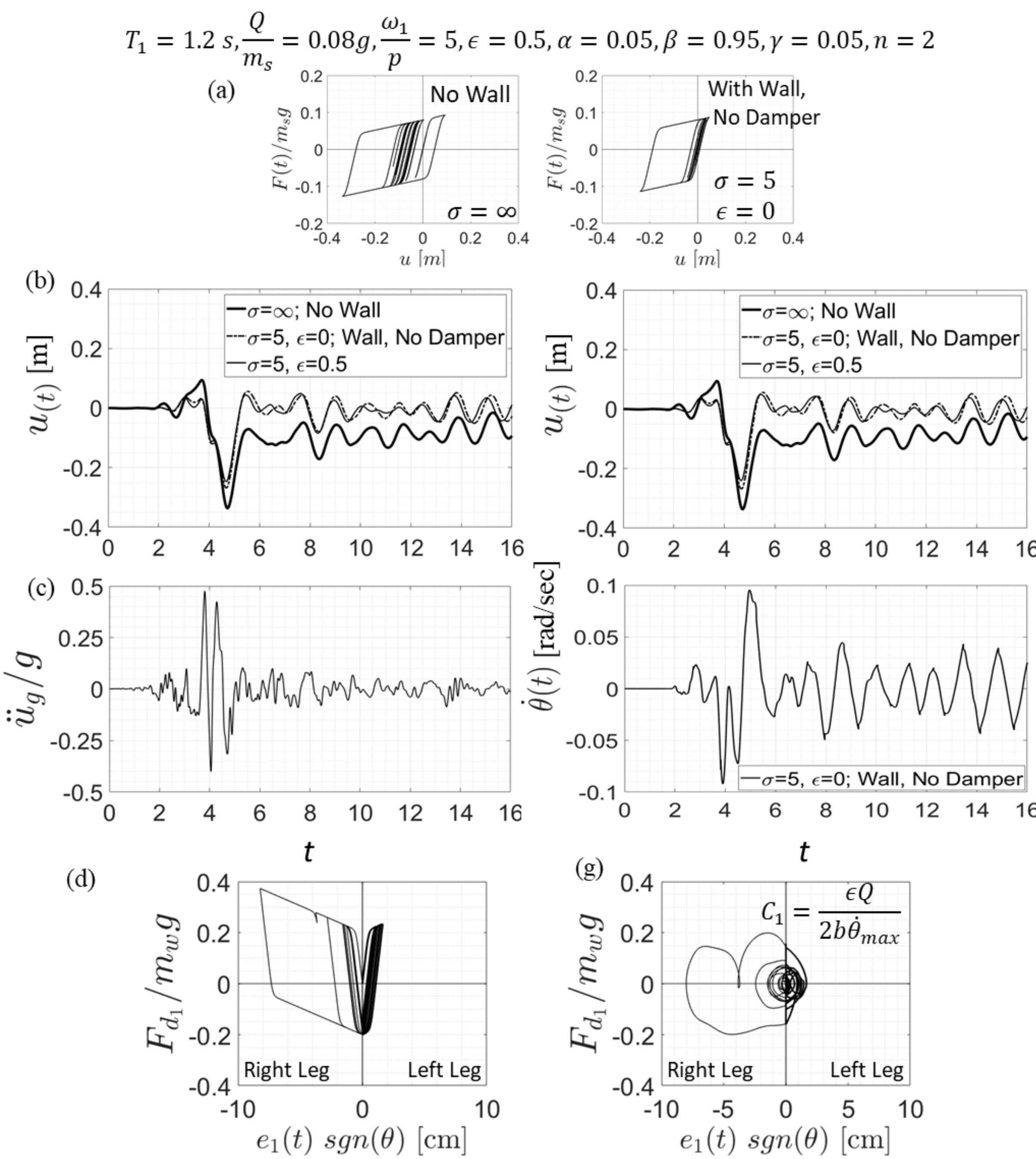

Figure 4-3 Time history analysis of a nonlinear SDOF oscillator coupled with a vertically damped stepping rocking wall with normalized strength $Q/m_s = 0.08g$, mass ratio, $\sigma = m_s/m_w = 5$, wall size, $\omega_1/p = 5$, and pre-yielding period of $T_1 = 1.2sec$, when subjected to the CO2/065 ground motion recorded during the 1966 Parkfield, California earthquake. Heavy solid lines: No wall. Heavy dashed lines: Rocking wall without damper. Thin solid lines: Wall with dampers (hysteretic (left) and linear viscous (right)) ($\epsilon = 0.5$ and $\dot{\theta}_{max} = 0.10\ rad/sec$) zero-length dampers. Bottom: Force-displacement loops of the hysteretic (left) and linear (right) dampers installed at each leg of the rocking wall.

$$T_1 = 1.2\ s, \frac{Q}{m_s} = 0.15g, \frac{\omega_1}{p} = 5, \epsilon = 0.5, \alpha = 0.05, \beta = 0.95, \gamma = 0.05, n = 2$$

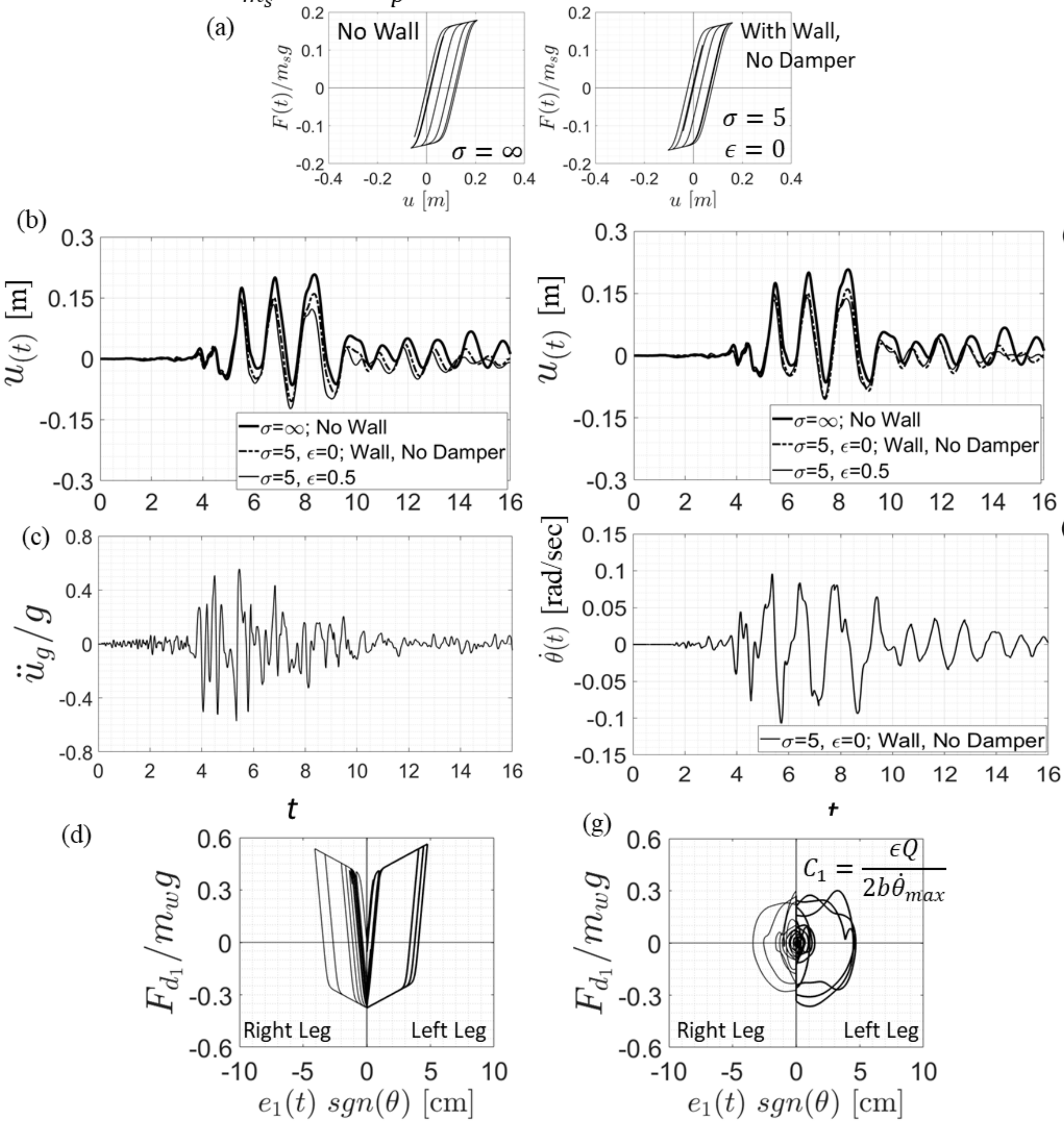

Figure 4-4 Time history analysis of a nonlinear SDOF oscillator coupled with a vertically damped stepping rocking wall with normalized strength $Q/m_s = 0.15g$, mass ratio, $\sigma = m_s/m_w = 5$, wall size, $\omega_1/p = 5$, and pre-yielding period of $T_1 = 1.2sec$, when subjected to the CO2/065 ground motion recorded during the Newhall/360 ground motion recorded during 1994 Northridge, California earthquake. Heavy solid lines: No wall. Heavy dashed lines: Rocking wall without damper. Thin solid lines: Wall with dampers (hysteretic (left) and linear viscous (right)) ($\epsilon = 0.5$ and $\dot{\theta}_{max} = 0.11\ rad/sec$) zero-length dampers. Bottom: Force-displacement loops of the hysteretic (left) and linear (right) dampers installed at each leg of the rocking wall.

4.3 EARTHQUAKE SPECTRA OF A YIELDING OSCILLATOR COUPLED TO A STEPPING ROCKING WALL WITH SUPPLEMENTAL DAMPING

The effect of supplemental damping, either hysteretic or viscous along the sides of a stepping rocking wall coupled to a medium-to-high rise, yielding building is investigated with the generation of inelastic response spectra. In addition to the 1994 Newhall 360 record shown in Figure 4-4, the Pacoima Dam/164 ground motion recorded during the 1971 Imperial valley, California earthquake, the Erzincan NS ground motion recorded during the 1997 Erzincan, Turkey earthquake, and the Sylmar ground motion recorded during the 1994 Northridge earthquake shown in Figure 4-5 are used for the generation of the inelastic response spectra.

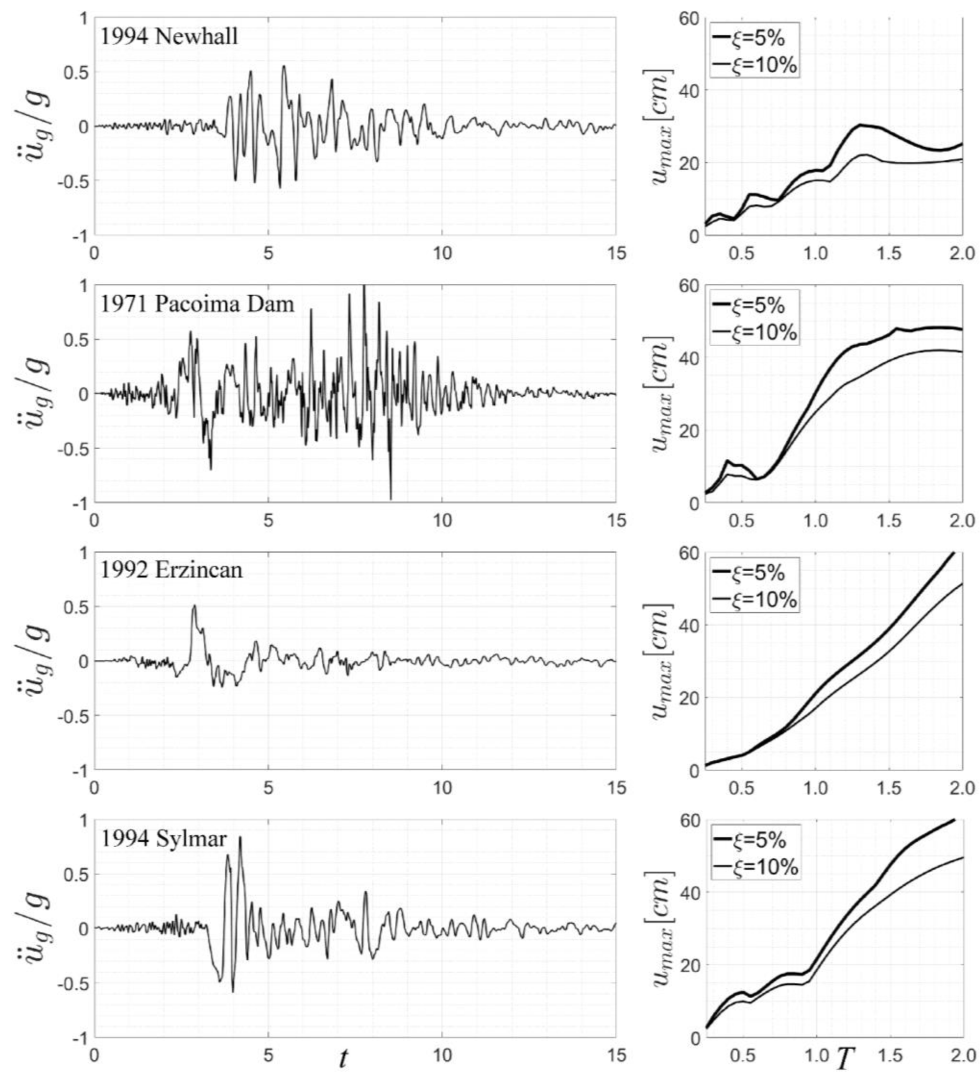

Figure 4-5 Recorded time-histories and elastic response spectra for damping ratio, $\xi = \frac{C}{2m\omega_o} = 5\%$ and 10% of the 4 ground motions used for the response analysis presented in this study.

These ground motions were selected based on the reasoning that the distinguishable coherent pulse of these motions has different duration, therefore each motion will amplify the inelastic structural response at different preyielding periods. With reference to (Makris et al. 2006) the Newhall record has a coherent pulse period $T_p = 0.75s$, the Pacoima Dam has coherent pulse duration $T_p = 1.3s$. the Erzincan record has a coherent pulse duration $T_p = 1.8s$, and Sylmar record has a coherent pulse duration $T_p = 2.3s$.

Figure 4-6 plots displacement response spectra of the yielding SDOF oscillator coupled to a rocking wall with vertical hysteretic dampers (say Buckling Restrained Braces) appended to the pivot corners of the rocking wall (d=0) with strength equal to 20% and 50% of the yielding strength of the structure $Q = 0.08m_s g$ and post-yield-to-pre-yield stiffness ratio equal to $a_d = 2.5\%$. The mass ratio $\sigma = m_s/m_w = 10$ on the left column and $\sigma = 5$ on the right column of Figure 4-6.

Figure 4-6 shows that when the input ground motion is the 1994 Newhall record, the vertical hysteretic dampers further suppress the inelastic displacements. In contrast, for the 1971 Pacoima Dam record, the 1992 Erzincan record, and the 1994 Sylmar record, Figure 4-6 reveals that the presence of supplemental hysteretic dampers at the pivot corners of the rocking wall has marginal effects and the reduction of the inelastic displacement is essentially due the coupling with the rocking wall. Furthermore, there are situations where the structural response when hysteretic dampers are used exceeds the structural response without dampers being appended at the pivot corners of the rocking wall. This “counter intuitive” finding should not be a surprise since it has been observed to also happen on the rocking response of solitary columns with supplemental damping (Makris and Aghagholizadeh 2019) and results from the way that inertia, gravity and damping forces combine. Figure 4-6 also plots the peak angular velocity, $\dot{\theta}_{max}$, of the rocking wall with the scale shown on the right of the plots. Clearly, as the preyielding period, T_1, of the frame structure increases, the peak angular velocity decreases. For each value of the preyielding period of the yielding oscillator appearing along the horizontal axis of the spectra, the value, $\dot{\theta}_{max}$, is fed to equation (4-25) to offer the equivalent viscous damping $c_1 = \epsilon Q_s / (2b\dot{\theta}_{max})$ that is needed to compute the corresponding spectra where the supplemental damping at the pivot corners of the rocking wall are linear viscous dampers.

Figure 4-7 plots displacement response spectra for the same structural configuration described when discussing Figure 4-6; however, now the strength of the inelastic frame is $Q = 0.15m_s g$ (left plots) and $Q = 0.20m_s g$ (right plots). The mass ration $\sigma = m_s/m_w = 10$ for both values of the strengths examined. Figure 4-7 reveals that supplemental damping along the sides of the rocking wall may have some limited beneficial effect for structures with long preyielding periods (say $T_1 > 1.0$ s). Nevertheless, no notable further response reduction is observed when larger values of hysteretic dissipation are used.

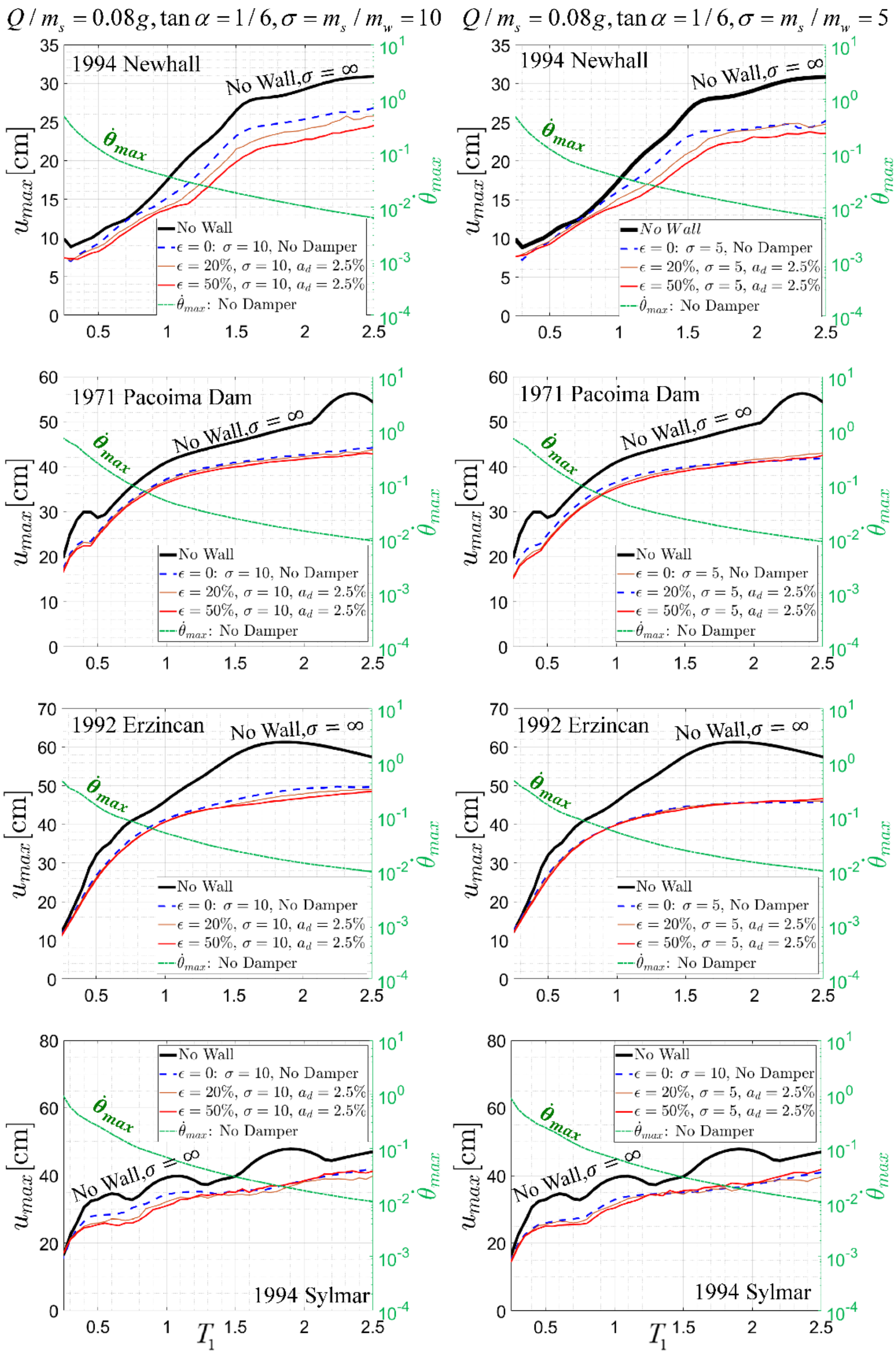

Figure 4-6 Peak response of SDOF yielding oscillator with strength of $Q/m_s = 0.08g$ coupled with a stepping wall with slenderness $tan\ \alpha = 1/6$ with zero-length supplemental hysteretic dampers appended at the pivoting points ($d = 0$) when excited by the 4 strong ground motions presented earlier in this study. Figures on the left correspond to a mass ratio $\sigma = m_s/m_w = 10$, whereas, for the figures on the right $\sigma = m_s/m_w = 5$.

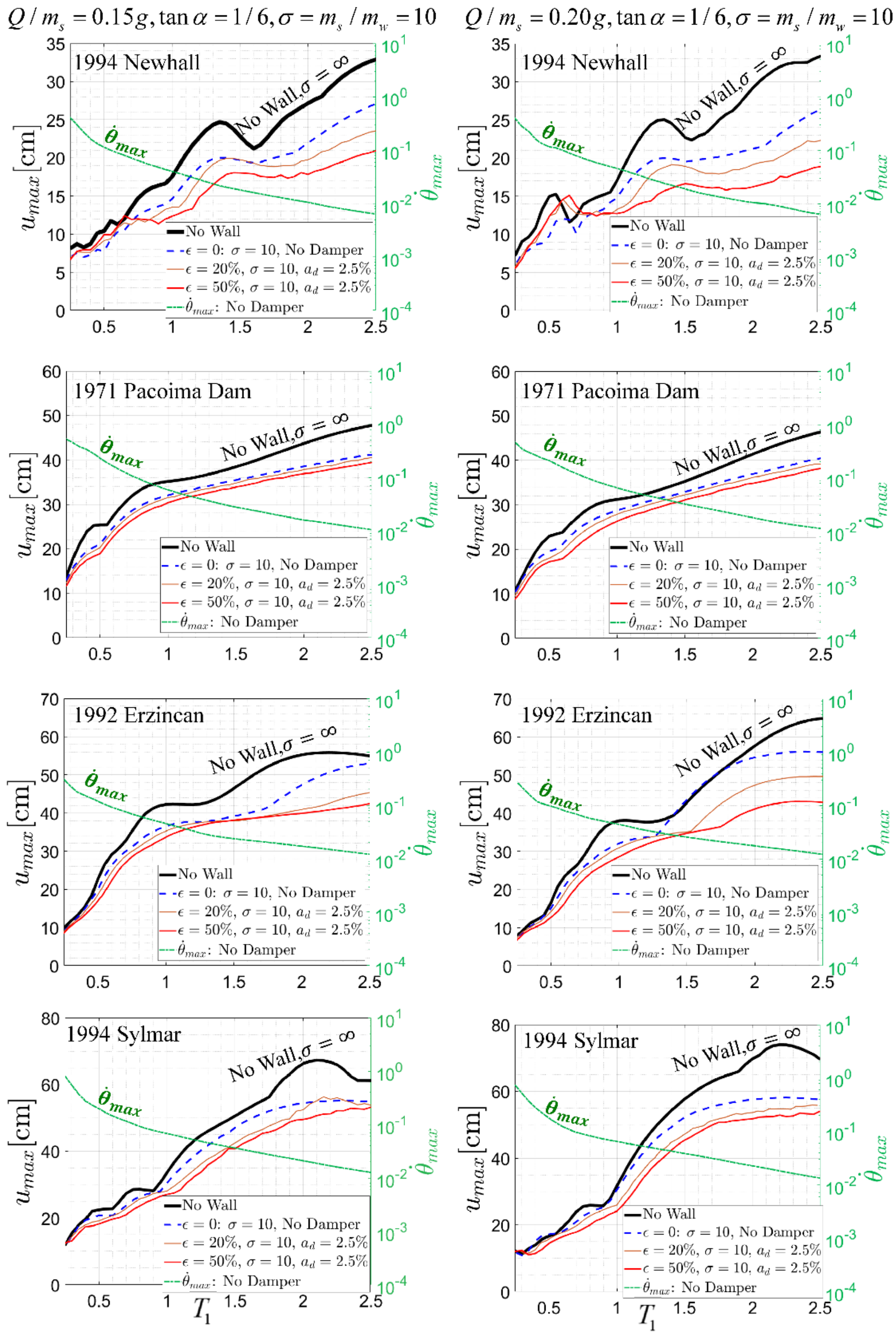

Figure 4-7 Peak response of SDOF yielding oscillator coupled with a stepping wall with slenderness $\tan\alpha = 1/6$ and mass ratio $\sigma = m_s/m_w = 10$ with zero-length supplemental hysteretic dampers appended at the pivoting points ($d = 0$) when excited by the 4 strong ground motions presented earlier in this study. Figures on the left correspond to a yielding structure with strength of $Q/m_s = 0.15g$ and on the right to a stronger yielding structure with strength of $Q/m_s = 0.20g$.

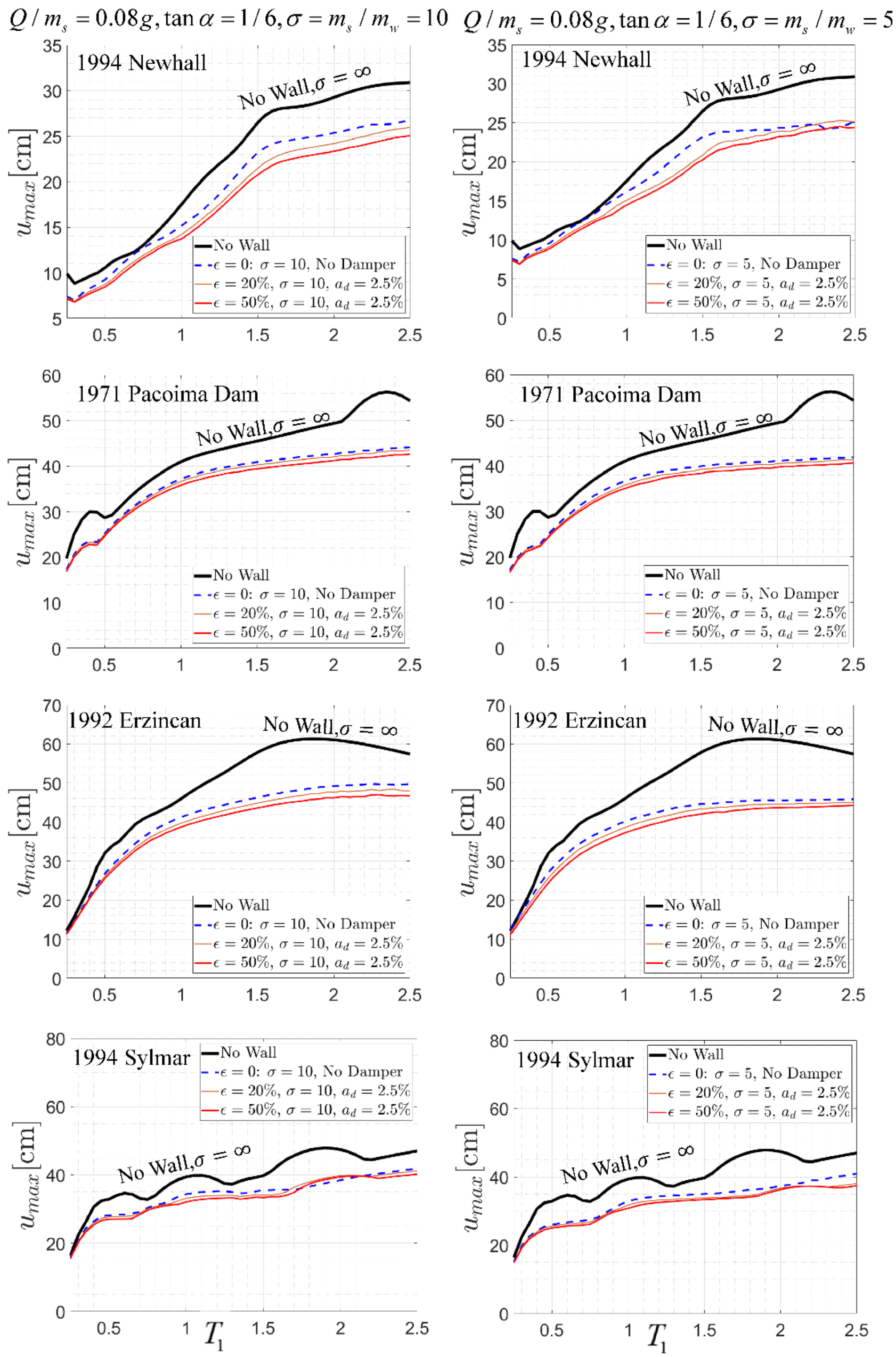

Figure 4-8 Peak response of SDOF yielding oscillator with strength of $Q/m_s = 0.08g$ coupled with a stepping wall with slenderness $\tan\alpha = 1/6$ with zero-length supplemental viscous dampers ($q = 1$) appended at the pivoting points ($d = 0$) when excited by the 4 strong ground motions presented earlier in this study. Figures on the left correspond to a mass ratio $\sigma = m_s/m_w = 10$, whereas, for the figures on the right $\sigma = m_s/m_w = 5$.

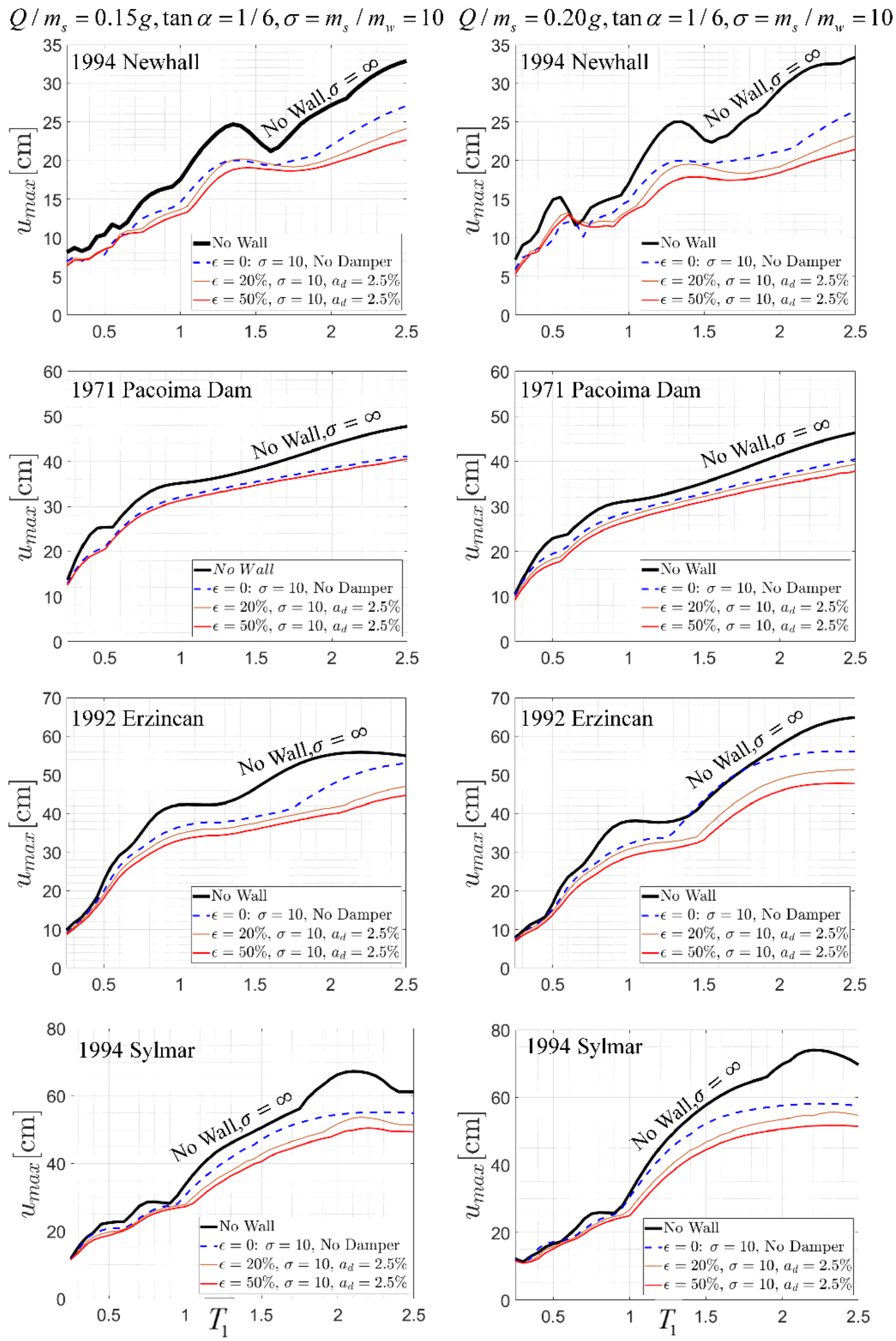

Figure 4-9 Peak response of SDOF yielding oscillator coupled with a stepping wall with slenderness $tan\ \alpha = 1/6$ and mass ratio $\sigma = m_s/m_w = 10$ with zero-length supplemental viscous dampers ($q = 1$) appended at the pivoting points ($d = 0$) when excited by the 4 strong ground motions presented earlier in this study. Figures on the left correspond to a yielding structure with strength of $Q/m_s = 0.15g$ and on the right to a stronger yielding structure with strength of $Q/m_s = 0.20g$.

Figure 4-8 and Figure 4-9 plot displacement response spectra of the yielding SDOF oscillator coupled to a rocking wall with vertical linear viscous dampers appended at the pivot corners of the rocking wall ($d = 0$) with damping constant $c_1 = \epsilon Q_s / (2b\dot{\theta}_{max})$ in which $\dot{\theta}_{max}$ is offered in Figure 4-6. Again, when the input ground motion is the 1994 Newhall record, the viscous dampers further suppress the inelastic displacements; whereas, for the other ground motion (1971 Pacoima Dam, 1992 Erzincan, and 1994 Sylmar) Figure 4-8 (which is for $Q = 0.08m_s g$) reveals that the presence of supplemental viscous dampers at the pivot corners of the rocking wall has a marginal effect. The same "counter intuitive" situations are observed where the structural response with supplemental damping matches or exceeds the structural response without dampers being appended at the pivot corners of the rocking wall. Whenever the damped response exceeds the undamped response, the exceedance is marginal. Figure 4-9 which plots the response for stronger inelastic structures ($Q = 0.15m_s g$ and $Q = 0.20m_s g$) when the rocking wall is equipped with viscous dampers reveals similar trend than those discussed in Figure 4-7 where hysteretic dampers were used.

4.4 CONCLUSIONS

This chapter investigates the dynamic response of a yielding SDOF oscillator coupled to a stepping rocking wall with supplemental damping (either hysteretic or viscous) along its sides. The full nonlinear equations of motion are derived, and the study presents a parametric analysis of the inelastic system in terms of inelastic response spectra and reaches the following conclusions:

- The participation of the stepping rocking wall suppresses invariably peak inelastic displacement; as has been shown in previous studies.
- In contrast, the effect of supplemental damping along the sides of the rocking wall is marginal for structures with preyielding periods lower that $T_1 = 1.0\ s$ and occasionally the damped response exceeds the undamped response. Whenever the damped response exceeds the undamped response, the exceedance is marginal.
- Supplemental damping along the sides of the rocking wall may have some limited beneficial effects for structures with longer preyielding periods (say $T_1 > 1.0\ s$).
- No notable further response reduction is observed when larger values of hysteretic or viscous damping are used

5 CONCLUSIONS

This report investigates the dynamics of a rocking walls when they are attached to moment-resisting frames. The effect of support condition of the wall for the cases of stepping rocking and pinned rocking wall is considered and compared. Moreover, the effect of using prestressing restrainers and dampers to the overall dynamics of the coupled rocking-wall-frame system under various earthquakes is examined.

For each case, the full nonlinear equations of motions are derived, and the dependability of the one-degree-of-freedom idealization is validated against the nonlinear time-history response analysis of the 9-story SAC steel building. Through a comprehensive parametric analysis, the study reaches the following conclusions.

1. When the yielding SDOF oscillator is coupled with a stepping rocking wall, the participation of the stepping wall suppresses the peak inelastic displacements in particular for more flexible structures with the heavier wall being most effective. Most importantly, the participation of the stepping rocking wall reduces drastically the permanent displacements which vanish completely as the weight of the wall increases.

2. When the yielding SDOF oscillator is coupled with a pinned rocking wall, opposite trends are observed:

    a. The participation of the pinned rocking wall increases in general the peak inelastic displacements with the heavier wall being most unfavorable.

    b. The participation of the pinned rocking wall increases the permanent displacements through a wide range of the response spectrum. This unfavorable response is mainly because the moment from the weight of a pinned rocking wall works against the stability of the system. Accordingly, the coupling a yielding frame with a pinned rocking wall may result to unfavorable response and should be used with caution.

3. The length of the coupling arm has a marginal effect on the response of the SDOF oscillator when coupled with a rocking wall. Nevertheless, the pinned wall amplifies the response for most of the range of the spectrum even when short arm lengths are considered.

4. The participation of the stepping rocking wall suppresses peak inelastic displacements with the heavier wall being in most cases more effective. In contrast, the effect of the vertical tendons even when they are stiff ($\frac{EA}{m_w g} = 200$) and highly prestressed ($P_o = m_w g$) is marginal.

5. Given than the vertical tendons increase the vertical reactions at the pivoting corners by more than 50%, this chapter concludes that for medium- to high-rise buildings, vertical tendons in rocking walls are not recommended.

6. The participation of the stepping rocking wall suppresses invariably peak inelastic displacement; as has been shown in previous studies.

7. In contrast, the effect of supplemental damping along the sides of the rocking wall is marginal for structures with preyielding periods lower that $T_1 = 1.0\, s$ and occasionally the damped response exceeds the undamped response. Whenever the damped response exceeds the undamped response, the exceedance is marginal

8. Supplemental damping along the sides of the rocking wall may have some limited beneficial effects for structures with longer preyielding periods (say $T_1 > 1.0\, s$).

9. No notable further response reduction is observed when larger values of hysteretic or viscous damping are used

10. The SDOF idealization presented in this report compares satisfactory with finite-element analysis of a 9-story steel SAC building coupled with a stepping rocking wall; therefore, the SDOF idealization can be used with confidence for preliminary analysis and design.

REFERENCE

Aghagholizadeh M. (2018). *Seismic Response of Moment Resisting Frames Coupled with Rocking Walls. Doctoral dissertation, University of Central Florida* [University of Central Florida]. https://stars.library.ucf.edu/etd/6156/

Aghagholizadeh M. (2020). A finite element model for seismic response analysis of vertically-damped rocking-columns. *Engineering Structures*, *219*(15), 110894. https://doi.org/10.1016/j.engstruct.2020.110894

Aghagholizadeh M., and Makris N. (2018a). Seismic Response of a Yielding Structure Coupled with a Rocking Wall. *Journal of Structural Engineering*, *144*(2), 04017196. https://doi.org/10.1061/(asce)st.1943-541x.0001894

Aghagholizadeh M., and Makris N. (2018b). Earthquake response analysis of yielding structures coupled with vertically restrained rocking walls. *Earthquake Engineering and Structural Dynamics*, *47*(15), 2965–2984. https://doi.org/10.1002/eqe.3116

Aghagholizadeh M., and Makris N. (2021). Response analysis of yielding structures coupled to rocking walls with supplemental damping. *Earthquake Engineering & Structural Dynamics*, *50*(10), 2672–2689. https://doi.org/10.1002/EQE.3466

Ajrab J. J., Pekcan G., and Mander J. B. (2004). Rocking wall-frame structures with supplemental tendon systems. *Journal of Structural Engineering*, *130*(6), 895–903. https://doi.org/10.1061/(ASCE)0733-9445(2004)130:6(895)

Aktan A. E., and Bertero V. V. (1984). Seismic response of R/C frame-wall structures. *Journal of Structural Engineering*, *110*(8), 1803–1821. https://doi.org/10.1061/(ASCE)0733-9445(1984)110:8(1803)

Alavi B., and Krawinkler H. (2004a). Behavior of moment-resisting frame structures subjected to near-fault ground motions. *Earthquake Engineering & Structural Dynamics*, *33*(6), 687–706. https://doi.org/10.1002/eqe.369

Alavi B., and Krawinkler H. (2004b). Strengthening of moment-resisting frame structures against near-fault ground motion effects. *Earthquake Engineering & Structural Dynamics*, *33*(6), 707–722. https://doi.org/10.1002/eqe.370

Baber T. T., and Wen Y.-K. (1981). Random Vibration of Hysteretic Degrading Systems. *Journal of the Engineering Mechanics Division, ASCE*, *107*(EM6), 1069–1087.

Beck J. L., and Skinner R. I. (1972). The seismic response of a proposed reinforced concrete railway viaduct. *Physics and Engineering Laboratory DSIR Report No 369*.

Beck J. L., and Skinner R. I. (1974). The seismic response of a reinforced concrete bridge pier designed to step. *Earthquake Engineering and Structural Dynamics*, *2*(4), 343–358. https://doi.org/10.1002/eqe.4290020405

Belleri A., Schoettler M. J., Restrepo J. I., and Fleischman R. B. (2014). Dynamic behavior of rocking and hybrid cantilever walls in a precast concrete building. *ACI Structural Journal*, *111*(3), 661. https://doi.org/10.14359/51686778

Bertero V. V. (1980). Seismic behavior of R/C wall structural systems. *Proceedings, 7th World Conference on Earthquake Engineering*, Istanbu, Turkey, Vol. VI: 323-330. https://www.iitk.ac.in/nicee/wcee/seventh_conf_Turkey/

Black C. J., Aiken I. D., and Makris N. (2002). Component testing, stability analysis, and characterization of buckling-restrained unbonded braces (TM). *PEER Report No. 2002/08, Pacific Earthquake Engineering Research Center, University of California, Berkeley, CA.*

https://peer.berkeley.edu/sites/default/files/0208_c._black_n._makris_i._aiken.pdf
Black C. J., Makris N., and Aiken I. D. (2004). Component testing, seismic evaluation and characterization of buckling-restrained braces. *Journal of Structural Engineering*, *130*(6), 880–894. https://doi.org/10.1061/(ASCE)0733-9445(2004)130:6(880)
Boardman P., Wood B., and Carr A. (1983). Union House-A crossbraced structure with energy dissipators Seismic Vulnerability Assessment. Retrofit Strategies and Risk Reduction View Project Damage Avoidance Design (DAD) View project. *Bulletin of the New Zealand National Society for Earthquake Engineering*, *16*(2).
Bouc R. (1967). Forced vibration of mechanical systems with hysteresis. *Proceedings, 4th Conference on Non-Linear Oscillations, Prague, Czechoslovakia*.
Charleson A. W., Wright P. D., and Skinner R. I. (1987). Wellington central police station, base isolation of an essential facility. *Proeeding, Pacific Conference on Earthquake Engineering*, *2*, 377–388.
Cheok G. S., and Lew H. S. (1993). Model Precast Concrete Beam-to-Column Connections Subject to Cyclic Loading. *PCI Journal*, *38*(4), 80–92. https://doi.org/10.15554/pcij.07011993.80.92
Chopra A. K., and Goel R. K. (2002). A modal pushover analysis procedure for estimating seismic demands for buildings. *Earthquake Engineering & Structural Dynamics*, *31*(3), 561–582. https://doi.org/10.1002/eqe.144
Constantinou M. C., and Adnane M. A. (1987). Dynamics of soil-base-isolated structure systems. Report 4: Evaluation of two models for yielding systems. In *Department of Civil Engineering, Drexel University, Philadelphia, PA.*
Elwood K. J. (2013). Performance of concrete buildings in the 22 February 2011 Christchurch earthquake and implications for Canadian codes. *Canadian Journal of Civil Engineering*, *40*(8), 759–776. https://doi.org/10.1139/cjce-2011-0564
Emori K., and Schnobrich W. C. (1978). *Analysis of reinforced concrete frame-wall structures for strong motion earthquakes*. Report no. SRS-457, University of Illinois at Urbana-Champaign. http://hdl.handle.net/2142/13919
Erkmen B., and Schultz A. E. (2009). Self-centering behavior of unbonded, post-tensioned precast concrete shear walls. *Journal of Earthquake Engineering*, *13*(7), 1047–1064. https://doi.org/10.1080/13632460902859136
Filiatrault A., Restrepo J., and Christopoulos C. (2004). Development of self-centering earthquake resisting systems. *Proceedings, 13th World Conference on Earthquake Engineering, Vancouver, British Columbia, Canada*. https://www.iitk.ac.in/nicee/wcee/thirteenth_conf_Canada/
Fintel M. (1975). Ductile Shear Walls in Earthquake-Resistant Multistory Buildings. *Proceeding, Seventh Joint Panel Conference of the US-Japan Cooperative Program in Natural Resources*, *470*, Tokyo, Japan.
Goda K., Hong H. P., and Lee C. S. (2009). Probabilistic characteristics of seismic ductility demand of SDOF systems with Bouc-Wen hysteretic behavior. *Journal of Earthquake Engineering*, *13*(5), 600–622. https://doi.org/10.1080/13632460802645098
Grigorian C. E., and Grigorian M. (2015). Performance Control and Efficient Design of Rocking-Wall Moment Frames. *Journal of Structural Engineering*, *142*(2), 4015139. https://doi.org/10.1061/(ASCE)ST.1943-541X.0001411
Grigorian M., and Grigorian C. (2016). An introduction to the structural design of rocking wall-frames with a view to collapse prevention, self-alignment and repairability. *The Structural*

Design of Tall and Special Buildings, *25*(2), 93–111. https://doi.org/10.1002/tal.1230
Gupta A., and Krawinkler H. (1999). Seismic demands for the performance evaluation of steel moment resisting frame structures. In *John A Blume Earthquake Engineering Center Technical Report 132. Stanford Digital Repository. Stanford University, Stanford, CA*. http://purl.stanford.edu/fm826wn5553
Gupta A., and Krawinkler H. (2000). Behavior of ductile SMRFs at various seismic hazard levels. *Journal of Structural Engineering*, *126*(1), 98–107. https://doi.org/10.1061/(ASCE)0733-9445(2000)126:1(98)
Holden T., Restrepo J., and Mander J. B. (2003). Seismic performance of precast reinforced and prestressed concrete walls. *Journal of Structural Engineering*, *129*(3), 286–296. https://doi.org/10.1061/(ASCE)0733-9445(2003)129:3(286)
Housner G. W. (1963). The behavior of inverted pendulum structures during earthquakes. *Bulletin of the Seismological Society of America*, *53*(2), 403–417.
Hu X., and Zhang Y. (2012). Seismic Performance of Reinforced Concrete Frames Retrofitted with Self-Centering Hybrid Wall. *Advances in Structural Engineering*, *15*(12), 2131–2143. https://doi.org/10.1260/1369-4332.15.12.2131
Kelly J. M. (1993). Earthquake-resistant design with rubber. In *Earthquake-Resistant Design with Rubber*. Springer London. https://doi.org/10.1007/978-1-4471-3359-9
Kelly J. M., Skinner R. I., and Heine A. J. (1972). Mechanisms of energy absorption in special devices for use in earthquake resistant structures. *Bulletin of NZ Society for Earthquake Engineering*, *5*(3), 63–88.
Kunnath S. K., Mander J. B., and Fang L. (1997). Parameter identification for degrading and pinched hysteretic structural concrete systems. *Engineering Structures*, *19*(3), 224–232. https://doi.org/10.1016/S0141-0296(96)00058-2
Kurama Y. C. (2000). Seismic design of unbonded post-tensioned precast concrete walls with supplemental viscous damping. *ACI Structural Journal*, *97*(4), 648–658. https://doi.org/10.14359/7431
Kurama Y. C., Sause R., Pessiki S., and Lu L.-W. (1999). Lateral load behavior and seismic design of unbonded post-tensioned precast concrete walls. *Structural Journal*, *96*(4), 622–632. https://doi.org/10.14359/700
Kurama Y. C., Sause R., Pessiki S., and Lu L.-W. (2002). Seismic response evaluation of unbonded post-tensioned precast walls. *Structural Journal*, *99*(5), 641–651. https://doi.org/10.14359/12304
Lanczos C. (1979). *The variational principles of mechanics*. Dover Publications.
Lu Y. (2005). Inelastic behaviour of RC wall-frame with a rocking wall and its analysis incorporating 3-D effect. *The Structural Design of Tall and Special Buildings*, *14*(1), 15–35. https://doi.org/10.1002/tal.254
Makris N. (1996). Near-source earthquakes, base isolated structures and semiactive damper. In G. D. Manolis & D. E. Beskos (Eds.), *1'st International Symposiom Earthquake Resisting Engineering Structures* (pp. 219–360).
Makris N. (2014a). A half-century of rocking isolation. *Earthquakes and Structures*, *7*(6), 1187–1221. https://doi.org/10.12989/eas.2014.7.6.1187
Makris N. (2014b). The role of the rotational inertia on the seismic resistance of free-standing rocking columns and articulated frames. *Bulletin of the Seismological Society of America*, *104*(5), 2226–2239. https://doi.org/10.1785/0120130064
Makris N., and Aghagholizadeh M. (2017a). The dynamics of an elastic structure coupled with a

rocking wall. *Earthquake Engineering & Structural Dynamics*, *46*(6), 945–962. https://doi.org/10.1002/eqe.2838

Makris N., and Aghagholizadeh M. (2017b, October). Earthquake Protection of a Yielding Frame with a Rocking Wall. *International Workshop on Performance-Based Seismic Design of Structures (Resilience, Robustness), Tongji University, Shanghai, China*. http://risedr.tongji.edu.cn/PBSD_Workshop/files/PBSD-Proceedings.pdf

Makris N., and Aghagholizadeh M. (2019). Effect of Supplemental Hysteretic and Viscous Damping on Rocking Response of Free-Standing Columns. *Journal of Engineering Mechanics*, *145*(5), 4019028. https://doi.org/10.1061/(ASCE)EM.1943

Makris N., and Black C. J. (2002). Uplifting and overturning of equipment anchored to a base foundation. *Earthquake Spectra*, *18*(4), 631–661. https://doi.org/10.1193/1.1515730

Makris N., and Chang S.-P. (2000). Effect of viscous, viscoplastic and friction damping on the response of seismic isolated structures. *Earthquake Engineering & Structural Dynamics, 29*(1), 85–107.

Makris N., and Kampas G. (2013). The engineering merit of the “effective period” of bilinear isolation systems. *Earthquakes and Structures*, *4*(4), 397–428. https://doi.org/10.12989/eas.2013.4.4.397

Makris N., and Roussos Y. (1998). Rocking response and overturning of equipment under horizontal pulse-type motions. *PEER Report No. 1998/05, Pacific Earthquake Engineering Research Center, University of California, Berkeley, CA*. https://apps.peer.berkeley.edu/publications/peer_reports/reports_1998/9805.pdf

Makris N., and Roussos Y. S. (2000). Rocking response of rigid blocks under near-source ground motions. *Geotechnique*, *50*, 243–262. https://doi.org/10.1680/geot.2000.50.3.243

Makris N., and Vassiliou M. F. (2014). Are some top-heavy structures more stable? *Journal of Structural Engineering*, *140*(5), 6014001. https://doi.org/10.1061/(ASCE)ST.1943-541X.0000933

Mander J. B., and Cheng C.-T. (1997). Seismic resistance of bridge piers based on damage avoidance design. *Technical Report NCEER-97-0014, National Center for Earthquake Engineering Research, University at Buffalo, State University of New York*. https://www.buffalo.edu/mceer/catalog.host.html/content/shared/www/mceer/publications/NCEER-97-0014.detail.html

McKenna F., Fenves G. L., and Scott M. H. (2000). Open system for earthquake engineering simulation. *University of California, Berkeley, CA*. https://opensees.berkeley.edu/

Meek J. W. (1978). Dynamic response of tipping core buildings. *Earthquake Engineering & Structural Dynamics*, *6*(5), 437–454. https://doi.org/10.1002/eqe.4290060503

Nakaki S. D., Stanton J. F., and Sritharan S. (1999). An overview of the PRESSS five-story precast test building. *PCI Journal*, *44*(2), 26–39. https://doi.org/10.15554/pcij.03011999.26.39

Nazari M., Sritharan S., and Aaleti S. (2017). Single precast concrete rocking walls as earthquake force-resisting elements. *Earthquake Engineering & Structural Dynamics, 46*(5), 753–769. https://doi.org/10.1002/eqe.2829

Nicknam A., and Filiatrault A. (2014). Numerical Evaluation of Seismic Response of Buildings Equipped with Propped Rocking Wall Systems. *Proceedings, 10th U.S. National Conference on Earthquake Engineering: Frontiers of Earthquake Engineering*.

NOAA National Geophysical Data Center. (2012). *Natural Hazard Images Database (Event: January 1995 Hanshin-Awaji (Kobe), Japan Images). NOAA National Centers for*

Environmental Information. https://www.ncei.noaa.gov/access/metadata/landing-page/bin/iso?id=gov.noaa.ngdc.mgg.photos:19

Paulay T. (1969). The coupling of reinforced concrete shear walls. *Proceedings, Fourth World Conference on Earthquake Engineering, Santiago, Chile,* Vol I: B2-75.

Paulay T. (1986). The design of ductile reinforced concrete structural walls for earthquake resistance. *Earthquake Spectra*, *2*(4), 783–823. https://doi.org/10.1193/1.1585411

Preti M., and Giuriani E. (2011). Ductility of a structural wall with spread rebars tested in full scale. *Journal of Earthquake Engineering*, *15*(8), 1238–1259.

Priestley M. J. N. (1991). Overview of PRESSS research program. *PCI Journal*, *36*(4), 50–57. https://doi.org/10.15554/pcij.07011991.50.57

Priestley M. J. N. (1996). The PRESSS Program—Current Status and Proposed Plans for Phase Ill. *PCI Journal*, *4*(2), 22–40. https://doi.org/10.15554/pcij.03011996.22.40

Priestley M. J. N., Sritharan S., Conley J. R., and Pampanin S. (1999). Preliminary results and conclusions from the PRESSS five-story precast concrete test building. *PCI Journal*, *44*(6), 42–67. https://doi.org/10.15554/pcij.11011999.42.67

Qu Z., Wada A., Motoyui S., Sakata H., and Kishiki S. (2012). Pin-supported walls for enhancing the seismic performance of building structures. *Earthquake Engineering & Structural Dynamics*, *41*(14), 2075–2091. https://doi.org/10.1002/eqe.2175

Restrepo J. I., and Rahman A. (2007). Seismic performance of self-centering structural walls incorporating energy dissipators. *Journal of Structural Engineering*, *133*(11), 1560–1570. https://doi.org/10.1061/(ASCE)0733-9445(2007)133:11(1560)

Robinson W., and Greenbank L. (1976). An extrusion energy absorber suitable for the protection of structures during an earthquake. *Earthquake Engineering & Structural Dynamics*, *4*(3), 251–259.

SAC Joint Venture. (2000). *Recommended Seismic Design Criteria for New Steel Moment-Frame Buildings: Program to Reduce the Earthquake Hazards of Steel Moment Frame Structures* (FEMA-350). https://www.fema.gov/media-library-data/20130726-1454-20490-9895/fema-350.pdf

Skinner R. I., Beck J. L., and Bycroft G. N. (1974). A practical system for isolating structures from earthquake attack. *Earthquake Engineering & Structural Dynamics*, *3*(3), 297–309. https://doi.org/10.1002/eqe.4290030308

Skinner R. I., Kelly J. M., and Heine A. J. (1974). Hysteretic dampers for earthquake-resistant structures. *Earthquake Engineering and Structural Dynamics*, *3*(3), 287–296. https://doi.org/10.1002/eqe.4290030307

Skinner R. I., Robinson W. H., and McVerry G. H. (1993). *An introduction to seismic isolation*. John Wiley & Sons, New York, NY.

Toranzo L. A., Restrepo J. I., Mander J. B., and Carr A. J. (2009). Shake-table tests of confined-masonry rocking walls with supplementary hysteretic damping. *Journal of Earthquake Engineering*, *13*(6), 882–898. https://doi.org/10.1080/13632460802715040

USGS. (2020). *The United States Geological Survey Library*. https://library.usgs.gov/

Vassiliou M. F., Mackie K. R., and Stojadinović B. (2014). Dynamic response analysis of solitary flexible rocking bodies: modeling and behavior under pulse-like ground excitation. *Earthquake Engineering & Structural Dynamics*, *43*(10), 1463–1481. https://doi.org/10.1002/eqe.2406

Vassiliou M. F., and Makris N. (2015). Dynamics of the Vertically Restrained Rocking Column. *Journal of Engineering Mechanics*, *141*(12), 4015049.

https://doi.org/10.1061/(ASCE)EM.1943-7889.0000953
Wada A., Qu Z., Motoyui S., and Sakata H. (2011). Seismic retrofit of existing SRC frames using rocking walls and steel dampers. *Frontiers of Architecture and Civil Engineering in China*, *5*(3), 259–266. https://doi.org/10.1007/s11709-011-0114-x
Wada A., Saeki E., Takeuchi T., and Watanabe A. (1989). Development of unbonded brace. *Nippon Steel*, *115*, 12.
Wen Y. K. (1975). Approximate method for nonlinear random vibration. *Journal of Engineering Mechanics*, *101*. https://doi.org/10.1061/JMCEA3.0002029
Wen Y. K. (1976). Method for random vibration of hysteretic systems. *Journal of the Engineering Mechanics Division*, *102*(2), 249–263. https://doi.org/10.1061/JMCEA3.0002106
Zhang J., and Makris N. (2001). Rocking response of free-standing blocks under cycloidal pulses. *Journal of Engineering Mechanics*, *127*(5), 473–483. https://doi.org/10.1061/(ASCE)0733-9399(2001)127:5(473)
Zhang Y., and Wang Z. (2000). Seismic behavior of reinforced concrete shear walls subjected to high axial loading. *Structural Journal*, *98*(5), 739–750. https://doi.org/10.14359/8809

The Pacific Earthquake Engineering Research Center (PEER) is a multi-institutional research and education center with headquarters at the University of California, Berkeley. Investigators from over 20 universities, several consulting companies, and researchers at various state and federal government agencies contribute to research programs focused on performance-based earthquake engineering.

These research programs aim to identify and reduce the risks from major earthquakes to life safety and to the economy by including research in a wide variety of disciplines including structural and geotechnical engineering, geology/seismology, lifelines, transportation, architecture, economics, risk management, and public policy.

PEER is supported by federal, state, local, and regional agencies, together with industry partners.

PEER Core Institutions

University of California, Berkeley (Lead Institution)
California Institute of Technology
Oregon State University
Stanford University
University of California, Davis
University of California, Irvine
University of California, Los Angeles
University of California, San Diego
University of Nevada, Reno
University of Southern California
University of Washington

Pacific Earthquake Engineering Research Center
University of California, Berkeley
325 Davis Hall, Mail Code 1792
Berkeley, CA 94720-1792
Tel: 510-642-3437
Email: peer_center@berkeley.edu

ISSN 2770-8314
https://doi.org/10.55461/MXXS2889